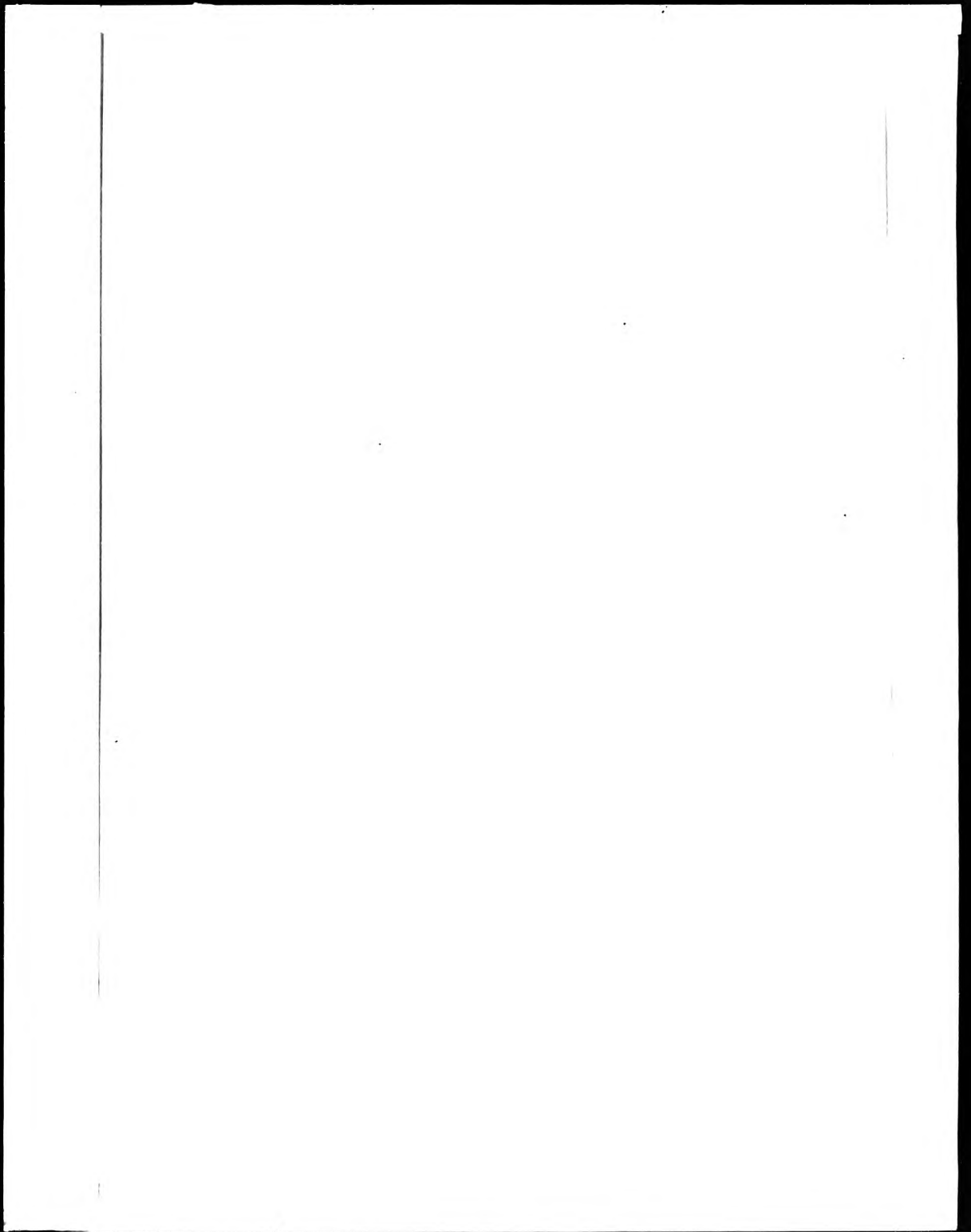


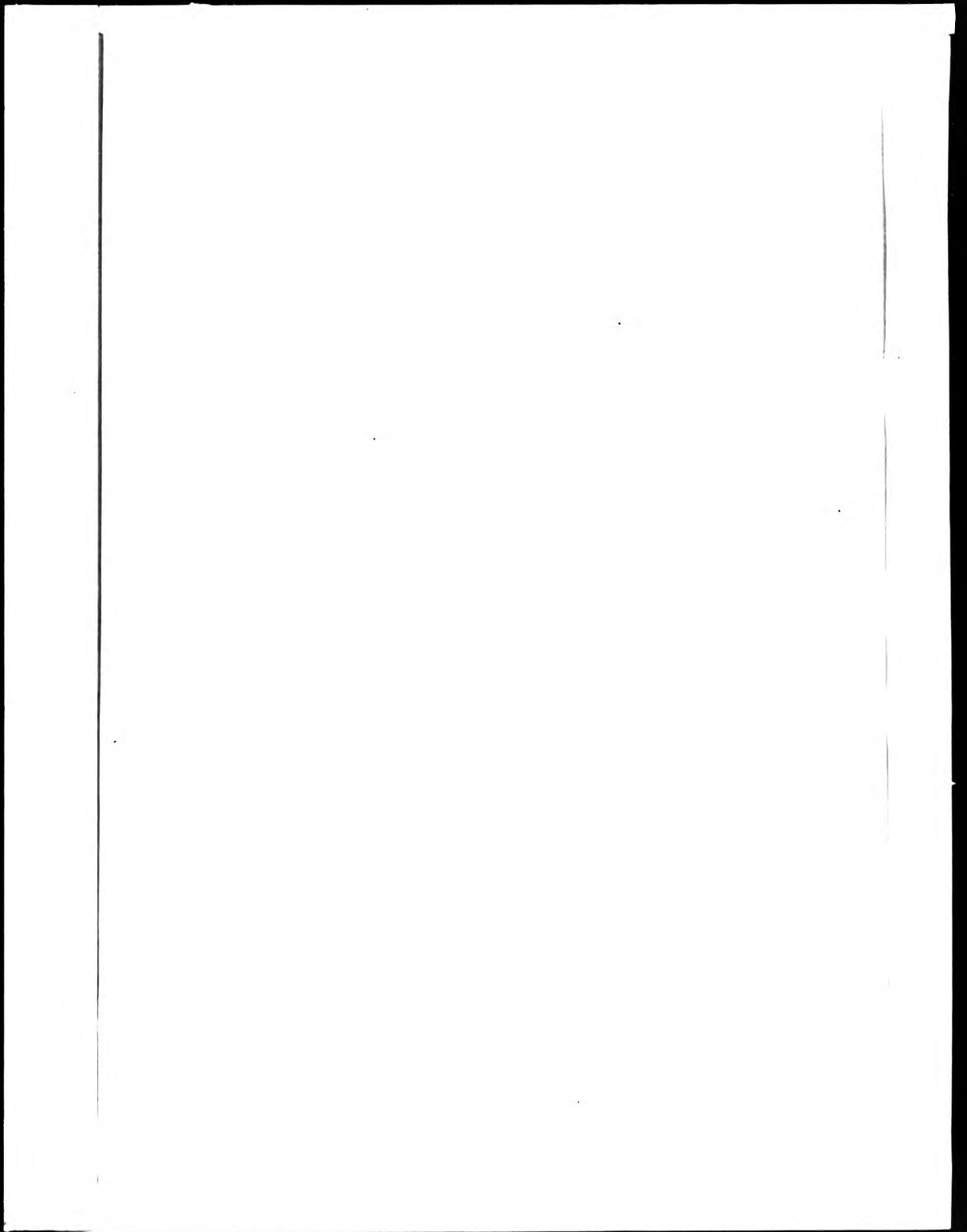
This PDF was created from the British Library's microfilm copy of the original thesis. As such the images are greyscale and no colour was captured.

Due to the scanning process, an area greater than the page area is recorded and extraneous details can be captured.

This is the best available copy



D82142



THE BRITISH LIBRARY DOCUMENT SUPPLY CENTRE

On the growth of (100) GaAs and (100)
InAs by molecular beam epitaxy

TITLE

.....

AUTHOR S.M. Newstead

Attention is drawn to the fact that the copyright of this thesis rests with its author.

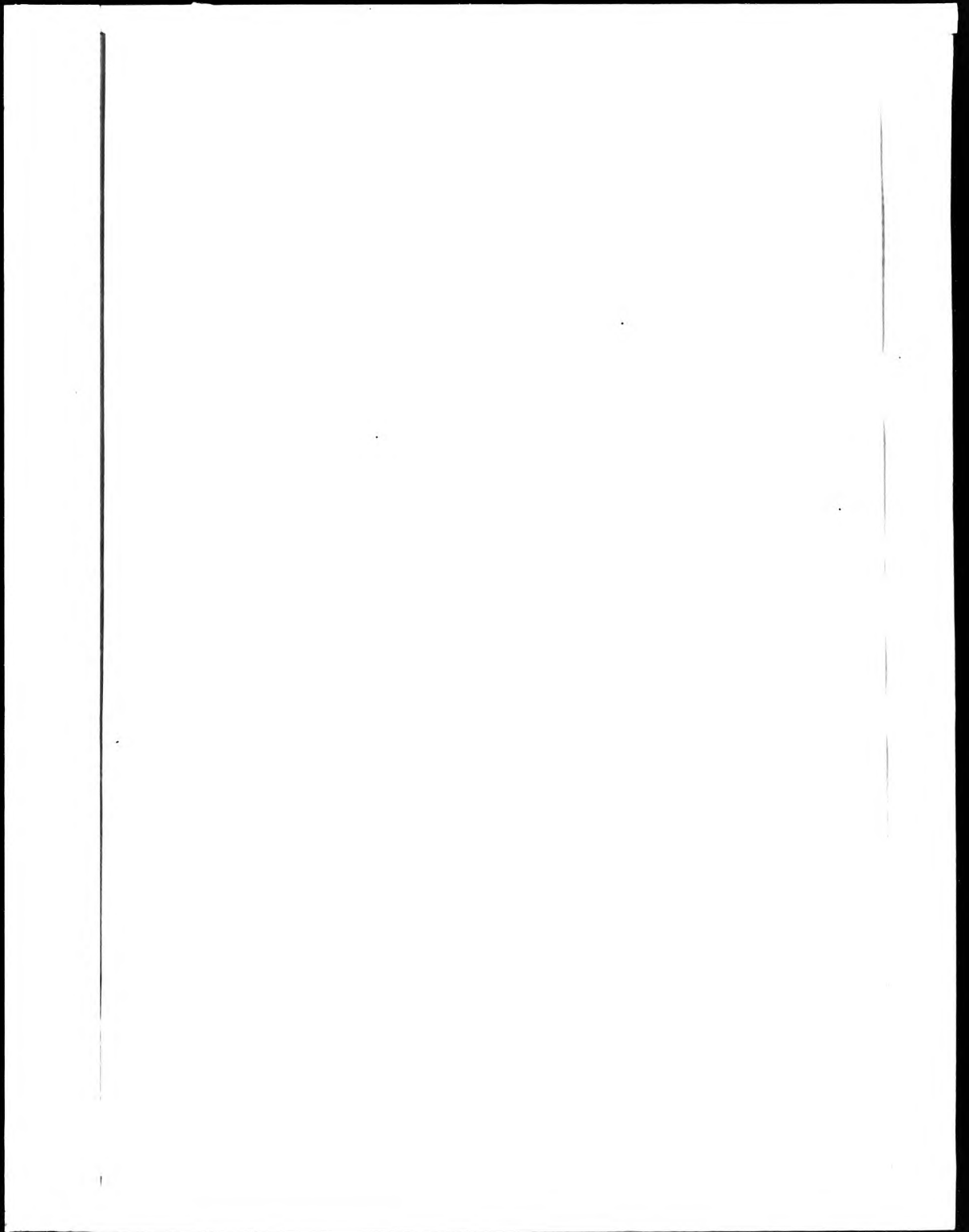
This copy of the thesis has been supplied on condition that anyone who consults it is understood to recognise that its copyright rests with its author and that no information derived from it may be published without the author's prior written consent.

THE BRITISH LIBRARY
DOCUMENT SUPPLY CENTRE
Boston Spa, Wetherby
West Yorkshire
United Kingdom

1	1	2	3	4	5	6	7	8
cms.								

21

REDUCTION X



On the growth of (100) GaAs and (100) InAs by Molecular
Beam Epitaxy

A thesis submitted for the degree of Doctor of Philosophy
in partial fulfilment of the requirements of the Council
for National Academic Awards

by

Simon Marc Newstead BSc

Department of Physics
Sir John Cass School of Science and Technology
City of London Polytechnic
31 Jewry Street
London EC3N 2EY

September 1987

CONTENTS

	Page
Abstract	(ii)
Acknowledgements	(iii)
Chapter 1 The Growth of III-V Compounds By Molecular Beam Epitaxy: Introduction and the Objectives of this Project.	1
Chapter 2 The Technology of Molecular Beam Epitaxy, and the factors influencing the design and operation of a new MBE facility at CLP	27
Chapter 3 The Commissioning of CLP1V, and an investigation into the functional relationship between surface reconstruction, growth conditions and the properties of GaAs epilayers.	61
Chapter 4 An Investigation Into the Optimum Conditions for the Nucleation and Growth of (100) InAs by Molecular Beam Epitaxy.	96
Chapter 5 The Electrical Properties of Si, Sn and Unintentionally Doped InAs grown by Molecular Beam Epitaxy.	126
Resume and Proposals	173
References	
Published Work	

On the growth of (100) GaAs and (100) InAs by Molecular Beam Epitaxy

S M Newstead

September 1987

ABSTRACT

Si and Sn doped GaAs epilayers were grown with electron concentrations from $8 \times 10^{14} \text{ cm}^{-3}$ ($\mu_{77} = 28 \times 10^3 \text{ cm}^2/\text{V-s}$) up to a peak of $1.16 \times 10^{19} \text{ cm}^{-3}$ (using Sn). The major mobility-limiting impurity was carbon. Unintentionally doped material was p-type, with $\mu_{300} = 380$ to $420 \text{ cm}^2/\text{V-s}$ at $N_A - N_D = 1.3 \times 10^{15} \text{ cm}^{-3}$. The range of applicability of the currently accepted GaAs growth model was investigated, leading to the construction of a detailed MBE surface phase diagram. Several surface phenomena are described with reference to this diagram.

Subsequent experiments investigated the growth of InAs. Good quality InAs could only be nucleated on (100) GaAs by using the minimum As_4 flux permitting stoichiometric growth at a temperature just below that at which InAs sublimates non-congruently. Phase diagrams were constructed to demonstrate the relationship between surface reconstruction, growth conditions and material quality. The homoepitaxial growth behaviour of InAs was essentially identical to that of GaAs.

Si and Sn were n-type dopants in InAs, exhibiting 100% electrically active incorporation and near-bulk mobilities at carrier concentrations from $\approx 1 \times 10^{16} \text{ cm}^{-3}$ to the solubility limit of Si, $2.3 \times 10^{19} \text{ cm}^{-3}$. The properties of n⁻ layers were influenced by interfacial accumulations of low mobility electrons. Etch profiling was used to derive a 77 K mobility of $\approx 90 \times 10^3 \text{ cm}^2/\text{V-s}$ at $N_D - N_A = 1.6 \times 10^{15} \text{ cm}^{-3}$ for the bulk-like region of a thick unintentionally doped layer. This figure is comparable to the best mobilities obtained from VPE and bulk grown InAs at similar carrier concentrations.

ACKNOWLEDGEMENTS

I would like to thank Dr J Goddard and the Department of Physics of the City of London Polytechnic for providing the resources necessary to undertake this project. I am particularly indebted to Drs E H C Parker (CLP) and J J Harris (Philips Research Laboratories) for their supervision and encouragement throughout this work. I would also like to acknowledge the excellent work of the technical staff at CLP (P Driscoll, W Hugkulstone, V B Manning, J Heal, R Elam, G J C Burton, A A Aldridge, K Burton and G Curtis), without which an experimental project of this nature would have been impractical. The photoluminescence measurements presented in this thesis were undertaken by S Hiscox and the low temperature Hall measurements by R Nichols, both of the GEC Hirst Research Laboratories.

I am especially grateful to the following people for their moral and/or professional support, without which the last few years would have been far less productive and enjoyable: R A A Kubiak, W Y Leong, D M^CPhail, M G Dows-ett, R M King, J S Barrett, R Houghton, H Fox and G Patel (of CLP); C T Foxon and J H Neave (PRL); D F Lee; J M Thomas and family; and my sister Gill.

Statement of advanced studies undertaken in accordance with
CMAA Regulations 3.8-3.10

Participation in postgraduate seminars in solid state physics arranged by Drs. E H C Parker and R A A Kubiak at CLP; attendance at UK MBE users group meetings 1983-1986.

Regular meetings with, and guidance by, industrial supervisor (Dr J J Harris, Philips Research Laboratories, Redhill UK).

Attendance at Nato Advanced Study Institute on 'Molecular Beam Epitaxy (MBE) and Heterostructures' Erice, Sicily, March 1983; Rank Prize Funds Symposium on Optoelectronic Devices, Malvern, UK, October 1983; Fourth International Conference on Molecular Beam Epitaxy, York, UK, September 1986. A paper based on the work reported in Chapters 3 and 4 of this thesis was presented by the author at the York conference.

CHAPTER 1

The Growth of III-V Compounds By Molecular Beam Epitaxy: Introduction and the Objectives of this Project

Contents

PART 1

- 1.1 Introduction
- 1.2 Molecular Beam Epitaxy
- 1.3 GaAs Surface Kinetics
- 1.4 GaAs Growth Models
- 1.5 Surface Reconstruction
- 1.6 Doping
 - (i) n-type dopants
 - (ii) p-type dopants
- 1.7 Defects in MBE Layers

PART 2

- 1.8 Objectives of this Project
- 1.9 GaAs Growth Study
- 1.10 InAs Growth Study
 - (i) review of earlier studies
 - (ii) objectives of this study
- 1.11 InAs Doping Study

1.1 Introduction

Many of the most useful and exciting properties of the III-V compound semiconductors can only be exploited through the use of epitaxial growth techniques. Until recently, most use has been made of LPE [Panish et al (1971)] and VPE [Dapkus (1984), Ludowise (1985)] technology. However, it is now possible to purchase an MBE system from one of several manufacturers (e.g. VG Semicon, UK; Varian and Perkin-Elmer, USA; and Riber, France) and apply a well established methodology to produce a wide range of commercially important GaAs/AlGaAs device structures. These include high electron mobility transistors [HEMTs, Solomon and Morkoc (1984)], heterojunction bipolar transistors [HBTs, Nakajima et al (1985)], heterojunction LASERS [Tsang (1985)] and other high speed logic, microwave and optoelectronic devices [Eastman (1983), Weimann (1985)]. Many of these applications require high purity layers to be grown to an accurately pre-determined thickness defined by morphologically abrupt heterojunctions. A high degree of control over composition and doping is also required. MBE offers several advantages over LPE and VPE for the growth of such layers;

- (i) A low growth rate of $\approx 1 \mu\text{m/h}$ (or 1 monolayer/sec) combined with essentially instantaneous interruption of growth and doping by rapid action shutters permits accurate and reproducible control over layer thickness [Cho and Arthur (1975)].
- (ii) The relatively low substrate temperatures used in MBE cause minimal diffusion-induced smearing of doping and compositional profiles [Cho (1975), Morkoc and Cho (1979)] and may also reduce the concentration of thermally induced defects [Kasano (1978)].
- (iii) The non-equilibrium nature of MBE allows growth within the miscibility gap of certain ternary and quaternary compounds of potential importance for the

production of long-wavelength optoelectronic devices [Stringfellow (1983)].

- (iv) The UHV environment necessary for MBE allows a wide range of diagnostic equipment to be used for fault finding and in-situ growth studies [Cho and Arthur (1975), Davies and Williams (1985)].

A further area of interest is the possibility of 'selective area epitaxy' by MBE, where masks [Cho and Reinhart (1972), Hiyanizu et al (1980)] or substrates pre-patterned with SiO_2 [Cho and Ballamy (1975)] are used for the lateral definition of active regions. In-situ ion beam lithography may be used to the same end [Davies and Williams (1985)]. These advantages are partially offset by the relative complexity and expense of MBE compared to rival growth techniques. It is also noteworthy that the lowest residual carrier concentrations in MBE grown GaAs are currently an order of magnitude higher than those reported for the best LPE material [10^{12} - 10^{13} cm^{-3} , Kunzel et al (1982)]. However, this does not cause problems in most intentionally doped device structures. More detailed comparisons between MBE, VPE and LPE have been made by Dapkus (1984) and Dorrity et al (1985).

The wider availability of MBE has opened up several areas of pure research. Phenomena associated with the quantum confinement of carriers are of particular importance at present [Tsui and Gossard (1981), Gossard (1984)]. Perhaps the most interesting low dimensional structures are superlattices, exemplified by the GaAs-AlGaAs and InAs-AlSb-GaSb systems [Sai-Halasz et al (1977), Chang and Esaki (1980), Chang (1983)]. Strained layer [Osbourne (1982)] or 'pseudomorphic' systems are also accessible via MBE. Technological spin offs from low dimensional studies include quantum Hall devices, of potential importance as precision resistance standards in instrumentation [Tsui and Gossard (1981)].

This chapter has two main objectives; firstly, to provide a general review of the physical processes involved in MBE growth and, secondly, to indicate why further experimental work was required in the areas addressed by this thesis. Specific objectives are described in Secs 1.8 to 1.11.

1.2 Molecular Beam Epitaxy

Molecular beam epitaxy derives from the three temperature vacuum deposition technique of Gunther (1958, 1961). The distinguishing feature of MBE (Fig 1.1) is that beams of neutral matrix (Ga, Al, In, As, etc) and dopant atoms or molecules are allowed to impinge upon a heated single crystal substrate to produce an epilayer, a single crystal deposit continuous with the substrate and having the same crystallographic orientation. Each molecular beam source is individually shuttered to allow abrupt changes to be made in compositional and doping profiles, and the whole process is carried out under ultra high vacuum (UHV) to minimise the unintentional doping of epilayers by residual gas species. For GaAs, the use of substrates orientated on, or close to, (100) yields the best quality material and provides orthogonal cleavage planes for the separation of samples or devices [Cho and Arthur (1975)].

To be useful for electronic purposes a III-V compound must be stoichiometric, i.e. composed of equal quantities of group III and group V atoms situated on their correct sublattices. Fortunately, surface effects make the MBE growth of compounds in the GaAs family quite straightforward: within a large temperature range, the group III (Ga, In, Al) flux has a unity sticking co-efficient and determines the growth rate, whilst any group V (As) flux in excess of that required for stoichiometry is desorbed. These processes will now be discussed in detail.

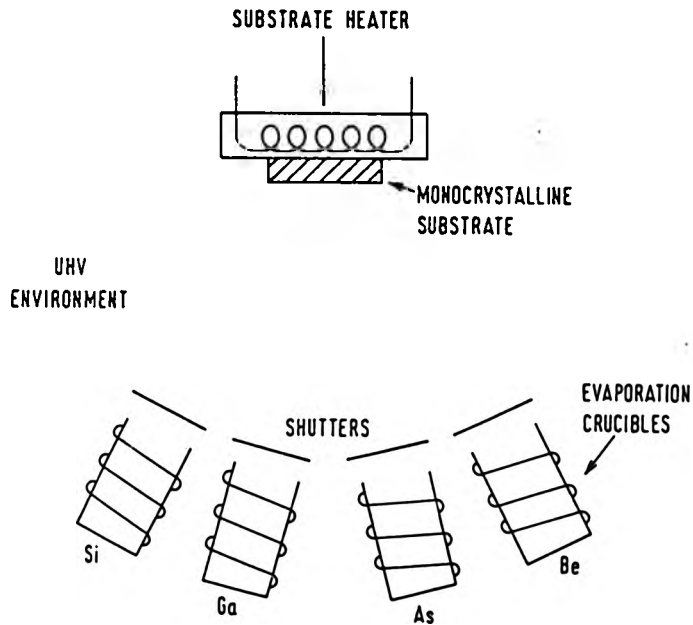


Fig 1.1 The essential components of a III-V MBE system

1.3 GaAs Surface Kinetics

Both dissociation (sublimation) and condensation (growth) processes can be important in MBE. Briefly, free (Langmuir) sublimation occurs from the surface of an epilayer which is heated under vacuum. At moderate temperatures group III and group V atoms are lost at the same rate, the smoothness of the surface is preserved and the sublimation is said to be congruent [Foxon et al (1973), Goldstein et al (1976)]. Above a critical 'non-congruent sublimation' temperature T_{nc} [approx. 640°C for (100) GaAs, 450°C for InAs and 365°C for InP, Wood et al (1983a)] the sublimation rate of the group V element exceeds that of the group III element and surface accumulations of group III metal occur, disrupting epitaxy. MBE is usually performed at temperatures well below T_{nc} (however, see also Sec 1.7).

The processes controlling MBE growth at moderate temperatures are adequately described by the models proposed by Foxon (1983) and Joyce (1985) to account for the results of their modulated beam studies [Foxon and Joyce (1975), (1977), (1978), (1980)] and the flash desorption experiments of Arthur (1973). Growth under both As_2 and As_4 fluxes was studied. Referring to (100) GaAs, the results which require interpretation are; (i) that the sticking probability of the Ga atoms is unity; (ii) only sufficient As_2 or As_4 molecules are incorporated to preserve stoichiometry and (iii) that the apparent sticking co-efficient of the arsenic flux is always ≤ 1 using As_2 and always ≤ 0.5 if As_4 is used. These observations are not confined to the growth of GaAs: most combinations of In, Ga and Al with As and Sb have been shown to behave similarly [Foxon (1983)]. At high growth temperatures, congruent sublimation reduces the growth rate of binary compounds [Fischer et al (1983)] and affects the composition of those III-III-V ternary compounds, such as InGaAs, from which one group III element sublimes more rapidly than the other [Foxon (1983)]. However, although these phenomena may present

practical difficulties, they do not alter the basic mechanisms of MBE growth.

1.4 GaAs Growth Models

The growth of (100) GaAs from Ga and As_2 fluxes is shown schematically in Fig 1.2a. According to the model, As_2 dimers are first adsorbed into a weakly bound ($\approx 0.15eV$) precursor state in which they are freely mobile. The dimers can only incorporate into the epilayer when they encounter occupied gallium lattice sites, which are often preferentially available at sites of high binding energy at vicinal and island step edges [Harris (1985)]. 'Layer by layer' growth results under certain conditions [Petroff et al (1984)], generally resulting in an overall smoothing of the crystal surface [Cho (1970)]. In the absence of free gallium the As_2 dimers have a measurable surface lifetime but, ultimately, a zero sticking probability. The excess dimers generally desorb unchanged, but may undergo a pairwise interaction and desorb as As_4 at low growth temperatures [Foxon and Joyce (1977)]. The As_2 sticking probability increases with the surface population of gallium, reaching unity when equal quantities of gallium and arsenic atoms are available. At this point the surface reconstruction (Sec 1.5) changes from (2×4) to (4×2) , marking the onset of gallium accumulation [Foxon and Joyce (1978)]. Ga atoms may be supplied to the surface from external fluxes or (at high growth temperatures) from the thermal decomposition of the epilayer [Neave and Joyce (1978b)]. Desorption or sublimation from the gallium adlayer is not significant at substrate temperatures below about $630^\circ C$ [Fischer et al (1983)].

The growth of (100) GaAs from Ga and As_4 fluxes is more complex, although many of the same concepts apply [Foxon (1983)]. As with As_2 , the As_4 tetramers are accommodated in a mobile precursor state for a limited period of time, and

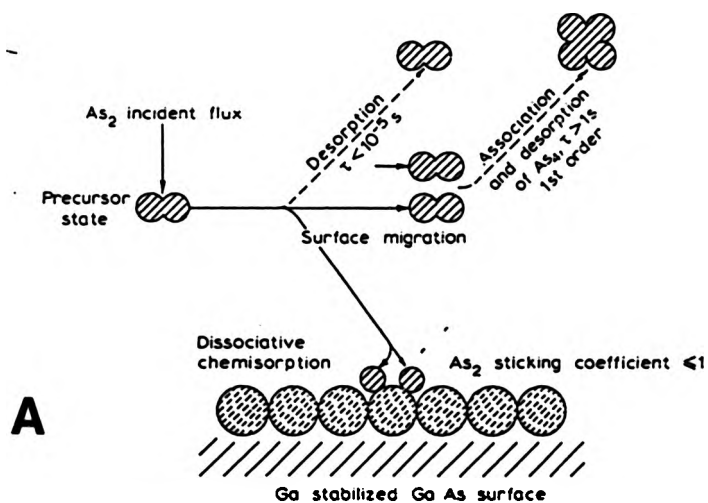
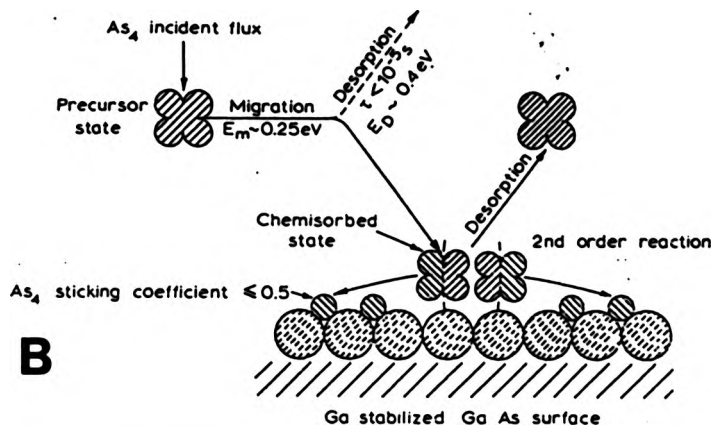


Fig 1.2 The processes involved in the growth of (100) GaAs from (A) Ga and As₂ and (B) Ga and As₄ fluxes [after Foxon (1983)].

it is the Ga adatom population which decides their ultimate sticking probability. The chief difference when using As_4 is that the sticking probability of the tetramers cannot exceed 0.5 even if a large excess of gallium atoms is present. This reflects the fact that growth from As_4 requires a pairwise dissociation of two tetramers, releasing four arsenic atoms for growth [Foxon and Joyce (1975); the process is shown schematically in Fig 1.2b]. The remaining four atoms are desorbed as a newly created As_4 tetramer.

The different processes involved in growth from As_2 and As_4 fluxes may affect the properties of films grown under otherwise identical conditions. Experimental results generally show that lower trap concentrations [Neave et al (1984)] and superior minority carrier properties [Duggan et al (1982), Tsang (1982, 1985)] are obtained in GaAs/AlGaAs structures grown from As_2 . However, factors such as dopant incorporation (Sec 1.6) and the effects of surface reconstruction on the physical mechanism of condensation (Sec 1.5) generally affect the electrical, optical and morphological properties of MBE grown GaAs more strongly than the choice of arsenic species.

1.5 Surface Reconstruction

Surface reconstruction is a re-ordering of the outermost atomic layer(s) of a crystal in order to reduce the free energy of the surface. The (100) surface of GaAs can support several reconstructions during MBE growth. Each represents a particular surface stoichiometry which is maintained over a limited range of flux ratios and growth temperatures [Cho (1970, 1971a, 1971b), Panish (1980)]. This makes surface reconstruction extremely useful as a system-independent monitor of the MBE growth conditions.

Reconstruction is easily monitored during growth using

reflection high energy electron diffraction (RHEED), in which 3 to 15keV electrons are reflected at a grazing incidence from the epilayer onto a florescent screen [Bauer (1969), Prutton (1975)]. The surface of the epilayer acts as a two dimensional grating which usually yields a streaked pattern because of the relaxation of the Laue scattering conditions in one dimension. A pattern of spots is generally indicative of a rough or contaminated surface [Cho and Arthur (1975), Ploog (1980)]. The periodicity of the RHEED pattern is the same as that of the reciprocal lattice of the surface mesh [Prutton (1975), Ashcroft and Mermin (1976)]. The surface mesh is usually described using the nomenclature of Wood (1964), in which 'the (2x4) reconstruction of a (100) surface' refers to a structure having twice the bulk lattice spacing in the [011] direction and four times bulk spacing in [011].

Early work by Cho (1970,1971a,1971b) showed that two stable reconstructions predominate on (100) GaAs during MBE growth. These are normally identified as the (2x4) and (4x2) reconstructions, although Neave and Joyce (1978a) have pointed out that the (2x4) and c(2x8) reconstructions cannot be distinguished by most MBE RHEED systems, which only display the zeroth order Laue zone. Epitaxial GaAs with good electrical properties may be grown under the (2x4) reconstruction. However, Neave et al (1984) have reported that growth under a (3x1) reconstruction [which occurs at higher temperatures than the (2x4), Massies et al (1976), Panish (1980), Van Hove and Cohen (1982)] yields material of improved photoluminescent efficiency. Growth under the (4x2) reconstruction yields material spoiled by surface accumulations of Ga metal. Neave and Joyce (1978a),(1978b) have used RHEED to investigate the range of substrate temperatures permitting epitaxial growth. Their results suggest that the minimum temperature ($\approx 130^{\circ}\text{C}$) is determined by the non-dissociative incorporation of As_4 tetramers and the maximum temperature ($\approx 600^{\circ}\text{C}$) by the thermal dissociation of the epilayer. In practice, GaAs

grown below about 480°C is so heavily trapped as to be semi-insulating [Murotani et al (1978)]; the exact temperature below which trapping becomes significant is determined by the arsenic flux [Newstead et al (1987), Chapter 3].

Several 'MBE surface phase diagrams' have been mapped out to show how the reconstructions of (100) GaAs change with the substrate temperature and matrix fluxes [e.g. see Cho (1971a,b), Massies et al (1976), and Van Hove et al (1985)]. Because of the practical difficulties involved in measuring MBE growth parameters, there is considerable spread in the reported positions of the boundaries separating the various reconstructions [Van Hove et al (1983), Wood et al (1983b)]. One objective of this project was to construct accurate surface phase diagrams for (100) GaAs and (100) InAs, self-calibrated against the change in surface reconstruction at $J_{As}:J_{Ga(In)}=0.5:1$ [Foxon et al (1978)]. These diagrams were useful for practical purposes, such as setting up the (rather restricted) optimum nucleation conditions of (100) InAs/GaAs [Newstead et al (1987), Chapter 4] as well as providing some information on the surface processes occurring during MBE growth.

A number of workers have used AES, XPS [Drathen et al (1978), Massies et al (1980), Bachrach et al (1981)] and static SIMS [Croydon et al (1985)] to estimate the surface compositions of reconstructed GaAs. Whilst all agree on the compositional ordering of the major reconstructions, there is disagreement over the absolute estimates of stoichiometry [Monch (1985)]. ARPES [angle resolved photoemission, Larsen et al (1981), Dobson et al (1982)] and integrated photoemission [Bachrach et al (1981)] have been helpful in determining some of the physical and electronic properties of GaAs surfaces but, as yet, no fully detailed understanding of the factors determining the dominant reconstruction modes of the III-V compounds has emerged. The interpretation of results can be complicated by the presence of

vicinal steps and disordered reconstructions [numerous adjacent domains of one or more reconstructions, Dobson et al (1982)]. However, these features can be exploited in surface studies. For example, the diffusion of gallium adatoms on GaAs has been investigated by examining the temperature dependence of the disappearance of RHEED intensity oscillations on slightly misorientated substrates [Neave et al (1985)]. RHEED oscillations, corresponding to monolayer depositions, are in themselves useful for accurately measuring group III fluxes [Harris et al (1981), Neave et al (1983)].

1.6 Doping

The choice of useful dopants for III-V MBE is small compared to the wide range of group II, IV and VI impurities which have been used successfully in LPE. The difficulty in MBE is that dopants must incorporate via the growing surface, so that volatile impurities (such as sulphur) tend to re-evaporate before incorporating at normal growth temperatures [Davies et al (1981)]. It is also found that large atoms (such as Sn in GaAs) tend to accumulate on the surface, hampering efforts to obtain sharp doping profiles [Cho (1975), Wood and Joyce (1978), Rockett et al (1982)]. Surface segregation can also cause non-uniform composition profiles in ternary compounds such as InGaAs [Foxon (1983)]. Size effects in MBE are increasingly the subject of debate [Patel et al (1987)]. The interplay between thermodynamics and kinetic processes in determining dopant incorporation is not understood in detail [Wood (1985)], although thermodynamics can be useful in identifying MBE dopants which are unlikely to be effective [such as Zn in GaAs, Heckingbottom et al (1983)]. Silicon and tin are the most useful donors and beryllium the best behaved acceptor in MBE GaAs. However, there are difficulties associated even with these elements, and the doping of III-V compounds still presents problems in the

more demanding applications of MBE.

1.6 (i) n-type dopants

On a simple valence basis, the group IV elements should be amphoteric in III-V compounds. This is true of Ge in GaAs which dopes either n- or p-type according to the ratio of Ga to As vacancies on the growing surface [Wood et al (1979), Metzger et al (1980)]. Si and Sn are, however, only slightly amphoteric [Chai et al (1981), Mendez et al (1983)] and incorporate as shallow donors in (100) GaAs. Si has a unity sticking probability and does not noticeably segregate [Cho (1975), Hiyamizu et al (1981)]. Si doping at moderate levels (10^{15} - 10^{18} cm⁻³) produces material with near-bulk electrical properties, but compensation is apparent in highly doped layers [Ilegems (1985)]; this may result from the inclusion of nitrogen, generated by the decomposition of the PBN Si crucible at high temperatures [Sacks and Shen (1985)]. The chief disadvantage of silicon is that it is difficult to dope to free carrier concentrations in excess of 6×10^{18} cm⁻³ in MBE-GaAs [Miller et al (1982), Sachs and Shen (1985)]. Higher carrier concentrations are attainable using Sn [1.1×10^{19} cm⁻³, Harris et al (1982)]. This to some extent offsets the the problems of surface segregation [Rockett et al (1982)] and rate limited incorporation [Wood and Joyce (1978), Harris et al (1984)] experienced when using Sn in GaAs, and Sn doping is most commonly used in devices requiring very low resistivity n⁺ layers [Harris (1985)].

S, Se and Te have been of limited use in MBE because of their volatility (which can cause problems during bakeouts) and their low sticking probabilities on GaAs surfaces at normal growth temperatures (580-600°C, Chapt 3). However, the chalcogens are useful n-type dopants for the III-V antimonides [Si and Sn are essentially amphoteric in Ga(Al)Sb, Gotoh et al (1981)]. Source volatility problems

have been overcome by the use of electrochemical cells to generate sulphur and selenium fluxes from stable compounds of silver [Davies et al (1981), Andrews et al (1984)]. It is also possible to dope with S, Se and Te derived from thermally generated fluxes of PbS, PbSe and PbTe [Wood (1978, 1985)]. Again, the greater stability of the compound over the element facilitates control of the effusion source. It is unclear whether the Pb component of the flux incorporates or is electrically active in GaAs. However, it has been reported that the concentration of electron traps in GaInP [Blood et al (1982)] and GaAs [Akatsu et al (1987)] may be reduced by the application of a small Pb flux during MBE growth.

The discussion above refers to growth on (100) surfaces. Dopants can incorporate differently on other surfaces; for example, Si doped (110) GaAs grown by MBE is always highly compensated or p-type [Ballingall and Wood (1982,1983)]. The same result is obtained when (111) substrates are used. These phenomena have been explored by Miller (1985), who selectively etched a (100) substrate to produce 2 μm wide (110) and (100) facets. A vertically orientated 'n-p-n-p' modulation doped structure resulted from subsequent overgrowth with Si doped GaAs.

1.6 (ii) p-type dopants

Beryllium is a well behaved shallow acceptor in (100) MBE GaAs permitting controllable doping with 100% electrically active incorporation at levels between $1 \times 10^{15} \text{ cm}^{-3}$ and $6 \times 10^{19} \text{ cm}^{-3}$ [Ilegems (1977)]. There are three problems associated with the use of this dopant; (i) Be is highly toxic; (ii) Be getters oxygen bearing residual gas species to form electrically inactive centres such as BeO in GaAs [Wood (1985)]; and (iii) Be exhibits anomalously high interstitial diffusion rates in GaAs at doping levels above about $1 \times 10^{19} \text{ cm}^{-3}$ [McLevige et al (1978)]. The latter

effect may preclude the use of Be as a dopant for very thin p^+ layers such as HBT base regions. These problems are not critically important to most users, especially compared to those encountered when using other p-type dopants in MBE.

The other usable p-type dopants in (100) MBE GaAs are Ge, Mg and Mn. Ge is only useful for heavy doping because of the compensation effects previously mentioned. Mn is a deep acceptor (appearing about 100 meV above E_v), which is almost completely frozen out at 77K. Mg is a well behaved shallow acceptor in GaAs, but is of limited use in MBE as a unity sticking probability can only be obtained at growth temperatures of 500°C or less [Wood et al (1982)]. Low energy (<500eV) ion beam doping has been investigated as a means of increasing the sticking probabilities of volatile doping species [Naganuma and Takahashi (1975), Esaki and McGroddy (1975), Bean and Dingle (1979)]. Most attention has been paid to the p-type dopants Zn and Mg. In general, the Hall mobilities obtained from such layers are lower than those obtained from co-evaporation doped MBE material, leading to speculation about the extent of the damage caused by subsurface implantation [Wood (1985)].

1.7 Defects in MBE Layers

The imperfections found in MBE grown material fall into three main categories; (i) point defects, (ii) impurities incorporated from the residual gas, impure cell charges or the outgassing products of heated components and (iii) gross morphological defects. Point defects essentially result from localised deviations in stoichiometry and may be manifest as deep level traps [Neave et al (1980), Stall et al (1980)] or through reductions in photoluminescent intensity [Tsang (1985)]. Thermodynamics may eventually be of assistance in identifying optimal growth conditions [Heckingbottom et al (1983)] but, at present, the most practical way of avoiding excessive intrinsic defect

concentrations is by reference to the results of actual growth studies. Grange (1985) has recently reviewed the relevant literature, concluding that most compounds should be grown under minimised group V fluxes as close as possible to their non-congruent sublimation temperature.

The level of unintentional doping in epilayers is highly dependent on the design and operation of a given MBE system; these factors are discussed in Chapter 2. For the present it is sufficient to note that unintentional acceptor levels of less than $1 \times 10^{14} \text{ cm}^{-3}$ can be obtained in carefully grown MBE GaAs [Dingle et al (1982), Hwang et al (1983), Heiblum et al (1983)]. Reducing the level of gross morphological defects is a more pressing problem. Inexpert ex-situ substrate cleaning, or the use of stale or insufficiently pure chemicals, can leave dust and drying marks on the substrate leading to poor nucleation over localised areas. These problems can be avoided with care [Sec 2.8(ii)], but the ubiquitous presence of oval defects on MBE grown GaAs is of greater concern. These defects are normally present at densities of between 10^2 and 10^5 cm^{-2} , vary in length from 1 to 10 μm and are aligned with the $[0\bar{1}1]$ direction if the epilayer is grown on (100) substrates [Ilegems (1985)]. Oval defects have been shown to result from several causes including; (i) 'spitting' from the gallium cell [Wood et al (1981)]; (ii) Ga_2O_3 and Ga_2O in the Ga charge [Ito et al (1984)], which may be avoided by cleaning and re-charging the gallium cell each time the MBE system is let up to air [Chai and Chow (1981)], or by pre-etching the gallium charge in HCL [Weng et al (1986)], or chemically reduced by the addition of a small amount of aluminium to the Ga cell charge [Kirchener et al (1981)]; (iii) arsenic oxides in the arsenic cell charge [Suzuki et al (1984)]; and (iv) microscopic dust particles on the substrate [Weng et al (1985)]. At the time of writing, oval defect densities of about $1 \times 10^2 \text{ cm}^{-2}$ are regularly attained by careful workers [Weng et al (1986)]. This is considered acceptable, although not ideal, by device processors

[Rezazadeh (1987)]. There is evidence that oval defects may be completely eliminated by employing Metal Organic MBE [Tsang (1984) (1987), Sec 2.3]. Splashes of Ga and Al metal generated by the action of the source cell shutters are a further source of defects.

1.8 The Objectives of this Project

This thesis reports on investigations into the growth of (100) InAs and (100) GaAs by MBE. A central objective of the project was to identify the optimum growth conditions for InAs. Previous studies at CLP [Meggitt et al (1978, 1979, 1980), Grange et al (1979, 1980), Kubiak et al (1983, 1984a)] had only been partially successful in meeting this aim, largely because the MBE systems then available offered limited control over the growth parameters. For this reason a new MBE system, CLP_{IV}, was constructed for the present work (Chapter 2).

1.9 GaAs Growth Study

Before starting on the InAs work, GaAs epilayers were grown to commission CLP_{IV} because; (i) the growth of GaAs by MBE was known to be straightforward, with information on substrate preparation, growth and doping being readily available in the existing literature and (ii) techniques for the optical and electrical characterisation of epitaxial GaAs were similarly well established. The first growths were directed towards identifying and eliminating hardware and operating problems. Subsequently, a series of Si and Sn doped layers were grown to provide data for a critical assessment of the new system. A central theme of this thesis is the use of surface reconstruction as a basis for accurately reproducible flux calibrations: the relevant experimental techniques were developed when growing GaAs. This involved the construction of an MBE surface phase

diagram, which also yielded some information on the surface processes occurring during growth and the range of applicability of the MBE growth model [Foxon (1983)]. The GaAs work is presented in Chapter 3.

1.10 InAs Growth Study: Introduction

InAs was studied because this compound, and its related ternaries, offer useful alternatives to GaAs/AlGaAs for certain applications, including

- (i) **Optoelectronic Devices**, where the tunable direct bandgaps of InGaAs [Cheng et al (1981)], InAlAs [Praseuth et al (1987)], InAsSb [Yen et al (1987)] and InGaAsSb [Chui et al (1987)] cover wavelengths inaccessible using GaAs/AlGaAs, including the minimum loss and dispersion windows of both silica [1.55 μm , Sze (1981)] and fluoride [2.55 μm , Tran et al (1986)] optical fibers. Experimental device structures have included laser emitters [Tsang (1985)] and InAsSb strained-layer superlattice detectors [Hughes (1987)]. Binary InAs has been used for the active layers of a MQW laser operating at 1.5 μm [Benchimol (1987)]

- (ii) **High Speed Logic and Microwave devices**, where the high electron mobilities and high saturation drift velocities of InAs and InGaAs [Littlejohn et al (1978), Kubiak et al (1984b)] offer improved high frequency performance [Barnard et al (1980), Bandy et al (1981)]. InGaAs/AlGaAs heterostructures have received particular attention as 'pseudomorphic HEMTs' [Liu and Das (1987), Hiyamizu et al (1987)]; this combination offers a wide enough bandgap for room temperature operation and low Al levels can be used in the AlGaAs, avoiding excessive levels of DX centres [Dhar et al (1986)].

(iii) **Structures of Scientific Interest**, which exploit the unusual bandedge lineup of InAs with GaSb (the conduction band of InAs lies below the valence band edge of GaSb). These structures are exemplified by the InAs-GaSb-AlSb polytype [Sai-Halasz et al (1977), Chang and Esaki (1980)] and the InAs-GaAs strained layer superlattices [Yao et al (1983), Fukui and Saito, Jap. J. Appl. Phys. 23 (1984) L521]

Epitaxially deposited InAs has also been used to obtain low-resistivity ohmic contacts to GaAs/AlGaAs device structures [Wright et al (1986a)].

Many of the structures and compounds described above have been grown by MBE. However, most publications have only included superficial descriptions of the growth conditions used. The implication is that the majority of structures were grown on the basis of trial and error. Whilst this approach may have been tolerable for preliminary studies, it was clear at the inception of this project (see review below) that more detailed work was required, both to improve device quality and to meet increasingly successful competition from rival growth techniques.

1.10 (i) Review of Earlier Studies

Early research into the vacuum deposition of InAs was restricted to polycrystalline growth on glass and (100) GaAs substrates [Gunther (1961), Johnson (1966), Kunig (1968), Howson (1968), (1970), Freller (1979)]. Godinho and Brunschweiler (1970) were the first to obtain epitaxial deposits on heated GaAs substrates of various orientations. Their results for growth on (100) surfaces are still pertinent; (i) mirror-shiny epitaxial layers were only obtained within a narrow range of substrate temperatures and As₄:In flux ratios, (ii) large, highly directional growth features were sometimes noticed on layers grown

under non-optimum conditions, and (iii) the electrical properties of the layers showed a strong dependence on the film thickness, an effect previously only seen in VPE material [Cronin et al (1966), McCarthy (1967)]. These results have been enlarged upon by Yano et al (1977), Meggitt et al (1978, 1979, 1980), Grange et al (1979, 1980), Parker et al (1981), Schaffer et al (1980, 1981, 1983), Kubiak et al (1983, 1984a), Hancock and Kroemer (1984), Sugiyama (1986) and Munekata et al (1987). As semi-insulating InAs is not available, these workers used SI (100) GaAs substrates to facilitate electrical measurements. Table 1.1 summarises their results: all found that mirror-shiny heteroepitaxial layers with low defect levels and high electron mobilities could only be grown within a limited range of parameters. Epilayers grown under non-optimum conditions had rough surfaces and severely degraded electrical properties. Such material has been designated as arsenic or indium rich, according to whether the arsenic flux was above or below its optimum value. Characteristic defects occur on epilayers grown under each regime [Yano et al (1977), Schaffer et al (1983), Kubiak et al (1984a)]. Experiments by Hancock and Kroemer (1984) and Sugiyama (1986) have indicated that the conditions required for homoepitaxial growth are not as demanding as those applying to (highly mismatched) heteroepitaxy.

To date, all unintentionally doped InAs grown by MBE has been n-type. As shown in Table 1.1, residual carrier concentrations of $2 \times 10^{16} \text{ cm}^{-3}$ and less have only been reported for epilayers grown at temperatures above about 500°C [the non-congruent sublimation temperature of InAs is approximately 490°C at low arsenic overpressures, Meggitt (1979), Wood et al (1983a)]. Table 1.1 shows that the residual carrier concentration tends to increase with decreasing growth temperature, reaching $1 \times 10^{18} \text{ cm}^{-3}$ at 400°C . This may imply that the carriers derive from stoichiometric defects [Heckingbottom et al (1983)], or from volatile impurities in the source charges or growth

Table 1.1 - Conditions leading to optimum morphology and carrier properties in unintentionally doped InAs grown on (100) GaAs by MBE

	Growth temperature (°C)	As ₄ :In Flux Ratio	Best 77K mobility (cm ² /V-s)	Minimum residual doping level (cm ⁻³)
Heggett et al (1978, 1980)	330	=1:1	5x10 ³	1x10 ¹⁶
Grange et al (1979)	370	0.5:1 to 4:1	8x10 ³ *	7x10 ¹⁶
Schaffer (1980)	400	2.9:1	not available	
	450	11:1	not available	
Yano et al (1977)	480	15:1 to 18:1	20x10 ³	2x10 ¹⁶
Schaffer et al (1983)	=520	3:1	10x10 ⁴	5x10 ¹⁵
Heggett et al (1978, 1980)	530	20:1	15x10 ³	6x10 ¹⁶
Rubiak et al (1984a)	530	16:1 to 18:1	20x10 ³	1x10 ¹⁶
This study	450-600	minimised	60x10 ³	5x10 ¹⁵

NB The data is arranged in order of increasing growth temperature, not chronologically; allowance should be made for general improvements in source hygiene etc. in the later systems. Caution should be exercised in comparing T_g growth and the As₄:Ga flux ratio between laboratories. * indicates a 300 K mobility. All electrical properties directly measured.

environment [sulphur is a persistent contaminant in indium, Lambert et al (1983)], or both. All of the workers referenced in Table 1.1 reported that, at a given growth temperature, the lowest residual carrier concentrations and highest electron mobilities were obtained from the smoothest and least defected epilayers.

The growth of InAs at temperatures above 500°C can be difficult, as even small changes in the large arsenic flux required to stabilise the epilayer surface can be sufficient to disrupt epitaxy [Yano et al (1977), Meggitt et al (1978, 1980), Kubiak et al (1984a)]. Nonetheless, the best 77K Hall mobilities reported for unintentionally doped material range from 60×10^3 to 105×10^3 cm²/V-s at $N_D - N_A \geq 5 \times 10^{15}$ cm⁻³ [Schaffer et al (1983), Newstead et al (1987)], approaching bulk mobilities in InAs doped to give similar carrier concentrations [Schillmann (1956)]. Only limited information is available on the intentional doping of InAs during MBE [Ilegems (1985)]. Those impurities which have been investigated behave similarly in InAs and GaAs; in both materials Mg and Be are acceptors [Yano (1977), Schaffer and Berg (1981)] and Si and Te are shallow donors [Kubiak et al (1984a)].

Meggitt (1979), Grange et al (1979), Kubiak (1983), Sugiyama (1986) and Wright et al (1986a) reported that their best heteroepitaxial InAs was grown under arsenic stabilised conditions (a (2x4) reconstruction was generally indicated). In one case [Grange (1979)] the minimum As₄ flux permitting stoichiometric growth was used. These conditions are analogous to those usually used for the growth of GaAs (e.g. see Chapters 1 and 3). Conversely, Schaffer (1980), Kowalczyk et al (1982), Schaffer et al (1983), Hancock and Kroemer (1984) and Munekata et al (1987) have reported that is essential to nucleate the (100) InAs/GaAs heterojunction under an In stable (4x2) reconstruction, which may subsequently be maintained throughout growth. These workers also indicate that InAs

epilayers grown under the (2x4) reconstruction have rough surfaces and poor electrical properties. Ignoring the possibility of misidentification, these conflicting reports may indicate potentially useful differences between InAs and GaAs. For example, the greater diffusivity of group III adatoms on the (4x2) surface [Neave et al (1985)] could lead to reductions in the concentration of point defects in InAs grown under this reconstruction (e.g. through an increased ability for adatoms to reach appropriate sites before incorporation).

1.10 (ii) Objectives of this Study

To summarise: at the inception of this project it was known that only a narrow range of arsenic fluxes would permit good quality (100) InAs/GaAs heterojunctions to be grown at a given temperature. It was also known that the electrical properties of the InAs layers tended to improve with increasing growth temperature, and that higher arsenic fluxes were generally required under these conditions. However, no qualitative relationship had been derived between the optimum growth parameters; there was uncertainty as to which surface reconstruction yielded the best quality InAs; there was little experience of controlled doping; and only limited information on homoepitaxial growth was available. In short, there were no simple operating precepts which would allow good quality InAs to be grown for experimental or device purposes. Therefore experiments were undertaken (i) to determine the functional relationship between the MBE growth parameters, epilayer quality and surface reconstruction, and (ii) to find out whether the arsenic and indium rich growth conditions were intrinsic to InAs or simply resulted from difficulties in nucleating the severely mis-matched (100) InAs/GaAs heterojunction. These investigations are reported in Chapter 4. Considerable importance was placed on the use of surface reconstruction as a means of rapidly finding the optimum

nucleation/growth conditions for InAs in a previously uncalibrated MBE system. The construction of an MBE surface phase diagram for (100) InAs provided a natural framework for this work.

1.11 InAs Doping Study

Further experiments, described in Chapter 5, were undertaken to investigate the electrical properties of Si, Sn and unintentionally doped InAs grown by MBE. This necessarily involved a doping study. The electrical data available at the start of this project was largely limited to the Hall properties of n-type epilayers¹ deliberately or unintentionally doped within the range $1 \times 10^{16} \text{ cm}^{-3}$ to $5 \times 10^{17} \text{ cm}^{-3}$ [Ilegems (1985)]. It was considered useful to supplement this,

- (i) By investigating the properties of heavily doped epilayers, as used for ohmic contacts and low resistivity buffer layers in microwave devices [Harris (1985)]. Although MBE grown n^+ InAs [Wright et al (1986a)] and compositionally graded n^+ $\text{In}_x\text{Ga}_{1-x}\text{As}$ [Woodall et al (1981)] epilayers had been used to obtain low resistivity ohmic contacts to a variety of GaAs/AlGaAs heterojunction devices, such basic parameters as the maximum doping levels and minimum resistivities attainable in MBE InAs had not been established.
- (ii) By investigating the properties of n^- InAs grown by MBE, i.e. to allow a critical comparison to be made

¹ The electronic properties of MBE grown InAs quantum wells have been studied in greater detail [Chang et al (1984), Mendez et al (1984)].

between the present capabilities of LPE, VPE and MBE. Previous attempts to do this had been hampered by the high n-type doping levels obtained in unintentionally doped MBE grown InAs [frequently in excess of $1 \times 10^{16} \text{ cm}^{-3}$, Table 1.1, compared to $2 \times 10^{15} \text{ cm}^{-3}$ in VPE grown material, Cronin et al (1966), McCarthy (1967)].

It was also considered useful to examine moderately doped (e.g. $5 \times 10^{16} < N_D - N_A < 1 \times 10^{18}$) n-type MBE-InAs grown under conditions leading to low unintentional doping levels. The experiments concentrated on Si doping, as this impurity has shown promise as a well behaved donor at all compositions of InGaAs grown by MBE [Kubiak et al (1984a,b), Wood (1985)].

CHAPTER 2

The Technology of Molecular Beam Epitaxy, and the factors affecting the design and operation of a new MBE facility at the City of London Polytechnic

Contents

- 2.1 General Considerations
- 2.2 The UHV Environment
 - (i) The choice of materials for UHV
 - (ii) UHV pumps and cryopanelling
 - (iii) Load-locked and multiple chamber systems
- 2.3 Flux Generation
- 2.4 Substrate Heater and Wafer Transfer Mechanism
- 2.5 Temperature control System
- 2.6 Flux Monitoring
- 2.7 Analytical Equipment
- 2.8 Operating Procedures
 - (i) Preparation of cell charges
 - (ii) Pumpdown and bakeout
 - (iii) Substrate preparation
 - (iv) Routine growth procedures

2.1 General Considerations

The basic components of a modern molecular beam epitaxy system are,

- (i) The UHV chamber(s) and associated vacuum hardware
- (ii) a load-locked substrate exchange system
- (iii) a substrate heater
- (iv) individually shuttered molecular beam sources
- (v) a control system to regulate cell temperatures, operate shutters, etc
- (vi) analytical and monitoring equipment including, as a minimum, RHEED and a beam flux monitor

A wide degree of flexibility is available within this basic framework and design of CLPIV, the MBE system commissioned for this project, was strongly influenced by the intention to grow InAs. As described in Chapter 1, a high degree of control over the MBE growth parameters is required in order to grow good quality InAs. Therefore, two problems were given particular attention when designing the new system: (i) the provision of a substrate heater which would allow an accurate and reproducible measurement of the growth temperature whilst remaining compatible with load-locked operation, and (ii) attaining good flux regulation and flux uniformity.

A two chamber system, built on a convenient scale for operation and maintenance by a single worker, was considered best able to meet the requirements of this project. Figures 2.1 and 2.2 show the overall layout of the equipment. In summary: CLPIV was based on a bakeable stainless steel vertical evaporation chamber (Sec 2.2) pumped by a 400 l/sec sputter ion pump supported by a titanium sublimation pump and extensive cryopanelling (Sec 2.2(ii)); the substrate exchange load lock (Sec 2.2(iii)) was independently pumped by a 15 l/sec ion pump and a sorption pump. The growth chamber was equipped with six

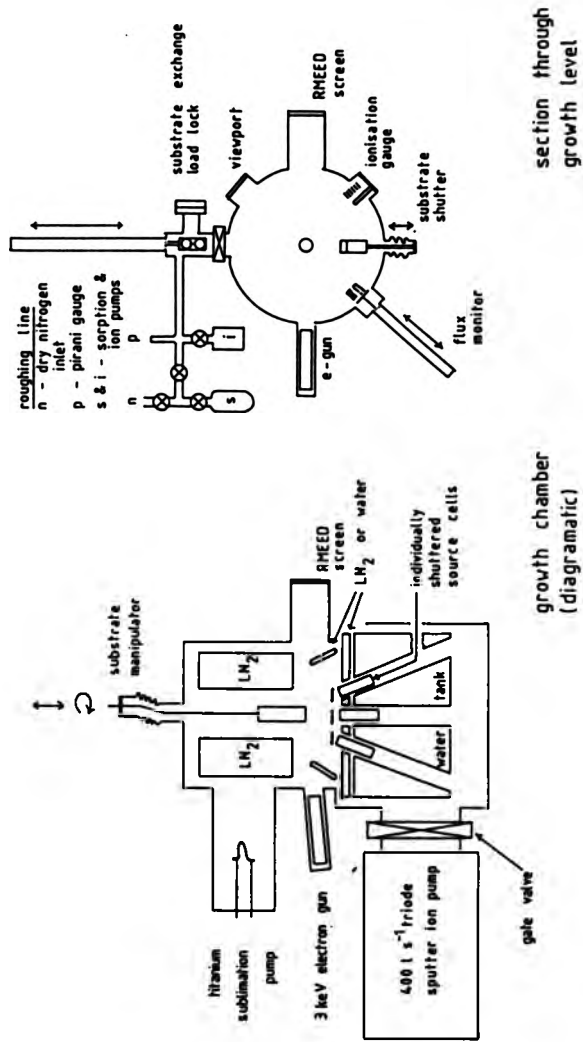


Fig 2.1 Schematic of the MBE system, CLPIV, used in this project.

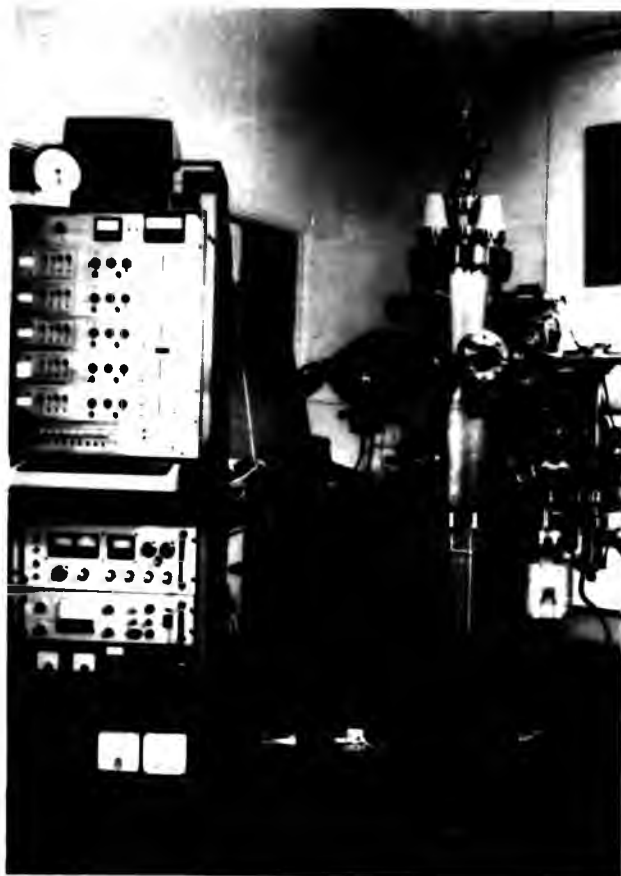


Fig 2.2 Photograph of the Apparatus. The load-lock is on the right hand side of the chamber, and the RHEED screen at the front. The temperature control and flux monitoring systems are mounted in the rack to the left of the photograph. The pump controllers, main ionisation gauge and quadrupole mass spectrometer were fitted in a second rack, not shown, to the right of the equipment.

individually shuttered source cells (Ga, In, Si, Sn and 2xAs, Sec 2.3), a substrate heater (Sec 2.4) and a computer based temperature control system (Sec 2.5); a fixed and a movable ionisation gauge for flux monitoring (Sec 2.6); 5keV RHEED for surface studies (Sec 2.7) and a quadrupole mass analyser (QMA) for residual gas analysis and leak testing. The factors affecting the choice or design of these components will now be discussed in detail.

2.2 The UHV Environment

The attainment of a clean UHV environment, in which the unintentional doping of epilayers by residual gases and vapours is reduced to below normal semiconductor doping levels (i.e. $<1 \times 10^{14} \text{ cm}^{-3}$), is the first requirement in MBE. Obtaining such an environment has three aspects; (i) the selection of a suitable vacuum chamber and pumping system, (ii) reducing outgassing from strongly heated components to acceptable levels, and (iii) adopting careful housekeeping techniques to maintain the clean environment when once it has been achieved.

2.2 (i) The Choice of Materials for UHV

Most modern UHV systems, and those MBE components which are not strongly heated, are manufactured from '304' or a closely allied grade of stainless steel. After several hours bakeout into vacuum, principally to remove adsorbed water vapour, the outgassing rate of these materials is sufficiently low to allow pressures of about 5×10^{-11} mbar to be achieved. The primary outgassing species after bakeout are H_2 and CO/N_2 . Stainless steel contains Mn which, if a component is heated much above 300°C , can sublime in sufficient quantity to cause compensation and trapping problems in MBE grown GaAs [Ilegems and Dingle (1975), Covington and Meeks (1979), Covington et al (1979),

Grange (1980, 1982)]. This problem is compounded by the relatively low thermal conductivity of stainless steel so that, in early MBE systems, poor material quality was often attributable to the use of stainless steel in close proximity to heated components. The efficient force cooling (or, better, designing out) of all stainless steel in such positions is clearly essential. All joins in stainless steel chambers should be internally argon arc welded to obtain oxide-free welds devoid of virtual leaks from pockets of trapped gas. Avoiding virtual leaks is in any case essential in UHV/MBE design: general UHV engineering techniques have been reviewed by Harris (1981) and Weston (1984a). Apart from stainless steel, materials used in general construction include OFHC copper (for conductors and as gaskets in demountable seals), borosilicate glass, fused quartz and sapphire (viewports and feedthroughs), high alumina ceramics (for feedthroughs and electrical insulation), and various thermocouple materials. Wheeler (1972) has reviewed the vacuum properties of these materials and the various techniques for welding, brazing or otherwise joining them.

Most of the materials discussed above are unsuitable for the fabrication of strongly heated components because of their chemical and/or thermal instability. Inert refractory materials must be used instead (i) to resist corrosion by the growth fluxes and (ii) to avoid contaminating the MBE system with volatile materials. The choice of suitable metals is restricted to tantalum, molybdenum and tungsten. Tantalum has several advantages over the other refractory metals for general use; it is readily available in several forms including rod, tube, plate and foil; it is readily cut, machined and shaped; it is easy to weld to itself and other materials; and it remains malleable after all but the most severe heat treatments (in vacuo). However, tantalum is relatively soft and slightly reactive with gallium at high temperatures. Molybdenum is fairly difficult to machine and almost impossible to weld but is physically

harder than tantalum, and has a greater resistance to attack by gallium. For these reasons, Mo is used for the manufacture of components such as substrate transfer plates. Tungsten is very inert but almost impossible to machine by any technique other than grinding. Consequently this metal has found limited application in MBE technology.

The choice of electrical insulators for use at high temperatures is similarly limited. The use of quartz (fused silica) and beryllium oxide heater insulators has been reported to lead to Si and Be doping as a result of reduction reactions with Ta filaments [Covington and Meeks (1979)]. High alumina (Al_2O_3) ceramics are more stable but reduction to Al and Al_2O by hot tantalum filaments has been demonstrated under extreme conditions [Farrow and Williams (1978)]. 99% Al_2O_3 /tantalum heater assemblies were used extensively in CLP-IV, although care was taken to operate these components within their limits, and no line-of-sight existed between the growth region and any heater. High alumina ceramics are mechanically strong and easy to shape by grinding. Pyrolytic boron nitride (PBN) exhibits superior thermal and chemical stability to alumina and is widely used as a crucible material in III-V beam sources (Sec 2.3). PBN is generally grown onto a graphite former by a CVD process and is available as sheets, rods, tubes and crucibles. Other shapes can be grown to order. PBN tends to delaminate under stress, and so is difficult to machine. There is evidence that nitrogen originating from the decomposition of PBN crucibles is sometimes present in MBE grown GaAs [Leroux et al (1986)]. Fortunately, significant incorporation has only been noticed when using Si doping sources at high temperatures [Sacks and Shen (1985)].

There is an obvious need for cleanliness when handling MBE components. New vacuum hardware may be cleaned by wiping with solvents, preferably having first been scrubbed with a phosphor-free surface decontaminant such as 'Decon 90' to remove oil, swarf and general engineering dirt. Small

components are best cleaned ultrasonically in a chlorinated hydrocarbon (such as 1,1,1-trichloroethylene) to remove oils and waxes. Rinsing with propan-2-ol and acetone facilitates drying. New molybdenum components may be etched back to bright metal using $3\text{H}_2\text{SO}_4:1\text{H}_2\text{O}_2:1\text{H}_2\text{O}$ or a weak solution of bromine in methanol. These etches are also suitable for removing GaAs deposits from used refractory components. Once clean, components should only be handled using nylon gloves. Any tools used on clean assemblies should be prepared with similar care. The cleaning of heated MBE components should be completed by outgassing into UHV at temperatures slightly higher than those used during normal operation. Typical procedures are discussed in Secs 2.3 and 2.8.

2.2 (ii) UHV Pumps and Cryopanelling

The extent and nature of unintentional doping from residual gas species must be examined before the choice of pumping systems for MBE can be discussed in detail. The prevalent residual impurities in MBE grown GaAs are carbon, which appears as an acceptor 25 meV above E_v [Cho and Arthur (1975), Ilegems and Dingle (1975), Wood (1985)] and oxygen, which is known to cause poor minority carrier properties and non-radiative recombination in GaAs/AlGaAs structures [Wicks et al (1981), Tsang (1985)]. Not unreasonably, gas species containing carbon and oxygen (e.g. CO, CO₂ and H₂O) are considered to be particularly deleterious to material quality. Thermodynamic arguments suggest that carbon and oxygen are less likely to be incorporated into GaAs from CO than from CO₂ or H₂O, and that Al bearing compounds have the greatest affinity for residual gas species [Prior et al (1984)]. However, experiments involving the deliberate introduction of high purity O₂, CO and CO₂ to the growth chamber have all yielded null or inconclusive results [Ilegems and Dingle (1975), Parker et al (1981), Wood (1985)]. This has led to speculation that carbon incorpor-

ation in MBE-GaAs results from residual hydrocarbon contamination on the substrate following cleaning [Tegayadi et al (1983), Sec 2.8 (iii)], or from exposure to thermally excited species generated by hot filaments in the growth region [Davies and Williams (1985)]. The consensus of opinion is that the partial pressures and the excitation states of CO_2 and H_2O (in particular) should be minimised by turning off all hot filaments not required during growth and by the extensive use of cryopanelling [Davies and Williams (1985), Wood (1985)]. It is interesting to note that, from thermodynamic arguments, the quantity of oxygen incorporated into AlGaAs from H_2O should decrease significantly as the H_2 pressure is increased [Prior et al (1984)]. This conclusion is supported by evidence that the introduction of hydrogen into the growth chamber can improve the optoelectronic properties of MBE GaAs [Calawa (1978), Bachrach and Bringans (1983), Pao et al (1986)].

When designing CLPIV (1982-3) the majority of III-V MBE systems used either a diffusion or a sputter ion pump, usually supported by a titanium sublimation pump. The use of diffusion pumps involves some risk of hydrocarbon contamination, e.g. due to oil vapour backstreaming into the growth chamber in the event of a backing pump failure. However, GaAs of excellent quality has been grown in carefully operated diffusion pumped systems [Davies and Andrews (1984)]. An ion pumped system, roughed out by a sorption pump, should not suffer any pump-derived hydrocarbon contamination and is generally considered to be inherently clean. For this reason, a triode sputter ion pump of large (400 l/sec) capacity was chosen for CLPIV. The selectivity of this pump, and the sublimation pump supporting it, precluded the rapid pumping of H_2 and the noble gases. This was not considered to be a problem because, as previously noted, an ambient of molecular hydrogen may actually be advantageous [Calawa (1978), Prior et al (1984)] and the noble gases, being inert, do not incorporate as active impurities. Helium cryopumps have also become

popular in III-V MBE. Cryopumps are less species selective in their pumping characteristics than ion pumps, have a better pumping speed to size ratio and have fallen in price in recent years [Weston (1984b)]. The choice of primary pump can be severely limited if phosphorous or mercury containing compounds are to be grown, in which case the removal of very heavy gas (P_2 or Hg) loads requires the use of non-saturating throughput (diffusion, turbomolecular etc.) pumps. These problems are not relevant to this thesis and have been adequately reviewed elsewhere [Davies and Williams (1985)].

In addition to the primary pumping described above, CLPIV was provided with extensive cryopanelling in order to reduce unintentional doping by condensable vapours (especially H_2O) and to deal with the large arsenic pumping load during growth. A continuous flow cryopanel around the growth region provided pumping close to the substrate (Fig 2.1) and served the secondary function of reducing the radiated heat load into the walls of the growth chamber. A co-axial LN_2 tank surrounded the upper part of the substrate heater and increased the effectiveness of the sublimation pump by baffling it from direct exposure to the group V flux. The source cells were thermally isolated from one another by a (continuous flow) water tank (Figs 2.1, 2.3). An internally baffled panel, mounted immediately above this tank, could be cooled by a continuous flow of either water or LN_2 . The panel was usually water cooled to allow the source cells to be kept at elevated temperatures overnight. This practice keeps the sources clean of condensable vapours and reduces the risk of cracking the crucibles through excessive thermal cycling [Heiblum et al (1983a)]. The use of LN_2 to cool the panel was not found to improve the majority carrier properties of n^- GaAs layers grown in CLPIV.



Fig 2.3 Source Cell Cluster (showing water tank and cryopanel, see also Fig 2.1)

2.2 (iii) Load-locked and Multiple Chamber Systems

A load lock is a small, independently pumped clean vacuum system connected to a UHV system via a wide-bore gate valve. The function of a load lock is to allow specimens (substrates in MBE) to be loaded without breaking the vacuum in the main UHV system, so avoiding time consuming bakeouts. Aside from increasing system throughput, the almost universal adoption of load locking in MBE has made an important contribution to material quality; repeated depositions over the internal surfaces of the growth chamber effectively bury and/or getter contaminants, leading to a steady reduction in unintentional impurity incorporation in successive growths. This effect has been repeatedly demonstrated by sequential improvements in majority carrier mobilities and photoluminescence intensities [Robinson and Ilegems (1978)], by the lowering of electron trap densities in GaAs [Weimann (1979)] and by improvements in the efficiency of MBE grown DH LASERS [Tsang (1982)]. The practice of load locking has recently been extended to include the loading of group V sources, normally the most rapidly depleted, via gate valves [Davies and Williams (1985)].

It is now common for large MBE systems to have three chambers; a load lock, a growth chamber and a preparation chamber separating them. The preparation chamber is routinely used to outgas substrates at temperatures of between 200°C and 400°C for a few hours before use. This practice is believed to make a useful contribution to material quality by preserving the cleanliness of the growth chamber [Hwang et al (1983), Heiblum et al (1983a)]. The preparation chamber is also often used for surface studies, removing delicate analytical equipment from the harsh environment of the growth chamber

2.3 Flux Generation

Molecular beam sources for III-V MBE fall into four categories; (i) resistively heated furnaces or 'source cells', (ii) gas cracking cells, (iii) electrochemical cells, and (iv) self heated charges, such as Si strip doping sources [Kilgore and Roberts (1963)]. Electron beam evaporators have been used for in-situ metallisation [Davies and Williams (1985)], but are uncommon in III-V MBE. As described in Chapter 1, electrochemical cells are used to generate controllable fluxes from stable compounds of volatile doping species. These cells are not used for the production of fluxes of matrix species. Gas cracking cells are used to generate beams of, for example, As₂ dimers by thermally decomposing arsene gas supplied (via an adjustable regulator) from outside of the MBE system. If a gas cracking cell is used it is, therefore, no longer necessary to periodically open the growth chamber in order to replenish the arsenic cell(s). This is an important advantage, as it is often the depletion of the group V cells which limits the length of an unbroken growth series when using conventional sources. Arsenic dimers can also be generated by cracking thermally sublimated As₄ tetramers on a hot (approx. 900°C) baffled surface [Krusor and Bachrach (1983)].

The widespread adoption of gas sources has been hampered by safety considerations. This position may be changed by the development of MOMBE (Metal Organic MBE, also known as 'chemical beam epitaxy' or CBE) techniques which have demonstrated considerable potential for the production of epilayers having very low defect levels [Tsang (1984, 1987)]. MOMBE techniques allow the advantages of MOCVD (e.g. semi-infinite source supplies for both group III and group V elements) to be combined with those of MBE (slow growth rates and rapid beam interruption for precise control of quantum well thicknesses, in-situ diagnostic instrumentation including RHEED and RGA, compatibility with

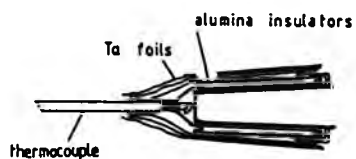
other UHV processes including metallisation and dry etching). Basic studies into the growth and doping of III-V compounds by MOMBE are currently being undertaken by several laboratories [Tsang (1987), Heinecke et al (1987), Kimura et al (1987), Werner et al (1987)].

By far the most common method of flux generation in III-V MBE is via evaporation from resistively heated source cells. Such cells are often referred to as 'Knudsen sources' but in practice, to fulfil the requirements of high mass transfer to the substrate at reasonable cell temperatures, the cell orifice must be made so large that the vapour and charge cannot remain in equilibrium. The distribution of fluxes under these conditions has been examined by Herman (1982). Any materials used in the construction of source cells must remain physically and chemically inert when exposed to corrosive elements at high temperatures: Si, Al and Ga cells are frequently operated at temperatures between 900°C and 1200°C. The most commonly used crucible materials are high purity graphite and PBN. Graphite is porous and difficult to outgas properly and it is probably for this reason that the highest mobility MBE-GaAs has been grown in systems equipped with PBN crucibles [Drummond et al (1982a), Hwang et al (1983), Heiblum et al (1983a)]. However, graphite may be competitive with PBN in other respects. For example, substituting a graphite gallium crucible for a PBN crucible in a Varian 360 system is believed to have caused a substantial reduction in the oval defect density on GaAs [Harris (1984)]. Experience in the authors present laboratory (GEC HRC) confirms this result, but suggests that lower residual p-type doping levels are obtained in GaAs if PBN crucibles are used.

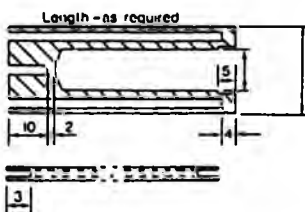
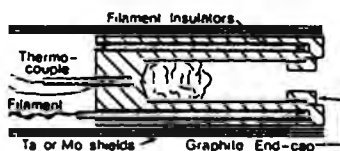
The design of the source cells used in MBE can strongly influence material purity and system reliability. It is essential that there is no line-of-sight between the heater filaments (generally tantalum wires or foils) and the substrate. It is also important to ensure that the heaters

and thermocouples are immune to contamination by gallium splash, e.g. from the shutter blades. CLPIV was equipped to deposit alloys of In, Ga and As doped with Si or Sn. The Si cell was built around a PBN crucible heated by a tantalum wire filament in a light tight enclosure (Fig 2.4). The In, Ga and Sn cells were made from high purity graphite to an in-house design [Kubiak et al (1982), Fig 2.4]. Graphite cells were chosen on the grounds of expense and ease of machining. The principal advantages of the design used are; (i) complete shrouding of the heater, (ii) efficient thermal contact between heater and charge, (iii) firmly located thermocouple (to prevent calibration shifts) and (iv) ease of manufacture. The Si, In, Ga and Sn cells were fitted with W-5%Re/W-26%Re thermocouples for stable high temperature performance. Two 50g capacity arsenic cells were fitted (Fig 2.4, the second cell was added to prolong the intervals between bakeouts). As noted in Chapter 1, the use of As₂ dimers instead of the tetramers generated by simple thermal sources may be beneficial in certain applications. However, the additional complication of constructing and operating arsenic crackers was not considered necessary to meet the objectives of this project.

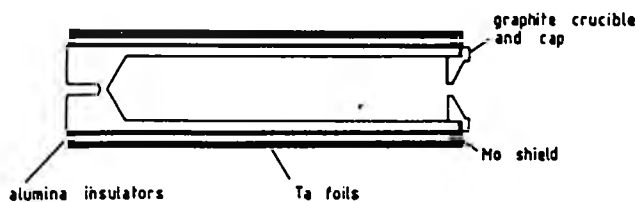
The outgassing of the newly constructed cells was found to be of crucial importance to obtaining GaAs of good electrical quality (see also Sec 3.2). Typically, after baking the MBE system overnight to obtain UHV, a cell would be heated to between 1100°C and 1200°C (estimated by thermocouple and/or optical pyrometer and power input) for between 8 and 48 hours. The system pressure was always maintained below 5×10^{-7} mbar when first heating a cell, and the other cells and the substrate heater were kept hot to minimise cross contamination (it was only possible to outgas new components in the growth chamber of CLPIV. This practice should be avoided if a preparation chamber or alternative clean UHV system is available). The gas load evolved when heating a new graphite cell consisted mainly of H₂ and CO. The same species, in lesser quantities, were



PBN silicon cell



Graphite high temperature cell



Graphite arsenic cell

Fig 2.4 Sectioned diagrams of the evaporation sources used in CLPIV: Top, PBN Si Cell; centre, graphite crucible with integral heater shroud as used for the In, Ga and Sn sources [after Kubiak et al (1982)]; bottom, 50g capacity arsenic source.

evolved when outgassing the PBN Si cell. When the temperature of a carefully outgassed uncharged graphite cell was increased from 400°C to 1000°C, the ultimate pressure rise (in a recently baked system with the cryopanelling filled) was less than 5×10^{-10} mbar. The procedures described above, although protracted, contributed to a marked improvement in the electrical properties of InAs and GaAs epilayers over those obtained when using essentially similar source cells in previous MBE systems built at CLP [Meggitt (1979), Grange (1980), Kubiak (1983), see also Chapters 3 and 5].

Each source cell was equipped with a solenoid operated shutter (Fig 2.5). These were designed to be easily interfaced to a switch panel, computer or timer to facilitate the growth of multi-layer structures. The use of three solenoids switched in pairs (Fig 2.5) was found to give an appreciably less violent action than using only two solenoids, reducing the level of defects derived from shutter splash.

2.4 Substrate Heater and Wafer Transfer Mechanism

The main requirements of a heater assembly for III-V MBE are (i) the ability to heat substrates to temperatures of up to about 750°C, (ii) provision for the accurate (or, at least, reproducible) measurement of the substrate temperature and (iii) compatibility with load locked operation. In addition, provision for substrate rotation may be necessary if good doping and compositional uniformity is required across large (i.e. 2" or 3" diameter) substrates. Two methods of substrate handling are in common use in III-V MBE. In the first, substrates are soldered to molybdenum transfer plates with high purity indium. The back face of the transfer block is radiantly heated during growth and (provided that the substrate is evenly wetted with In) the high thermal conductivity of Mo ensures even heating of the substrate. Alternatively, direct radiant

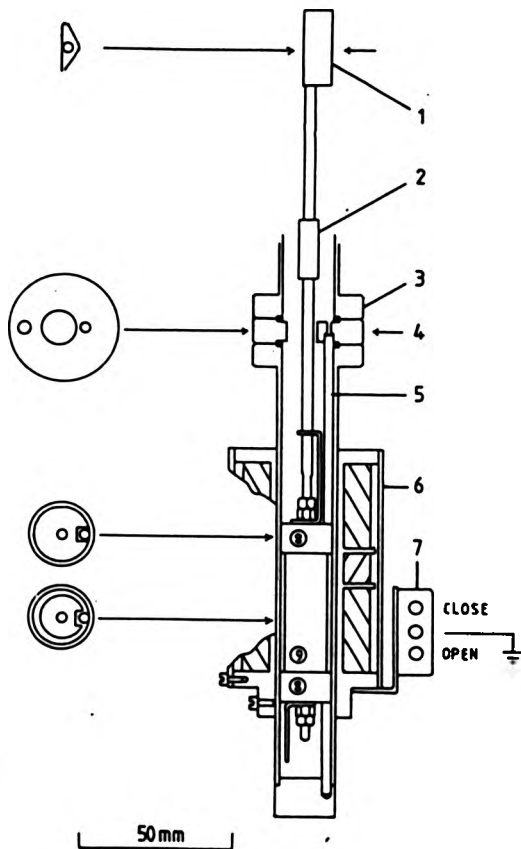


Fig 2.5 Solenoid Operated Shutter. The solenoid (6) was wound in three sections. These were switched in pairs so that the Swedish iron slug (9) was already part of the way into the solenoid at the start of its travel. This gave a 'soft' action without resort to electronic techniques. The slug was of the same length as the paired solenoids and so was self centring. PTFE bearings (8) were used: these slid along an anti-rotation rod (5) to prevent the shutter blade (1) from mis-aligning. Tantalum or molybdenum were used for all components to the right of the collar (2).

heating of the substrate may be employed [Palmateer et al (1984), SpringThorpe and Mandeville (1986)]. This approach is often used in production laboratories where the removal of two processing steps (indium soldering and post-growth lapping to leave a clean back face to the substrate) is an obvious advantage. However, indium free mounting does have disadvantages for research applications. Firstly, only substrates of a standard size (normally 2" diameter) may be used which precludes, for example, simultaneous growth on a variety of substrates. More importantly, it is not possible to measure the substrate temperature directly. Either an infra-red pyrometer must be used [which can be complicated by emissivity changes between materials when growing heterojunctions, pyrometer port fogging, etc., Wright et al (1986b)], or else the temperature must be scaled from a thermocouple fixed to some part of the heater assembly. If the latter approach is taken the indicated and actual temperatures can differ by as much as 250°C (e.g. in a VG V80H system). This temperature offset varies according to the backside finish of the substrate [SpringThorpe and Mandeville (1986)].

Accurate measurement of the substrate temperature is far from straightforward even if indium mounting is used. The best results were obtained in early MBE systems in which substrates were indium soldered to a Mo plate which was an integral part of the heater assembly. The growth temperature could then be measured using a thermocouple permanently mounted in the Mo block. This technique is clearly incompatible with load-locked operation and so alternative methods have been developed. Perhaps the most successful of these (as used in early Varian systems) is to use a two or three metal thermocouple pressed into well(s) in the back of the Mo transfer plate. Provided that care is taken to avoid radiant heating of the thermocouple wires, run-to-run reproducibility to within about 30°C can be achieved using this technique (although obtaining a reproducible contact between the thermocouple and transfer block is not a

trivial problem, Croydon [1985]).

The heater designed for CLPIV circumvented most of the problems described above. The assembly was based on a 1" diameter Ta tube with a flat Mo plate fitted into one end to form a light tight enclosure around the heating element, which was non-inductively wound onto a PBN former (Fig 2.6). The thermocouple junction was permanently mounted in a 1.2 mm diameter hole bored through the width of the Mo plate. The thermocouple leads, insulated by alumina tubes, ran along the outside of the Ta tube and so were not exposed to direct radiant heating. The whole assembly was surrounded by heat reflecting Ta foils as indicated in Fig 2.6. The lower surface of the Mo plate was thinly coated with 6N purity indium. Substrates were transferred into the growth chamber soldered to a Mo transfer plate, which was then itself indium soldered to the substrate heater (Fig 2.7). The transfer plate was keyed to fit over a peg in the transfer tray, allowing the plate to be dismantled by firmly twisting the heater. The light-tight construction of the heater enclosure completely protected the Ta element from exposure to corrosive fluxes and prevented light spillage from reducing the contrast of patterns on the RHEED screen.

This design proved very satisfactory in practice. Careful calibration of the heater against the sharply defined phase boundaries on (100) GaAs under static conditions [Newstead et al (1987); see also Chapter 3] indicates that a run-to-run temperature reproducibility of about 5°C was attained in CLPIV. Indeed, it was found that the substrate temperature could be reproduced to within about 15°C even after replacing the thermocouple when servicing the heater. The absolute accuracy of measurement was also reasonable; the In solder fixing the transfer block was found to melt at indicated temperatures within the range 160-185°C (cf. the MP of In, 157°C) and GaAs cleanup (oxide desorption) temperatures of 590-600°C were normally adequate [XPS

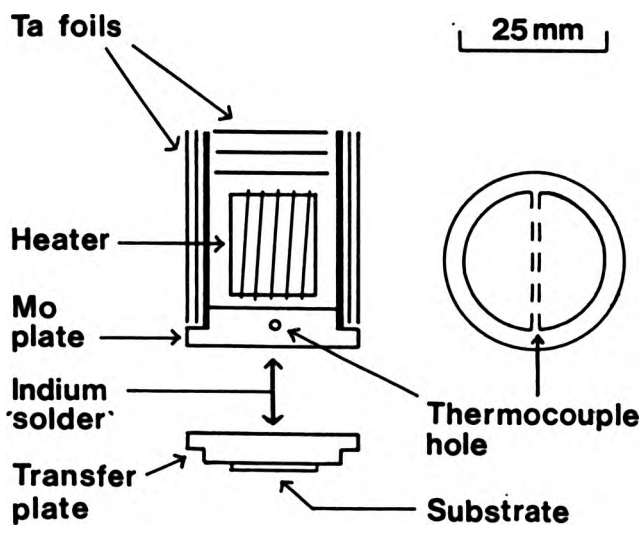


Fig 2.6 CLPIV Substrate Heater (Schematic), see also Fig 2.7

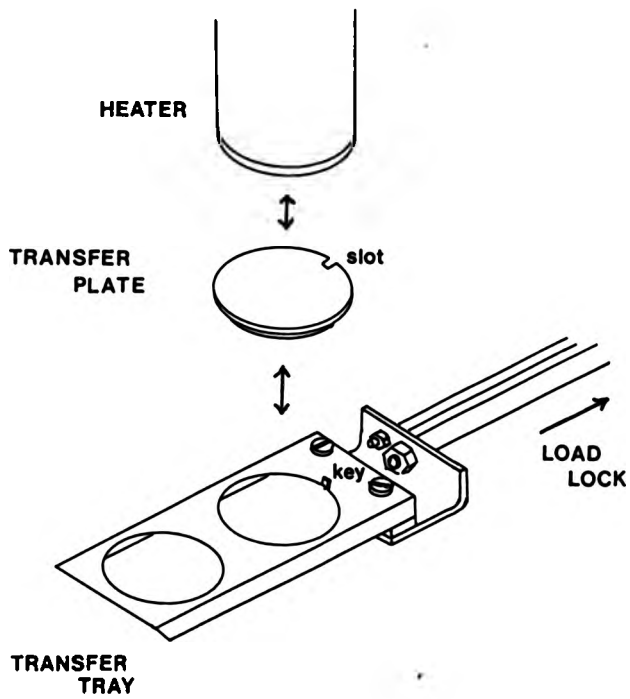


Fig 2.7 Wafer Transfer Mechanism. The 'key and slot' arrangement allowed the heater to be rotated whilst the transfer plate remained stationary. This motion was generally necessary to shear the Ga(In)As deposits formed at the join between the heater and the transfer plate during growth.

measurements made under carefully controlled conditions have shown that the thermally grown oxide of GaAs desorbs suddenly at $582 \pm 1^\circ\text{C}$, SpringThorpe et al (1987)]. It would be difficult to modify the present design for continuous rotation, but this was not required in CLPIV as the matrix fluxes did not vary noticeably over the small substrate areas employed (see also Chapters 3 and 4).

2.5 Temperature Control System

A control system which regulates the substrate and source cell temperatures to within 2°C is required if stable and reproducible doping profiles are to be obtained. Three term or 'PID' [proportional, integral and derivative, DeBarr (1962)] control of the heater current in response to thermocouple feedback is necessary to achieve this accuracy. The use of proportional control alone tends to result in an unstable system which will oscillate in temperature in response to any change in conditions (such as opening the shutter above a source cell). The differential error term damps these oscillations and the integral term corrects for 'offset', a condition where the system temperature stabilises at some fixed interval from the set temperature. PID control can be implemented by analogue or digital circuits. In practice, analogue circuit design is complicated as widely adjustable weighting is required on each of the error terms. A more flexible approach is to interface a computer or microprocessor to thermocouple and current buffers and to perform the control calculations with a software algorithm. Interfacing to pressure gauges, pump controllers and other UHV/MBE hardware allows alarm facilities and 'intelligent' safety cutouts to be included in the control routines.

A control system based on a BBC Model B microcomputer was designed and built in-house for CLPIV (Fig 2.8). A multiplexing system allowed up to eight temperatures to be

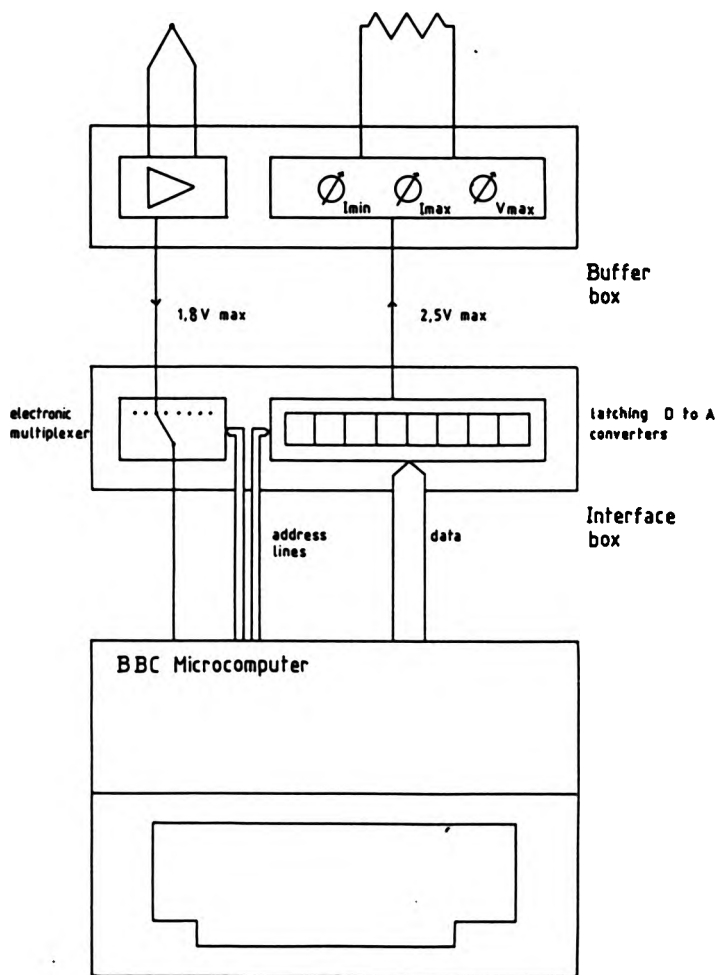


Fig 2.8 CLPIV Temperature Control System, see Sec 2.5

controlled. Each channel had a buffer unit containing a thermocouple amplifier with switchable gain (for use with W-Re or Cr-Al thermocouples) and a 250 Watt constant current buffer. The thermocouple output was linearised in software. The control program accessed the high temperature cells more frequently than those having long time constants; for example, the Ga and Si cell currents were adjusted every 1.5 seconds, eight times more frequently than the arsenic cell currents. Provision was made to ramp the cell temperatures between setpoints, e.g. to protect the cells from thermal shock when large changes in temperature were required. The main system ionisation gauge was interfaced to the computer, allowing the cell heaters to be switched off automatically in the event of a sudden pressure rise. The mains power supply to the buffer units was switched off automatically in the event of a computer diagnostic check failing. The optimum PID weighting factors are functions of the system temperature, so the control programme used whichever of three sets of factors were appropriate to the set temperature of a given channel. It was possible to control the Ga cell temperature to within 1.5°C at its normal set temperature ($\approx 1000^\circ\text{C}$). Dead beat recovery was obtained within 15 seconds of unshuttering the Ga cell, the maximum deviation being 5°C.

2.6 Flux Monitoring

The flux-temperature characteristics of evaporation sources can change significantly with time, e.g. due to depletion and/or deposition around the crucible orifice. Consequently, techniques have been developed to allow the matrix fluxes to be checked and adjusted during or immediately prior to growth. The most common method involves the use of an ionisation gauge to measure the beam equivalent pressures ('BEP') of the individually shuttered fluxes [Wood and Joyce (1978)]. Quadrupole mass spectrometers have been used in a similar manner as species specific detectors

[Chang et al (1973), Kawamura et al (1981)], although there have been some problems with the stability of these devices. Crystal oscillation monitors have also been found useful, but can only provide an estimate of the group III flux [Maissel and Glang (1970)]. Electron impact emission spectroscopy (EIES, e.g. Inficon "Sentinel" type) monitors have been applied with some success to Si-MBE [Kubiak et al (1986)] and III-V MBE [McClintock and Wilson (1987)] but again do not permit an estimate of the group V flux as (for example) the arsenic photoemission lies outside of the usable range of wavelengths. All of the techniques described above are non-absolute and require the measured quantities to be calibrated against the thicknesses or crystal compositions of grown layers. RHEED oscillations, corresponding to monolayer growths, may be used for absolute calibrations [Harris et al (1981), Neave et al (1983)].

CLPIV was provided with a movable ionisation gauge flux monitor which employed novel design features to facilitate a long linear motion [Newstead et al (1984); it is essential to be able to withdraw any monitor from the growth region to avoid heavy contamination from the growth fluxes limiting its useful lifetime]. Whilst measurements made with this monitor were reproducible, some non-linearity was noticed in measurements of the arsenic flux made at low III-V flux ratios. Various hardware modifications and changes in operating technique were tried but did not alleviate this problem. Consequently, the IGPM was only used to measure the group III fluxes and other techniques were developed to measure the group V flux (Chapter 3).

2.7 Other Analytical Equipment

Apart from the flux monitoring equipment described above, CLPIV was equipped with a 5 keV RHEED system based on a Vacuum Generators LEG 31 electron gun. This facility was

adequate for the work reported here, although experience at other laboratories has shown that 10 to 15 keV RHEED offers a significant improvement in definition. The system was also fitted with a quadrupole mass spectrometer for leak testing and residual gas analysis.

MBE systems in general may also be equipped with surface analytical equipment such as Auger electron spectroscopy (AES) and x-ray photoelectron spectroscopy (XPS). These techniques allow, within limits, surface composition, oxidation and contamination to be investigated. Such facilities are particularly useful for investigating surface passivation [Kerr et al (1987)] and substrate cleaning problems. CLPIV was not fitted with XPS or AES as these techniques are ill suited to the environment of a two chamber system, and in any case did not offer any capability of central importance to this project.

2.8 Operating Procedures

The procedures used during the day-to-day operation of CLPIV are described below. The discussion is divided into four sections; (i) preparation of cell charges, (ii) pumpdown and bakeout procedures, (iii) substrate cleaning prior to growth and (iv) routine growth procedures.

2.8 (i) Preparation of Cell Charges

It is essential to use high purity cell charges in MBE. Material of 6N (i.e. 99.9999%) or higher purity is usually specified. 6N purity gallium is available from several manufacturers as shot and small ingots, and also packed in polythene bottles. The last form of packaging is particularly convenient for dispensing small quantities (gallium melts at 27°C). It is not usual to pre-treat gallium in any way, although an HCL dip has been found useful in removing

surface oxides from Ga ingots and so reducing the levels of impurity incorporation and the oval defect densities of GaAs epilayers [Weng et al (1986)].

Indium is available as shot, sheet and ingots. It is not possible to melt indium in air without heavily oxidising the charge so, for the experiments described here, 2g 6N purity indium ingots (MCP) were loaded as supplied. Some workers have found it desirable to bake their In source materials at 800°C in a reducing (H_2) atmosphere in order to partially remove silicon contamination [Schaffer et al (1983)]; low levels of silicon and sulphur are almost inevitably present in refined indium [Janson (1983), Lambert et al (1983)]. Although the In used in the work reported here was not pre-treated, the InAs grown in these experiments compares favourably with the best epitaxial material grown worldwide [Chapter 5].

Arsenic is available as two isomorphs, alpha and beta. The beta form is stable in air but undergoes a violently exothermic phase change to the alpha form when heated, and so is unsuitable for MBE [Meggitt (1979)]. The alpha form is available as polycrystalline lump packed under vacuum or an inert gas to prevent oxidation. This material is loaded as supplied; Canyonlands 7N and MCP 6N material was used for the experiments reported here. Solid arsenic charges, shaped to fit the source cells of most commercial systems, are also available. Solid charges allow more material to be packed into each cell and so offer the possibility of extended growth series. There are, however, some problems with flux uniformity when using these charges [Poxon (1987)]. Impurity levels in the ppm range in MBE arsenic charges can have a dramatic effect on GaAs quality, even though As_4 sources are generally operated at temperatures below 300°C [Kubiak and Parker (1984)].

The tin charges (5N Nordico) were cut from a bar and etched for two minutes in Aristar grade HCL to remove visible

surface oxidation before rinsing, drying and loading. The silicon charges (better than 6N, Wacker and GEC) were etched for one minute in CP4A (5:3:3: HNO₃: HF:Acetic Acid) to remove surface oxides, then rinsed well and dried before loading.

2.8 (ii) Pumpdown and Bakeout Procedures

Having recharged the source cells and completed any other maintenance, the system would be roughed out to a pressure of $<1 \times 10^{-3}$ mbar with a sorption pump, then ion pumped for a short period. Large leaks were sought using helium search gas with the QMA at this stage. The high temperature components were always lightly outgassed prior to bakeout; this involved partially filling the LN₂ cryopanel to achieve a pressure of 1×10^{-7} mbar or lower, heating the Ga, In, Si and Si cells to 500°C, the arsenic cells to 200°C and the substrate heater to 600°C for about thirty minutes, and supplying the normal operating current of 50A to the sublimation pump filaments for several minutes. Any new or recently etched Mo substrate transfer plates were individually outgassed at this stage. These procedures significantly reduced the gas load encountered when fully outgassing the heated components after bakeout, therefore making a worthwhile contribution to system cleanliness. (The ion gauge heads and the sublimation pump filaments were further outgassed during bakeout).

The system was usually baked at 200°C for between 12 and 48 hours after which a further 8 hours were required for the ion pump magnets to cool. Barring leaks, a base pressure of between 1×10^{-10} and 5×10^{-10} mbar was obtained. Fig 2.9 shows a typical residual gas spectrum. The dominant peaks correspond to H₂, H₂O and CO/N₂. Following bakeout and leak testing, and before growing any epilayers, the high temperature sources and the substrate heater would be heated to approximately 50°C above their normal maximum

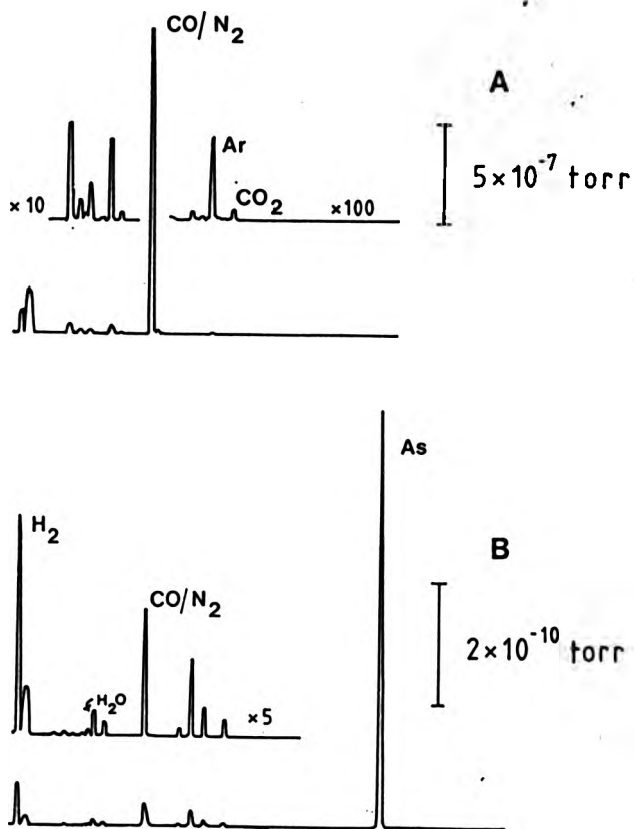


Fig 2.9 Residual gas spectra taken (a) whilst outgassing a new graphite crucible, recorded 2 hours after first reaching a temperature of 1100°C, and (b) during the growth of a GaAs epilayer under normal conditions (growth rate of 1 μm/h, JAs₄:JIn=4:1, T_{subs}=580°C). The calibrations refer to the main traces: the subsidiary traces should be scaled as indicated.

operating temperatures for a few hours. The arsenic cells were outgassed at their normal operating temperatures, as this was sufficient to eliminate the AsO peak from the residual gas spectrum without depleting the volatile arsenic charges.

2.8 (iii) Substrate Preparation

Single crystal boules of GaAs and related III-V semiconductors are normally grown either by the Bridgeman ('melt grown') or the liquid encapsulated Czochralski ('LEC') techniques [Kirkpatrick et al (1985)]. Both conducting and semi-insulating (nominally undoped or Cr trapped) GaAs boules are available. Substrates prepared from Bridgeman material generally have low dislocation densities compared to LEC grown substrates, and are preferred for the production of optoelectronic devices, especially LASERS [Tsang (1985)]. However, Bridgeman grown wafers are relatively expensive, and are of an inconvenient shape to handle if indium-free mounting is to be used, and the majority of material used in MBE is LEC grown.

The substrates used in MBE are normally orientated on, or close to, the (100) axis for the reasons given in Chapter 1. Substrates are usually bought 'pre-polished for epitaxy' from the manufacturer, in which case the saw cut blanks will have been cleaned up using successively finer grades of diamond or carborundum paste before being polished to a flat, featureless surface with a chemically buffered pad (e.g. using Br-Me or Syton). These procedures are described in detail by Jensen (1973), Tuck (1975) and Fynn and Powell (1979). The finished wafers are nominally 0.4 mm thick. Recently, wafers have been prepared from LEC grown GaAs isoelectronically doped with indium to a concentration of about $1 \times 10^{20} \text{ cm}^{-3}$. Although there are some problems with internal stress, the ultimate surface dislocation/defect density of these wafers is comparable to

Bridgeman grown material [Osaka et al (1985), Shinohara et al (1985)].

Subsequent treatments, usually performed immediately before the wafers are loaded into the MBE system, are designed to remove any contamination arising from packing and storage and to leave a thin, easily desorbed protective oxide 'cap' on the substrate. The procedures used at CLP were typical of current practice. GaAs substrates of the required size were cleaved from 2" wafers (MCP and ICI Wafer Tech); blown free of dust and GaAs fragments with filtered dry nitrogen; degreased by ultrasonic cleaning in Aristar grade trichloroethylene, acetone and methanol [the use of a chlorinated solvent is essential to remove certain waxes used in manufacture, Harris (1984)]; rinsed in 'MilliQ' filtered deionised water; etched in 8:1:1 H_2SO_4 : H_2O_2 (100 vol): H_2O for one minute under constant agitation; rinsed with MilliQ water; blown dry with filtered dry nitrogen and soldered with 6N purity indium to molybdenum plates (at 185°C) for transfer into the MBE system as described in Sec 2.4. A PTFE beaker was dedicated to each wet stage. The only substrate cleaning problems encountered arose from the limited shelf life of the etching chemicals, particularly the H_2O_2 . Although some authors have found a post-etch HCL rinse successful in removing contaminants [including S, Chai et al (1985)] arising from the use of stale chemicals, replacement should be considered more satisfactory.

Until recently it was believed that the volatile surface oxides were formed during the etching or final rinsing of the GaAs substrate [Cho and Arthur (1975), Ploog (1980), Vasquez et al (1983)]. However it is now known that the surface oxides mainly develop during air exposure, a process greatly enhanced if the substrate is heated, e.g. during indium soldering [Massies and Contour (1985a)]. It may be possible to reduce (or eliminate) the need for in-situ thermal cleaning if the substrate is mounted and

handled under an inert gas [light oxidation may be removed using running deionised water, Massies and Contour (1985b)]. Such a treatment may be effective in controlling defects originating at the film-substrate interface, some of which have been attributed to thermal cleaning processes [Massies et al (1983)].

After loading into the growth chamber the oxide cap was removed by heating under the arsenic growth flux. Although a few minutes at 590-600°C was sufficient to produce a properly reconstructed surface, this temperature was usually held for ten minutes for surety. In previous studies AES and XPS have been used to show that the arsenic oxides of GaAs begin to desorb at temperatures just below 400°C and the gallium oxides at 550-600°C [Vasquez et al (1983), Massies and Contour (1985a), the exact surface chemistry involved is uncertain]. More recently, SpringThorpe et al (1987) have used XPS under carefully controlled conditions to show that the thermally grown gallium oxide(s) of GaAs desorb suddenly at 582+/-1°C whereas oxides grown via exposure to ozone (an alternative MBE precleaning process which avoids the use of wet etching) desorb at about 630°C. The levels of carbon and oxygen on the substrate lie below the detection limits of AES (=0.1 monolayer) after oxide desorption [Cho and Arthur (1975)].

2.8 (iv) Routine Growth procedures

The procedures used during this project were typical of current practice in MBE in that much of the routine effort was directed towards the preservation of a clean UHV environment in the growth chamber. To this end, the Mo transfer plates were stored in the load lock and only removed from the system for the short periods necessary for wafer exchange. Substrates were normally used within a few hours of preparation.

The load-lock was roughed out using a sorption pump (opened very slowly to minimise turbulent gas flow, which can stir up particles and contaminate the substrate) and then ion pumped for at least one hour. To discourage contamination by condensable vapours, all cryopanelling in the growth chamber was filled and all cells were held close to their operating temperatures during transfer. The pressure in the growth chamber rose to about 5×10^{-8} mbar during transfer, although this was often masked by the arsenic ambient. When used, the titanium sublimation pump would be operated shortly after transfer. Use of the sublimation pump within a growth series was discontinued after early experiments showed that it made no detectable difference to the majority carrier properties of lightly doped GaAs grown in the system.

The matrix fluxes were checked before growth using the IGPM, although latterly the arsenic flux was checked against a fixed monitoring gauge as described in Chapter 3. Substrate cleanup and the first few minutes of growth were monitored using RHEED (some caution was exercised as Chang (1982) has shown that the exposure of an oxidised substrate to an electron beam, especially at temperatures below 350°C , can increase the surface density of carbon remaining after oxide desorption). At the end of growth the epilayer was cooled to 220°C and exchanged for a fresh substrate using the load-lock transfer mechanism. Whether heating or cooling, the substrate temperature was never ramped at rates greater than $2^{\circ}\text{C}/\text{sec}$ in order to avoid thermally induced slip lines. Overnight, and between growth runs, the Ga, In and dopant cells were held at 400°C , the arsenic cells at 150°C and the substrate heater at 250°C to discourage contamination from condensable vapours evolved from the warming cryopanelling.

Chapter 3

The Commissioning of CLPIV, and an investigation into the functional relationship between surface reconstruction, GaAs epilayer properties and the MBE growth conditions.

Contents

- 3.1 Introduction
- 3.2 Commissioning Growths
 - (i) Initial experiments; Si and Sn doping
 - (ii) Basic material properties
- 3.3 Range of Parameters Permitting the Growth of GaAs
 - (i) Experimental: Flux Monitoring
 - (ii) The Surface Phase Diagram of (100) GaAs
 - (iii) Stability of the Phase Boundaries
 - (iv) Activated Phase Boundaries
 - (v) Variation of Growth Rate
- 3.4 Epilayer Properties and the GaAs Phase Diagram.
- 3.5 Summary and Discussion

3.1 Introduction

GaAs epilayers were grown to commission CLP1V because; (i) the growth of GaAs by MBE was known to be straightforward, with extensive information on substrate preparation, growth and doping being available in the existing literature; (ii) techniques for the optical and electrical characterisation of epitaxial GaAs were similarly well established; and (iii) because a considerable volume of data was available for the comparative assessment of material quality.

3.2 Commissioning Growths

All of the commissioning layers were grown under conventional conditions, i.e. using a growth rate of about 1 $\mu\text{m}/\text{h}$, a (2x4) surface reconstruction and substrate temperatures of 580-600°C. The discussion below compares the properties of series of epilayers grown between bakeouts, as this approach gives a clear demonstration of the effects of hardware modifications. The results demonstrate that operating technique (specifically, the outgassing of high temperature components) is as important as system design in determining material quality.

3.2 (i) Initial Experiments; Si and Sn doping

Series 1: Si doped GaAs (six epilayers). Graphite cells, built to the design described by Kubiak et al (1982), were used for the high temperature (Ga and Si) sources. The arsenic cell, also constructed from graphite, was built to a simpler design offering a larger capacity (Fig 2.4). The cells were outgassed at an estimated 1200°C for 15 hours as described in Sec 2.3 and the cell charges were prepared as described in Sec 2.8(i). Although the morphology of the layers was reasonable, with oval defects being the dominant feature, typical Si-doped epilayers were p-type and highly

resistive at room temperature. The layers were semi-insulating at 77K. The series was ended to adjust or modify several components of the system. During this work the gallium cell was seen to be cracked and was replaced.

Series 2: Si doped GaAs (fourteen epilayers). As with Series 1, the Si doped epilayers grown in Series 2 were mirror-shiny but exhibited low mobility p-type conduction, implying that the cracked gallium cell was not wholly responsible for the degraded electrical properties. The series was ended following the development of a small leak in the continuous flow cryopanel surrounding the growth region (Figs 2.1, 3.7). It is possible that this leak was present at a lower magnitude throughout Series 1 and 2, although base pressures of less than 2×10^{-10} mbar were obtained at the beginning of both.

Extensive reduction of the alumina heater insulators in the Si and Ga sources was noticed at the end of Series 2, implying that these components had been outgassed at too high a temperature. Accordingly, these cells were replaced. The new Ga cell was made to the same design as before. A graphite Sn doping cell, of the same design as the Ga cell, was also fitted. The replacement Si cell was built around a PBN crucible as shown in Fig 2.4. This crucible had been used as a Ga cell in an earlier MBE system at CLP, and so was etched clean in $5\text{HNO}_3:3\text{HF}:3$ Acetic acid before use (NB - Varian has recently recommended that new PBN crucibles should be pre-cleaned in aqua regia. This etch may also be suitable for reconditioning used crucibles). Before charging, the new cells were outgassed for a total of twelve hours at temperatures estimated to be $\approx 1100^\circ\text{C}$, i.e. about 100°C below those previously used. The arsenic cell was emptied and recharged but otherwise left unaltered.

Series 3: Si and Sn doped GaAs (twenty-five epilayers). Series 3 consisted mainly of Sn doped epilayers: these were

n-type with mobilities appropriate to the free carrier concentration at $N_D - N_A > 5 \times 10^{15} \text{ cm}^{-3}$ (Figs 3.1, 3.2). The maximum free carrier concentration attainable through Sn doping was $1.16 \times 10^{19} \text{ cm}^{-3}$, in good agreement with previous estimates [$1.1 \times 10^{19} \text{ cm}^{-3}$, Harris et al (1982)]. The Si doped layers were also n-type, but with relatively low mobilities. The electrical properties of the Si doped films only became comparable to those of the Sn doped layers in Series 4, during which the Si source was outgassed at a temperature high enough to partially melt its charge [i.e. approaching 1410°C , Kaye and Laby (1973)]. High levels of H_2 and CO/N_2 were seen in the residual gas spectrum during this procedure and, at the end of the growth series, the PBN crucible and alumina heater insulators were seen to be partially decomposed. However, it was found that similarly vigorous outgassing of the Si cell was necessary to regain acceptable material quality after any air exposure of the MBE system. Although some danger of damage was incurred by this treatment, the source operated reliably for twenty growth series.

Series 4: Si and Sn doped GaAs (twenty-three epilayers). Preparations for Series 4 involved fitting a replacement for the continuous flow cryopanel removed at the end of Series 2 and replenishing the arsenic cell. Although the quality of the Sn doped material was very similar to that obtained in Series 3, the additional cryopanel was useful in that it protected the viewports from fogging. Improved electron mobilities were obtained from Si doped epilayers (Figs 3.1, 3.2) for the reasons already described. Subsequent modifications to the system were relatively minor; an In source was added at the end of Series 5 and a second arsenic cell, to increase capacity, at the end of Series 8.

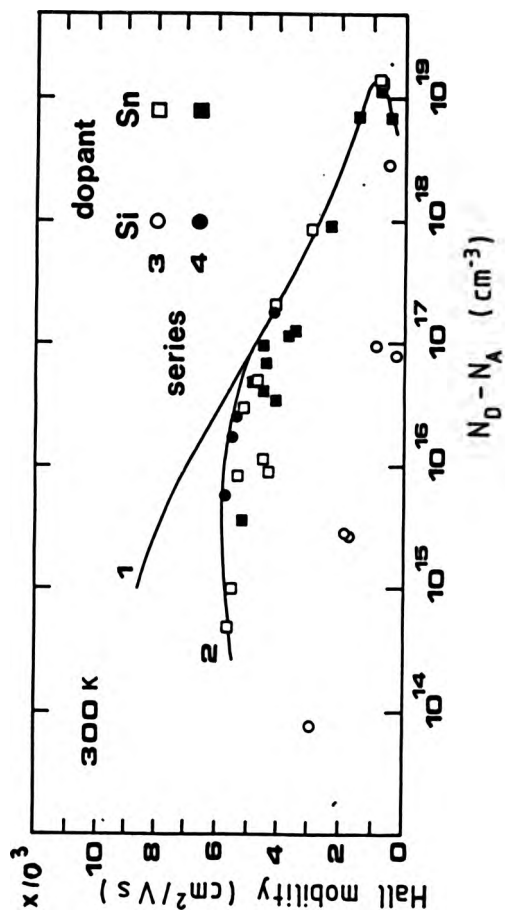


Fig 3.1 300 K Hall mobility versus carrier concentration of Si and Sn doped GaAs epilayers grown in CLPIV. Curve 1 is an empirical fit to the best recent MBE Data [Ilegems (1985)]. Curve 2 is fitted to the experimental data as a guide for the eye.

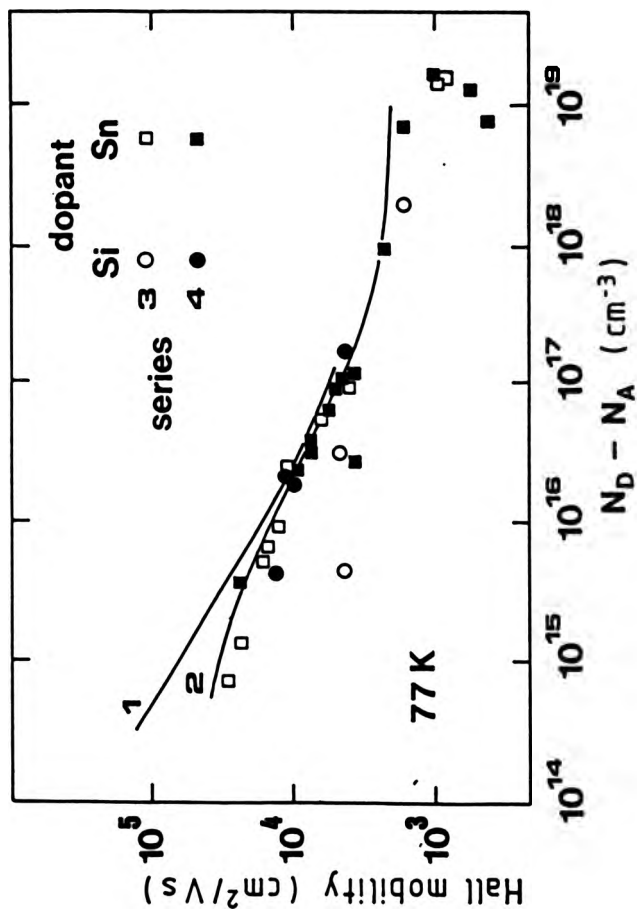


Fig 3.2 77K Hall mobility versus carrier concentration of Si and Sn doped GaAs epilayers grown in CLPIV. Curve 1 is fitted to data from lightly compensated MBE grown GaAs [Davies and Andrews (1984)]. Curve 2 is fitted to older MBE/VPE data [Poth et al (1979)].

3.2 (ii) Basic Material Properties

All of the layers included in Figs 3.1 and 3.2 were mirror shiny with oval defect densities of $\approx 5 \times 10^3 \text{ cm}^{-2}$. In subsequent experiments, the oval defect density was typically found to increase from $\approx 1 \times 10^3 \text{ cm}^{-3}$ (at a growth rate of $1 \mu\text{m/h}$ and when using a fresh gallium charge) to $\approx 1 \times 10^4 \text{ cm}^{-2}$ at the end of an extended growth series. This substantial increase was believed to originate from the use of a two-chamber system, in which regular exposure to low levels of O_2 and H_2O from the load-lock could partially oxidise the strongly heated gallium cell charge [gallium oxides in the Ga source are believed to be persistent sources of oval defects, Chai and Chow (1981), Kirchner et al (1981), Weng et al (1986)]. A grey skin was generally found to cover the surface of the Ga charge at the end of an extended growth series. This was believed to consist mainly of Ga-As-GaAs, but may also have contained carbon¹ and oxides as removing the skin tended to reduce the oval defect density obtained at the start of the following growth series.

As shown by Fig 3.2, the electron mobilities of Si and Sn doped GaAs grown in CLPIV lay close to the 77K mobilities obtained from representative LPE and VPE grown material [Poth et al (1979)] at carrier concentrations in excess of about $5 \times 10^{15} \text{ cm}^{-3}$. The 77 K mobilities did not, however, approach those of the best MBE grown GaAs [Davies and Andrews (1984)] until $N_D - N_A = 1 \times 10^{16} \text{ cm}^{-3}$. Similar, although slightly more exaggerated behaviour was seen at 300 K (Fig 3.1). The shape of the μ versus n curve implies that significant levels of compensation occurred at lower doping

¹ Croydon (1985) found that the skin formed on a Ga charge held in a similar graphite crucible had a carbon content of $\approx 0.11\%$.

levels. This is consistent with the properties of unintentionally doped GaAs epilayers grown in CLPIV, which were always p-type with 300 K carrier concentrations of between 1×10^{15} and $3 \times 10^{15} \text{ cm}^{-3}$. The corresponding 300 K mobilities, 380-420 $\text{cm}^2/\text{V-s}$, were comparable to those of VPE and LPE grown material at similar hole concentrations [Wiley (1975)]. Photoluminescence studies, described more fully below, showed that carbon was the dominant residual acceptor in these layers, as is usually the case with MBE grown GaAs [Cho and Arthur (1975), Wood (1985)].

A quantitative estimate of the compensation occurring in the doped layers was obtained by comparing the mobilities measured at a given free carrier concentration (e.g. $N_D - N_A$) with theoretical calculations [Rhode (1975), Walukiewicz et al (1982)]. Figure 3.3 shows the variation of the residual acceptor level, N_A , with the 77K free carrier concentration. This relationship was determined, using the results of Walukiewicz et al (1982), from the data in Fig 3.2 (excluding the low mobility Si doped epilayers grown in Series 3). It is apparent that N_A tends to a fixed value of $\approx 1.5 \times 10^{15} \text{ cm}^{-3}$ as $N_D - N_A$ is reduced below $5 \times 10^{15} \text{ cm}^{-3}$. As would be expected, this value is closely similar to the acceptor densities obtained in unintentionally doped material (between 1×10^{15} and $3 \times 10^{15} \text{ cm}^{-3}$, see above). An almost constant compensation ratio (N_A/N_D) of 0.38 was derived at carrier concentrations in excess of $1 \times 10^{16} \text{ cm}^{-3}$. This behaviour has been observed in bulk and epitaxial GaAs by several workers, including Wolfe and Stillman (1975), Poth et al (1978), and Kuphal (1981). It is currently believed that high levels of autocompensation do not occur in GaAs at these doping levels, and that the behaviour shown in Fig 3.3 results from limitations in the theoretical treatment [Anderson and Apsley (1986)]. In particular, no fully satisfactory calculations are available for the case where ionised impurities are present at concentrations in excess of $1 \times 10^{16} \text{ cm}^{-3}$ [Chattopadhyay and Queisser (1981), Anderson et al (1985)]. However, it is believed

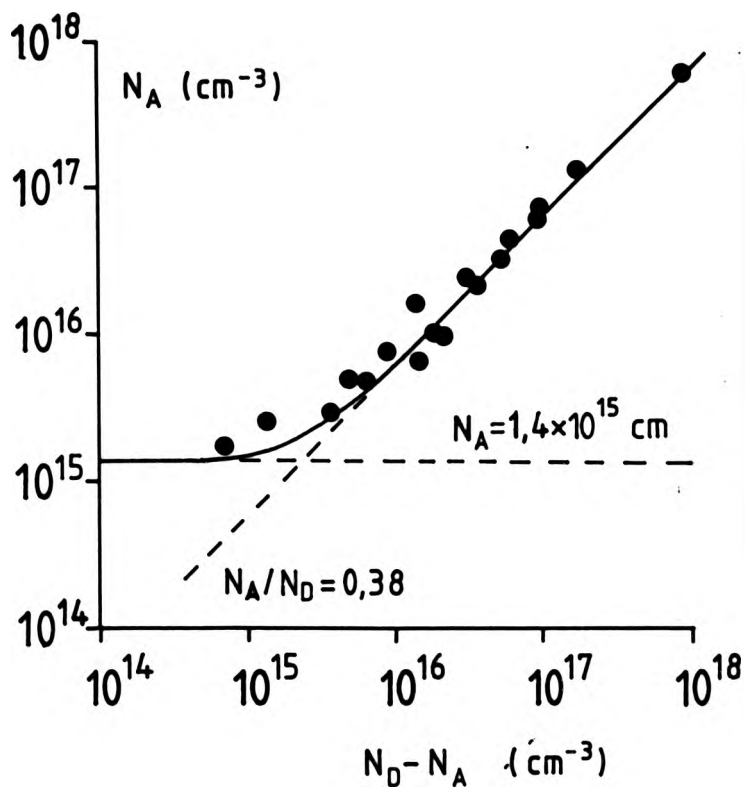


Fig 3.3 Acceptor population at 77 K as a function of the (compensated) carrier concentration, derived from the data in Fig 3.2 using the theoretical results of Walukiewicz et al (1982).

that the analysis presented is accurate for doping levels below about $1 \times 10^{16} \text{ cm}^{-3}$ [Anderson and Apsley (1986)] and, therefore, that the residual acceptor level determined from Fig 3.3 is a reasonable estimate of the true value.

Figure 3.4 shows the variation of the Hall mobility and carrier concentration with temperature for a Sn doped GaAs epilayer grown in CLPIV. The peak in mobility at about 90 K is typical of both bulk and epitaxial GaAs [Landolt-Bornstein (1982)]. The mobility falls off because of lattice scattering at temperatures above 90 K and because of ionised impurity scattering at lower temperatures [Seeger (1982)]. The temperature dependence of the carrier concentration is also conventional, with donor freezeout starting just below room temperature. The activation energy of the freezeout is 2.72 meV, which is approximately half of the existing estimates for the ionisation energy ' E_i ' of Sn in GaAs [5-7 meV, Casey and Panish (1978)]. This is consistent with a moderately high compensation ratio, which can cause the activation energy to vary between E_i and $E_i/2$ [Seeger (1982)]. The compensation ratio N_A/N_D of the sample shown in Fig 3.4 was ≈ 0.7 by Walukiewicz' analysis.

The freezeout became less rapid at temperatures below about 30 K, and $N_D - N_A$ actually increased slightly as the temperature fell from 15 K to 4.2 K (Fig 3.4). Similar behaviour has been observed in other III-V compounds [Brostowski et al (1955), Fritzsche and Lark-Horovitz (1955), Schklovskii and Efros (1984), see also Chapter 5] and has been attributed to both impurity band and hopping conduction at comparably low doping levels. Impurity band conduction is only possible when there is appreciable overlap between the ground state wavefunctions of the impurity atoms. This condition occurs when

$$a(4\pi N_D/3)^{1/3} > 1 \quad 3.1$$

where a is the electronic radius of the impurity atom

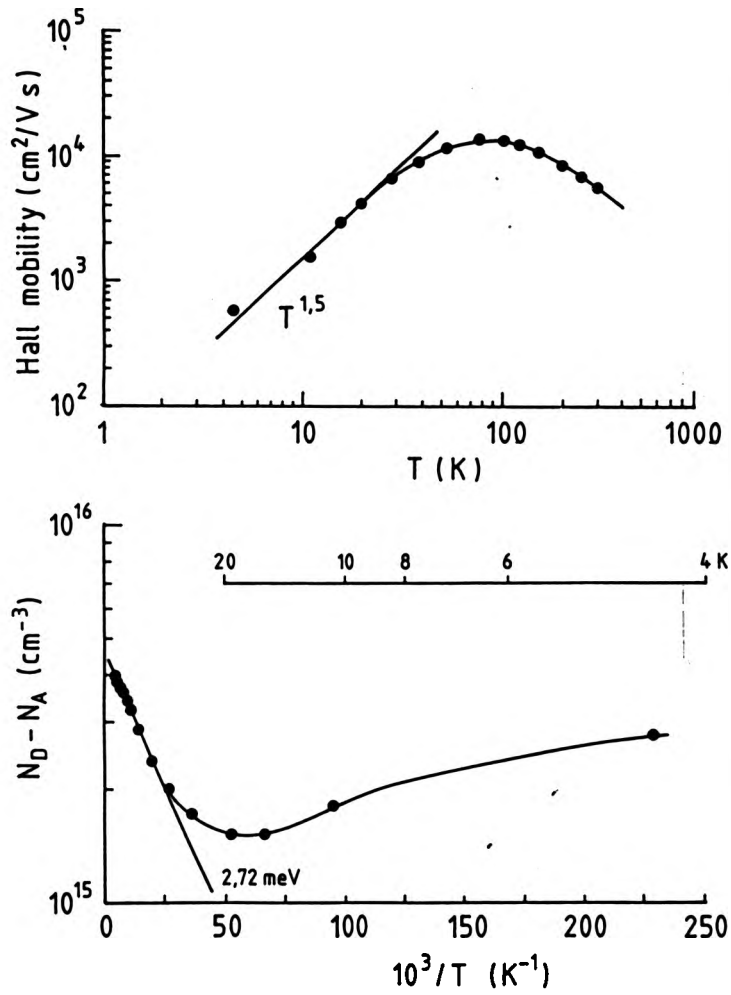


Fig 3.4 Temperature variation of Hall mobility and carrier concentration in a GaAs epilayer, lightly doped with Sn, grown in CLPIV.

[Pearson and Bardeen (1948)]. By analogy with a hydrogen-like atom, a is given by the Bohr formula

$$a = (\epsilon a_0 m) / m^* \quad 3.2$$

where a_0 is the ground state electronic radius of the hydrogen atom ($=0.53 \times 10^{-8}$ cm). Inserting the appropriate values for GaAs ($m^*/m=0.07$, $\epsilon=12$) yields the condition $N_D > 3.2 \times 10^{17} \text{ cm}^{-3}$; thus it is unlikely that impurity band conduction is occurring in the data shown in Fig 3.4, where $N_D - N_A$ is only $2-3 \times 10^{15} \text{ cm}^{-3}$ at the temperatures of interest. The mechanism for hopping conduction requires far less overlapping of the ground state wavefunctions of the impurities and a compensated sample [Blakemore (1958)] and is, therefore, more likely to be applicable to the layer under discussion. Hopping mobilities are typically of the order of $1 \text{ cm}^2/\text{V-s}$ in the acceptor bands of lightly doped Ge [Blakemore (1959)] and InSb [Hrostowski et al (1955)]. However, if shallow ($\ll 50$ meV) impurities are present, hopping may also occur via the conduction or valence band [Schklovskii and Efros (1984)]. Somewhat larger mobilities may be expected under these circumstances, commensurate with the present results (the 4.4 K mobility of the GaAs sample shown in Fig 3.4 is $543 \text{ cm}^2/\text{V-s}$).

If hopping conduction is not operative, the cessation of freezeout may indicate the presence of a two dimensional electron gas. However, it is not easy to see why a 2DEG should occur in homoepitaxial GaAs. It should be noted that the behaviour shown in Fig 3.4 was seen in all low temperature measurements made on lightly doped GaAs and InAs (Chapter 5) grown in CLP1V; that the contacts to the Hall samples remained ohmic at the temperatures of interest; and that similar results were obtained whether the ohmic contacts were annealed in air (the usual procedure) or in a reducing environment.

Several of the unintentionally (p^-) and lightly doped (n^-) epilayers were examined using photoluminescence (PL) techniques. The interpretation of PL data is treated succinctly by Pankove (1975) and Ilegems (1985). The results obtained confirmed that the layers were compensated with carbon acceptors, as indicated by strong peaks at 1.4900 eV (D^0, C_{As}^0) and 1.4935 eV (e, C_{As}^0). It was not possible to search for Mn or Cu, which may have been present as system-generated impurities [Grange (1980)], due to the limited spectral response of the detectors available. The excitonic region was dominated by broad peaks (commensurate with the level of compensation and/or doping) at 1.5110 eV (exciton bound to Ga-site defect), 1.5134 eV (D^+, X), 1.5140 eV (D^0, X) and 1.5156 eV (free exciton). A broad peak was seen at an energy of between 1.47 and 1.48 eV in several epilayers. This energy corresponds to the transition between a free (conduction band) electron and a Ge acceptor. However, Ge is not a common impurity in MBE source materials and it has been argued that this peak may be associated with carbon vacancy complexes [Briones and Collins (1982)]. This conclusion is supported by Akimoto et al (1984), who presented evidence that the peak results from the incorporation of CO from the gas ambient. As noted in Sec 2.2(i), attempts to obtain high carbon levels in GaAs by the deliberate introduction of CO into the MBE growth environment have been unsuccessful, leading to speculation that the carbon species must be thermally excited [e.g. by a hot filament, Davies and Williams (1985)] before incorporation can take place. With regard to the present results, it should be noted that Ploog (1980) ascribed high acceptor levels to the generation of excited carbon species by a reaction between a graphite crucible and its alumina support tubes. Essentially similar sources were used in CLPIV (Sec 2.3), implying that some improvement may have been possible through the use of PBN crucibles. Experience in the authors present laboratory (GEC HRC) suggests that the carbon backgrounds obtained in GaAs grown from graphite crucibles

are significantly higher than those obtained in GaAs grown from PBN crucibles under otherwise identical conditions.

3.3 Range of Parameters Permitting the Growth of GaAs

Having completed commissioning, experiments were undertaken to identify the range of growth conditions permitting the growth of good quality GaAs. This work had three aims;

- (i) To extend upon existing RHEED studies into the range of temperatures permitting the epitaxial growth of GaAs [Neave and Joyce (1978a), (1978b)]. The range of applicability of the kinetic growth model [Foxon (1983), Chapter 1] was also examined. An initial objective was to determine the temperature dependence of the arsenic flux required to just stabilise a (2x4) surface (and/or stoichiometric growth). The effects of varying the growth rate were also investigated.
- (ii) To investigate the behaviour of the boundaries separating the surface reconstructions of GaAs at higher flux ratios. These boundaries had been mapped out by several workers, and were known to be Arrhenius functions of the growth temperature and arsenic flux [see, for example, Panish (1980), Van Hove et al (1983)]. However, most observations had been confined to relatively high arsenic fluxes and there was appreciable spread in the reported positions of the phase boundaries. Furthermore, it was not clear to what extent (if any) the positions of the boundaries were affected by the growth rate or by factors related to the history of the layer.
- (iii) To correlate changes in epilayer properties with any changes in growth behaviour noticed when investigating (i) and (ii) above.

3.3 (i) Experimental: Flux Monitoring

It was considered desirable to obtain (as far as possible) absolute estimates of the growth fluxes, in particular to facilitate an eventual comparison between the growth of GaAs and InAs. Given the importance of the measurements, the techniques used will be described in detail.

The gallium flux was measured with a movable ionisation gauge flux monitor [described elsewhere, Newstead et al (1984)] calibrated via the growth of stepped films. The calibration of the As_4 flux followed directly from the experiments outlined under (i) above. In brief, a GaAs epilayer was set growing under a (2x4) reconstruction using a low substrate temperature (c. 520°C) and a known growth rate. The As_4 flux was then slowly reduced until a transition to a (4x2) surface reconstruction was induced. As non-congruent sublimation does not occur from GaAs at growth temperatures below about 630°C [Foxon et al (1973), Goldstein (1976)], this transition could be identified with the onset of non-stoichiometric growth at an $As_4:Ga$ flux ratio of 0.5:1 [Foxon et al (1980)]. Varying the growth rate allowed the arsenic flux to be calibrated across a range of intensities.

Steps were taken to check the validity of this calibration, even though similar techniques had been used by Grange (1980), Schaffer et al (1983) and Sugiyama (1986). A particular concern was that the minimum flux ratio permitting stoichiometric growth on (100) GaAs could be a weak function of the growth temperature even at 520°C [as indicated by Neave and Joyce (1978b)]. However, no such variation was noticed when performing the measurements reported here. This can be seen most clearly in Fig 3.5, which is the surface phase diagram of GaAs growing at 0.65 $\mu\text{m}/\text{h}$. This diagram will be fully described in Section 3.3 (ii). With regard to the present discussion, it should be noted that the (2x4) reconstruction occurred within

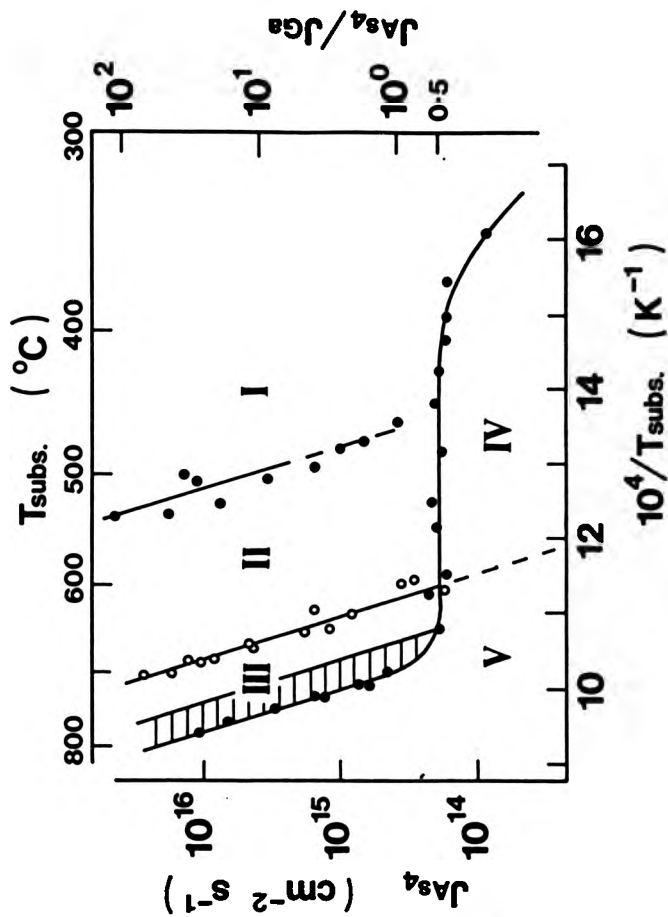


Fig 3.5 The MBE surface phase diagram of (100) GaAs at a growth rate of $0.65 \mu\text{m/h}$. The (2x4) and (4x2) surface reconstructions occurred in Regions II and IV respectively.

Region II and the (4x2) reconstruction within Region IV of the phase diagram. These regions are separated by a horizontal line indicating that, within experimental error, a constant $As_4:Ga$ flux ratio was just sufficient to maintain stoichiometric growth at all temperatures between 400°C and 630°C. An $As_4:Ga$ flux ratio of 0.5:1 was assigned to this boundary for the reasons already described.

Similar wide plateaux in the minimum As_4 flux were found at all other GaAs growth rates investigated, covering a range from 0.07 to 3.0 $\mu\text{m/h}$ (Fig 3.6). The availability of this range of calibration revealed difficulties in measuring $As_4:Ga$ flux ratios below about 3:1 with the conventional ion gauge flux monitor [Sec 2.6; similar problems were reported by Panish (1980)]. For this reason, all As_4 fluxes reported in this thesis were estimated from the background pressure of arsenic in the growth chamber during deposition. The arsenic pressure was measured using a fixed ionisation gauge (Vacuum Generators type VIG22) mounted close to the growth region but not directly exposed to any of the growth fluxes. Fig 3.7 shows the experimental geometry. This technique was considered satisfactory for the following reasons;

- (i) The As_4 overpressure at the 'low temperature' (2x4) to (4x2) transition was a linear function of the growth rate, with a slope of unity for over two orders of magnitude (Fig 3.8). Note that the As_4 flux was calibrated against the growth of InAs as well as GaAs. The two calibrations are in excellent agreement, indicating a close similarity between the basic MBE growth mechanisms of the two compounds.
- (ii) The arsenic cell calibration exhibited Arrhenius behaviour for all flux ratios greater than 0.25:1 (Fig 3.9), even when flux variations of up to three orders of magnitude were encountered.

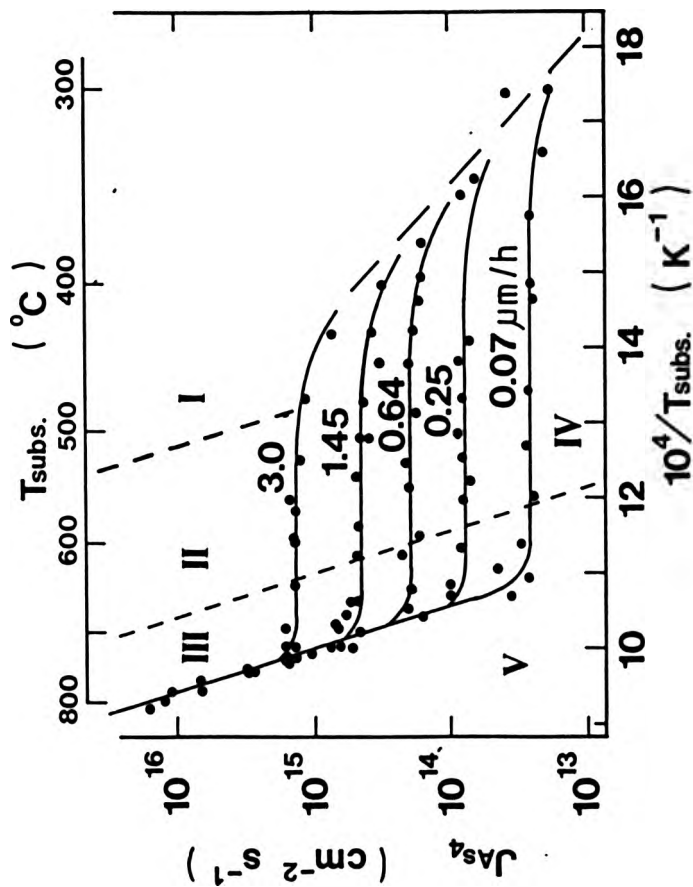


Fig 3.6 A superposition of the MBE phase diagrams of (100) GaAs at five fixed growth rates in the range 0.07 to 3.0 $\mu\text{m/h}$.

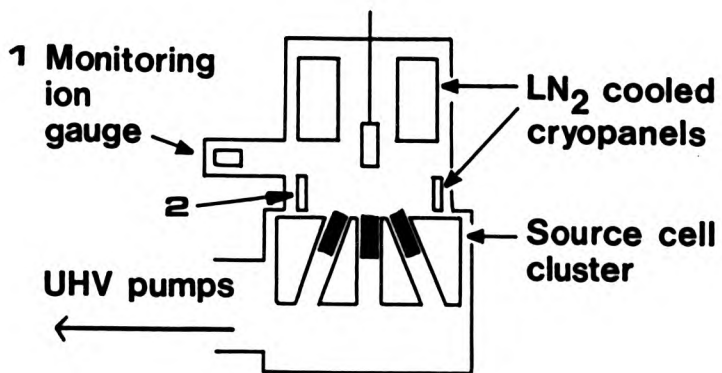


Fig 3.7 System geometry, showing (1) the arsenic flux monitoring gauge and (2) the continuous flow LN₂ cryopanel.

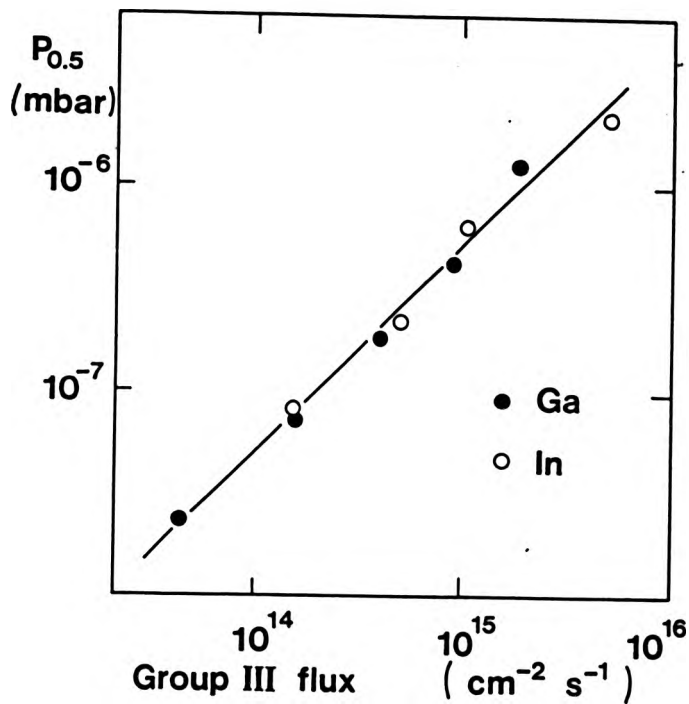


Fig 3.8 The minimum arsenic overpressure supporting a (2x4) surface reconstruction ($P_{0.5}$) as a function of the group III flux. The relationship is linear, with a slope of unity, for over two orders of magnitude.

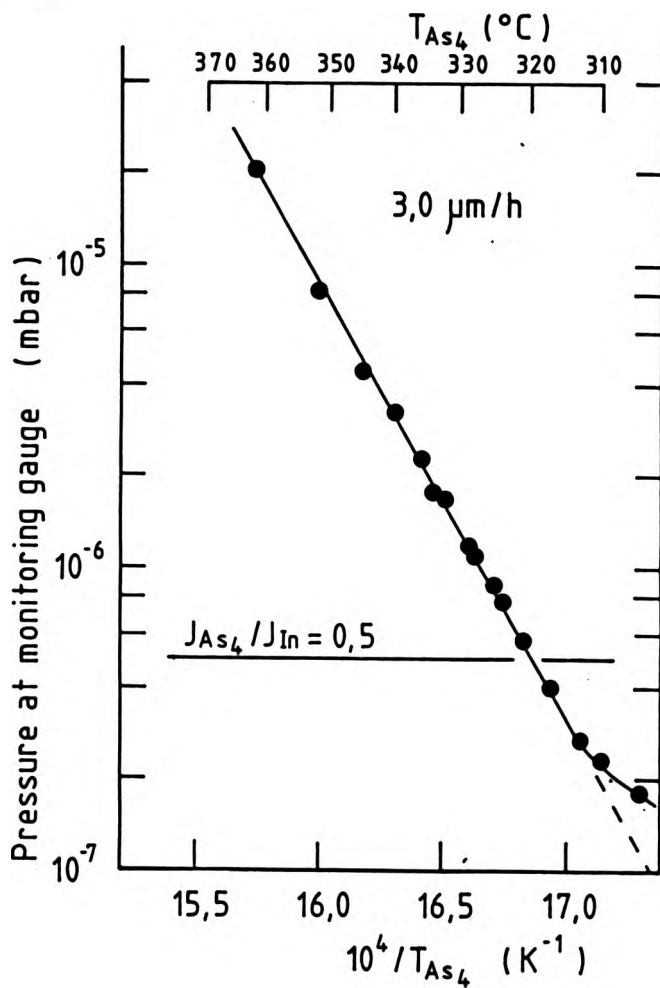


Fig 3.9 Graph showing Arrhenius behaviour of arsenic cell calibration (during deposition at 3 $\mu m/h$) at flux ratios in excess of 0.25:1.

(iii) The calibration of the arsenic overpressure was unchanged whichever of the two arsenic cells fitted to CLPIV was in use. It is not expected that this would be the case if the monitoring gauge were in line of sight with the source cells, as is the case with a conventional movable gauge monitor, because of variations of geometry.

(iv) The monitoring gauge did not shadow the substrate (Fig 3.7), allowing continuous monitoring of the arsenic flux during growth. This was particularly convenient when mapping RHEED boundaries, Sec 3.3 (ii).

3.3 (ii) The Surface Phase Diagram of (100) GaAs

Figure 3.5 is the surface phase diagram of (100) GaAs growing at $0.65 \mu\text{m/h}$. The purpose of the diagram is to show the functional relationship between surface reconstruction and the MBE growth parameters, providing a frame of reference for investigations into changes in growth behaviour or epilayer properties with reconstruction.

The reconstructions seen during growth (using 5 keV RHEED) were;

Region I	mixed (2x4)/c(4x4)	
Region II	(2x4)	
Region IIIa	(1x1) bulk streaks	
Region IIIb (shaded area)	initially (1x1), but unstable	{see below}
Region IV	(4x2)/c(8x2)	{see below}
Region V	(4x2)/c(8x2)	{see below}

A clear $c(4 \times 4)$ RHEED pattern could only be seen under large $As_4:Ga$ flux ratios in Region I. The pattern seen under practical growth conditions (i.e. $JAs_4:JGa < 50:1$) was a composite of the (2×4) and $c(4 \times 4)$ patterns. A clear $c(4 \times 4)$ pattern could, however, be obtained at low arsenic fluxes under static (no gallium flux) conditions.

The identification of the reconstructions seen in Regions IV and V is open to speculation. As shown in Fig 3.10, the RHEED patterns seen in these regions both had periodicities indicative of a (4×2) reconstruction. However, the patterns were readily distinguishable from one another by the length and definition of the $1/4$ order streaks in $[011]$ azimuth. This may indicate that the two patterns correspond to two reconstructions of similar periodicity, for example the (4×2) and the $c(8 \times 2)$. It was not possible to decide this during the experiments reported here. Indeed, Neave and Joyce (1978b) have argued that the RHEED patterns of the (4×2) and $c(8 \times 2)$ reconstructions are indistinguishable in the zeroth order Laue zone. However, Cho (1976) and Ludeke (1978) both clearly imply that they have been able to distinguish between the reconstructions using RHEED. The ordering reported by Cho (1976) indicates that the $c(8 \times 2)$ reconstruction occurs over a higher range of temperatures than the (4×2) .

As noted in Chapter 1, several workers have reported a (3×1) reconstruction on GaAs during growth under As_2 [Massies et al (1976), Panish (1980), Neave et al (1984)] and As_4 [Van Hove and Cohen (1982)] fluxes. The fact that a (3×1) reconstruction was not observed during the experiments reported here, or included in the phase diagrams reported by Van Hove et al (1983), Van Hove et al (1985) or Briones et al (1985) suggests that this reconstruction may only be visible with a critically adjusted RHEED geometry. With reference to the publications cited above, the (3×1) reconstruction is expected to occur between the (1×1) and (4×2) reconstructions, i.e. at the



Fig 3.10 The RHEED patterns seen on (100) GaAs in these experiments.

higher temperatures encompassed by Region III of Fig 3.5. (Experiments at the author's present laboratory (GEC HRC) have confirmed this, also showing that the (3x1) reconstruction, which is relatively diffuse, is often visible when using 15 KeV RHEED, but not when using 5 KeV RHEED, in a VG V80H MBE system).

It is interesting to note that the (2x4)/c(8x2) reconstruction usually converts to a (4x6) reconstruction as the substrate is cooled below $\approx 500^{\circ}\text{C}$ under static (no Ga flux) conditions [Croydon et al (1985)]. Although this phenomenon was repeatedly demonstrated in CLPIV, it proved impossible to obtain a (4x6) reconstruction during growth e.g. by lowering the temperature of an epilayer growing in Region II, or by lowering the As_4 flux whilst growing a layer in Region I

3.3 (iii) Stability of the Phase Boundaries

The boundaries separating the reconstructions shown in Fig 3.5 were mapped out by varying the substrate temperature at a fixed As_4 flux or vice versa. The boundaries were approached by both increasing and decreasing the variable parameter in order to check for hysteresis. The substrate temperature was generally altered by about 1°C in five seconds, and the arsenic cell temperature by about 2°C per minute. Hysteresis was not seen at any boundary, implying that (within the timescale of the experiments) the reconstructed surfaces remained in equilibrium with the growth fluxes. Note, however, that the surfaces of epilayers grown within Region IIIb (the shaded area of Region III, Fig 3.5) were temporally unstable, initially showing (1x1) bulk streaks but becoming (4x2)/c(8x2) gallium rich within the first five minutes of growth. It would be misleading to describe this behaviour as hysteresis, because the ultimate position of the boundary between Regions IIIb and V did not depend on the

history of the epilayer. The phenomenon is more consistent with the outdiffusion of a limited supply of arsenic from within the epilayer, as proposed by Neave and Joyce (1978b). It was not possible to find a simple relationship between the substrate temperature and the time taken for the transition, although it was apparent that there were distinct discontinuity at the boundary between the stable and unstable areas of Region III. In previous investigations Cho (1971a/b), (1983) and Van Hove et al (1985) have reported hysteresis of the activated boundaries between the (2x4), (1x1) and (4x2) reconstructions; however Panish (1980) reported that no hysteresis occurs, supporting the results presented above.

Referring to Fig 3.5, a fixed $As_4:Ga$ flux ratio (assumed to be 0.5:1 as previously described) was found to be just sufficient to maintain an arsenic stabilised reconstruction over a wide range of temperatures (400-635°C), indicating the range of applicability of the MBE growth model at 0.64 $\mu m/h$. At temperatures below 400°C the transition from an arsenic stable (2x4) reconstruction occurred at flux ratios below 0.5:1, and at temperatures below about 320°C the arsenic stabilised reconstruction became 'frozen in' and no change to a gallium rich (4x2) reconstruction could be induced, the RHEED pattern becoming slightly spotty and fading away as the As_4 flux was reduced. This behaviour may be related to the reducing ability of the gallium and As_4 adatoms to migrate to appropriate sites before incorporation, as it is reasonable to expect surface mobility to decrease at low temperatures. Foxon and Joyce (1975) have attributed some apparent differences in the surface chemistry of $As_4-Ga-(100)GaAs$ above and below 330°C to the formation of an intrinsic population of Ga atoms at the higher temperatures. It is also known that a proportion of the As_4 flux incorporates non-dissociatively at temperatures below about 180°C [Foxon and Joyce (1975)].

3.3 (iv) Activated Phase Boundaries

Several of the growth regions shown in Fig 3.5 are separated by parallel boundaries (i.e. between Regions I and II, II and III, III and V) having an activation energy of 3.9 eV. Within experimental error, the same activation energy has previously been obtained from (i) independent observations of some of the phase boundaries reported here [Panish (1980)], (ii) from the temperature dependence of time taken to evaporate a layer of pre-deposited arsenic from MBE grown (100) GaAs [Cho (1971); the result of this experiment did not rely on an accurate measurement of the arsenic flux], and (iii) from the temperature dependence of the vapour pressure of As_2 over GaAs [Foxon et al (1973), Goldstein et al (1976)]. These observations strongly suggest that the activation energy of the boundaries can be associated with the sublimation of chemisorbed arsenic (3.9 eV is comparable with chemical bond strengths). The fact that same activation energy characterised all of the activated phase boundaries shown in Figs 3.5 and 3.6 implies that the As-Ga bond was not severely strained under any of the reconstructions investigated.

Independent estimates of the strength of the As-Ga bond on the (100) surface can be derived from other properties. For example, Van Hove and Cohen (1987) have shown that both surface reconstruction and the arsenic overpressure influence the diffusion of Ga adatoms on GaAs, indicating that the diffusion co-efficient is a relatively weak function of temperature under the (2x4) reconstruction, but increases rapidly (with an activation energy of 4.0 eV) on crossing the boundary into the (1x1) reconstruction. This was taken to imply that some new bond-breaking process was operating, presumably liberating a proportion of the Ga atoms 'grown in' at island and vicinal step edges.

3.3 (v) Variation of Growth Rate

Figure 3.6 is the superposition of the surface phase diagrams of (100) GaAs for five fixed growth rates covering the range from 0.07 to 3.0 $\mu\text{m/h}$. Two points are of especial interest;

- (i) The activated phase boundaries are common to all growth rates, as would be expected from the mechanism proposed above.
- (ii) The low temperature decrease in the minimum flux ratio occurs at lower temperatures for lower growth rates. This behaviour is most probably related to the ability of the gallium and As_4 adatoms to migrate to appropriate sites before incorporation. For example, longer diffusion lengths may be expected at low growth rates (e.g. because of the reduction in surface population combined with the requirement for pairwise interaction), thus permitting lower growth temperatures (and the accompanying reductions in surface mobility) to be tolerated.

With reference to Fig 3.6, it is apparent that the low temperature deviation from the minimum flux ratio can be extrapolated to intersect the boundary between Regions III and V of the phase diagram. This intersection sets an upper limit to the growth rate at which GaAs can be deposited under the (2x4) or (1x1) arsenic stable reconstructions. Allowing for the use of a reasonable flux ratio, this limit is in excess of 60 $\mu\text{m/h}$, which is unlikely to be restrictive in practice.

3.4 Epilayer Properties and the GaAs Phase Diagram

The basic properties of GaAs epilayers grown in CLPIV under

'normal' conditions ($1 \mu\text{m/h}$, $T_{\text{subs}}=580-600^\circ\text{C}$, (2x4) reconstruction; i.e. within the upper range of temperatures encompassed by Region II) have already been described in Sec 3.2(ii). Essentially similar majority carrier properties were measured on all epilayers grown within Regions II and IIIa of the phase diagram [(2x4) and (1x1) reconstructions]; however, it is expected that the use of minimised As_4 fluxes and/or the higher growth temperatures associated with the (3x1) reconstruction would yield material with improved minority carrier properties [Grange (1985)]. No significant or reproducible variation in the oval defect density occurred on layers grown within Regions II or IIIa.

Epilayers grown in Region I [Mixed c(4x4)/(2x4) reconstruction] were also mirror shiny and, with the exception of oval defects, substantially undefected. However, these layers had poor electrical properties, often being highly resistive (with $N_D^+ - N_A^- \ll N_D$) even if doped at $1 \times 10^{17} \text{ cm}^{-3}$ with Si or Sn. This is illustrated by Fig 3.11, an electrochemical CV profile through a $2 \mu\text{m}$ thick Sn doped epilayer grown at $0.65 \mu\text{m/h}$ at an $\text{As}_4:\text{Ga}$ flux ratio of 5:1. The substrate temperature was increased from 450°C to 600°C in four steps during the deposition. The dips in $N_D - N_A$ accompanying the temperature steps were caused by transient changes in the Sn accumulation density. Note that the steady state carrier concentration was independent of the growth temperature at 500°C and above, but fell by 1.5 orders of magnitude at 450°C . This temperature is just within Region I of the phase diagram at the growth rate and flux ratio used (Fig 3.4, verified using RHEED during the deposition).

Several other workers have reported similar results [Murotani et al (1978), Stall et al (1980), Metze et al (1983), Missous and Singer (1986)], the consensus being that MBE grown GaAs becomes highly resistive or semi-insulating at growth temperatures below about 450°C because

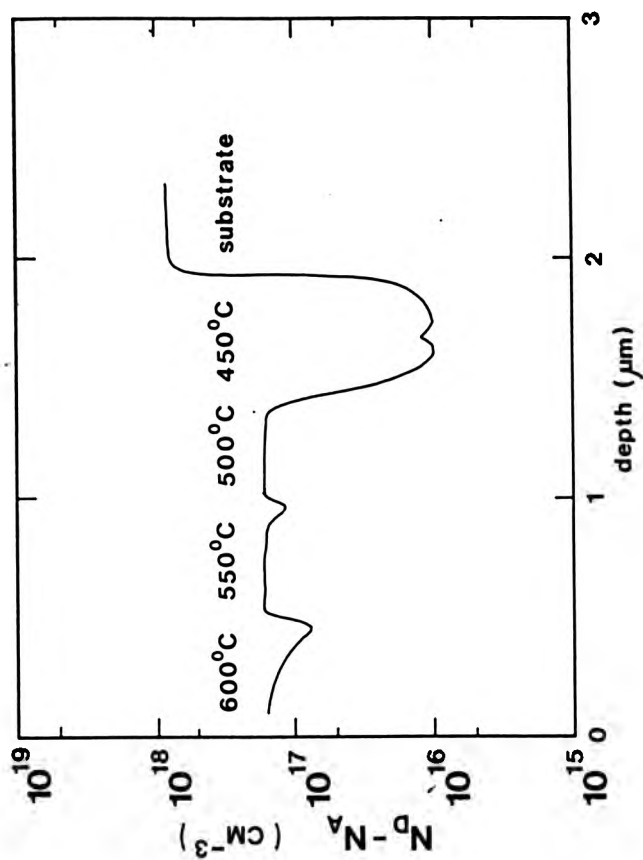


Fig 3.11 An electrochemical CV profile through a 2 μm thick Sn doped epilayer grown at $0.65 \mu\text{m/h}$ at an $\text{As}_2:\text{Ga}$ flux ratio of $5:1$. The growth temperature was increased from 450°C to 600°C in three steps.

of a sharp rise in the density of deep level traps. Metzger et al (1983) indicated that the minimum temperature permitting the growth of reasonable quality films decreased with the growth rate, being $\approx 450^{\circ}\text{C}$ at $0.2 \mu\text{m/h}$ and $\approx 380^{\circ}\text{C}$ at $0.02 \mu\text{m/h}$. As shown by Figs 3.6 and 3.11, these results are in agreement with the findings of this thesis. The advantage of using a phase diagram is that the activated boundary separating Regions I and II may be extrapolated to find the 'cut off temperature' at any desired growth rate and arsenic overpressure (Figs 3.5, 3.6).

Epilayers grown under a $(4 \times 2)/c(2 \times 8)$ reconstruction within Regions IV and V of the phase diagram were milky in appearance due to the presence of droplets of gallium metal (Fig 3.12) resulting from non-stoichiometric growth or, in Region V, non-congruent sublimation. Epilayers grown in Region IIIb (the temporally unstable area of Region III) were marred by elongated hillocks, similar in appearance to those seen on InAs grown under In-rich conditions (Chapter 4). As with oval defects, these features were aligned with the [011] direction. The exact appearance of the hillock features on GaAs was to some extent dependent on the arsenic flux, with 'terracing' becoming apparent at $\text{As}_4:\text{Ga}$ ratios in excess of about 10:1 (Fig 3.12).

3.5 Summary and Discussion

Si and Sn doped GaAs epilayers grown under 'normal' conditions (i.e. $\approx 1 \mu\text{m/h}$, $T_{\text{subs}} = 580\text{--}600^{\circ}\text{C}$, (2×4) reconstruction) showed bulk-like mobilities at carrier concentrations from $\approx 1 \times 10^{16} \text{ cm}^{-3}$ up to the maximum attainable doping level ($1.16 \times 10^{19} \text{ cm}^{-3}$ using Sn). Lightly doped material was compensated by an acceptor concentration of approximately $1.5 \times 10^{15} \text{ cm}^{-3}$. The highest electron mobilities [$\mu(300 \text{ K}) = 6 \times 10^3 \text{ cm}^2/\text{V-s}$, $\mu(77 \text{ K}) = 28 \times 10^3 \text{ cm}^2/\text{V-s}$] were obtained from epilayers doped to $N_{\text{D}} - N_{\text{A}} = 1 \times 10^{15} \text{ cm}^{-3}$. Unintentionally doped layers were always p-type,

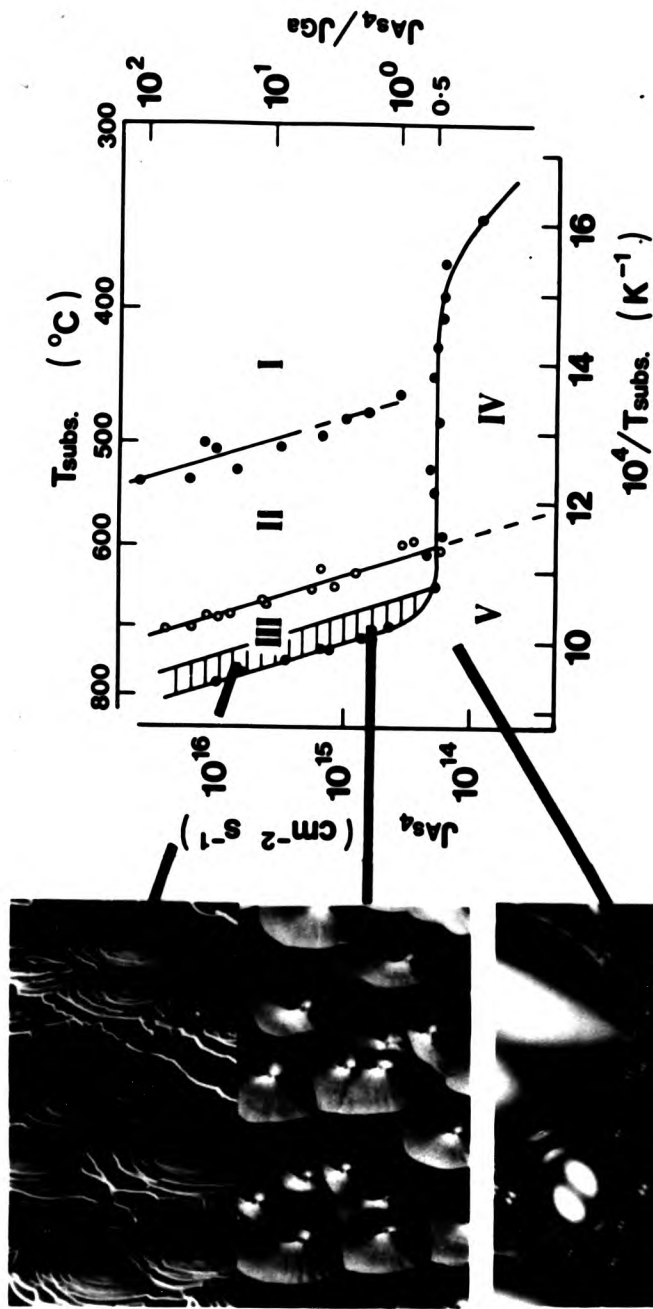


Fig 3.12 Showing the surface morphologies of 2 μ m thick epilayers grown within the temporally unstable area of Region III of the GaAs surface phase diagram.

with typical 300 K mobilities of 380 to 420 cm²/V-s at $1 \times 10^{15} \text{ cm}^{-3} < N_A - N_D < 3 \times 10^{15} \text{ cm}^{-3}$. Photoluminescence was used to identify carbon as the main unintentionally incorporated acceptor. Oval defect densities of between 1×10^3 and $1 \times 10^4 \text{ cm}^{-2}$ were obtained, according to the degree of oxidation of the Ga source charge.

The electrical properties of the doped layers were obviously limited by the (by 1987 standards) relatively high degree of compensation occurring at low doping levels. If, as was argued in Sec 3.2 (ii), this resulted from the incorporation of excited carbon species evolved from the graphite crucibles, some improvement may have been possible through the use of PBN crucibles in all of the high temperature sources. However, the electrical properties of the GaAs grown in CLPIV were superior to those of material grown in earlier home-built systems at CLP [Grange (1980), Kubiak (1983), Croydon (1985)], and the performance of the system was considered adequate for the purposes of this project.

The development of techniques to allow reproducible measurements of the growth temperature (Chap 2) and matrix fluxes (Sec 3.3) in CLPIV enabled a self-consistent MBE surface phase diagram to be constructed for (100) GaAs. This was the first such diagram to show the effects of all of the independently variable growth parameters, including the growth rate, in a systematic fashion. An absolute calibration of the As₄ flux was obtained by observing the (2x4)-to-(4x2) RHEED transition at the minimum As₄:Ga flux ratio (0.5:1) permitting stoichiometric growth. The substrate temperature was checked (see Chap 2) against the melting point of indium (157°C) and the GaAs oxide desorption temperature (580°C). On the basis of these calibrations, an activation energy of 3.8 eV was derived for the arsenic overpressure required to stabilise several surface reconstructions occurring within the range 400-800°C. This energy was identified with the bond-breaking involved in

the sublimation of chemisorbed arsenic, a conclusion supported by reference to independent measurements on related phenomena.

The onset of high trap densities in MBE GaAs grown at low temperatures was shown to occur as one of the activated phase boundaries (between the (2x4) and composite (2x4)/c(4x4) reconstructions) was crossed. The phase diagram allows this boundary to be extrapolated to any growth rate and As_4 overpressure. A second low-temperature phenomenon was also observed: the ability to grow under an arsenic stabilised reconstruction at an $As_4:In$ flux ratio of less than 0.5:1. The temperature at which this phenomenon first became apparent was found to increase with increasing growth rate. The slope of the increase is less than that of the activated phase boundaries and the results indicate that, unless an undiscovered effect occurs at growth rates in excess of $3 \mu\text{m/h}$, growth under the normal (2x4) reconstruction would not be possible at growth rates much in excess of $60 \mu\text{m/h}$. This is, of course, not a practical limitation.

Many workers [see, for example, Cho (1971a,b), Massies et al (1976), Panish (1980), Van Hove et al (1982, 1983, 1985), Schaffer et al (1983), Wood et al (1983b), Briones et al (1985)] have realised the value of specifying their MBE growth conditions against a system independent phenomenon, such as the boundary between two surface reconstructions. Several of these have produced GaAs phase diagrams as an aid to reproducing a given set of MBE growth conditions. The diagram presented in this thesis has three practical advantages: firstly, that the reported temperatures and fluxes are reasonably accurate; secondly, that the effects of varying the growth rate are included; and thirdly, that the Arrhenius type plot allows the data to be extrapolated to any desired growth rate. Taken together, these factors should allow the data to be used to calibrate the substrate heater of, for example, an MBE system of the type which

does not permit a thermocouple to be placed in intimate contact with the substrate (Chapter 2). The data may also be of use to cross-check pyrometer measurements. In the present study, the GaAs phase diagram was found to be of greatest value as a basis for comparison when investigating the growth of InAs. This aspect of the work is described in Chapter 4.

Chapter 4

An Investigation Into the Optimum Conditions for the Nucleation and Growth of (100) InAs by Molecular Beam Epitaxy.

Contents

- 4.1 Introduction
- 4.2 Experimental
- 4.3 The Nucleation of InAs on (100) GaAs
 - (i) Indium accumulation
 - (ii) Indium rich growth
 - (iii) Optimum growth conditions
 - (iv) Cross-hatched morphology
 - (v) Arsenic rich growth
 - (vi) Growth on GaAs buffer layers
- 4.4 Homoepitaxial Growth of InAs
 - (i) Growth on thick InAs buffer layers
 - (ii) Growth on (100) InAs substrates
- 4.5 The MBE Surface Phase Diagram of (100) InAs
 - (i) Surface reconstructions of (100) InAs
 - (ii) Nucleation phase diagram of InAs
 - (iii) Comparison with phase diagram of GaAs
 - (iv) Activation energy of the phase boundaries
- 4.6 Effects of Varying the Arsenic Species
- 4.7 Critique of Previous InAs Growth Studies
- 4.8 Summary and Discussion

4.1 Introduction

At the inception of this project there was, as described in Chapter 1, disagreement as to the optimum surface reconstruction to use at nucleation or during growth; little systematic understanding of the effects of varying the growth rate and other growth parameters; little experience of controlled doping; and only limited information on homoepitaxial growth available. Therefore, specific experiments were undertaken (i) to determine the functional relationship between the MBE growth parameters, epilayer properties and the surface reconstruction during growth, and (ii) to find out which non-optimum growth conditions are intrinsic to InAs and which result from difficulties in nucleating the severely mis-matched (100) InAs/GaAs heterojunction. Subsequent work on the controlled doping and electrical characterisation of InAs is reported in Chapter 5.

4.2 Experimental

The general procedures used when operating CLP IV have already been described in Chapter 2, and the techniques used to calibrate the matrix fluxes in Sec 3.3 (i) of Chapter 3. It is worth repeating that the As_4 flux was calibrated against the boundary between the (2x4) and (4x2) surface reconstructions when growing InAs (and GaAs) at low substrate temperatures. The $As_4:GpIII$ flux ratio at this boundary was taken to be 0.5:1 [e.g. using the results of modulated beam studies, Foxon et al (1978)]. Any discussion of the '0.5:1 flux ratio' in this chapter is, therefore, to some extent self-referential (although the detailed discussion in Sec 3.3 (i) should also be noted).

It should also be noted that the Hall properties quoted in this chapter were derived from measurements made at $B_H=0.3$ T and $I_H=1.0$ mA on etched cross samples. Such

measurements can considerably underestimate the Hall mobility in lightly-doped heteroepitaxial InAs, principally because of the effects of parallel conduction through electron accumulations at the free surface and the epilayer/substrate interface [Washburn et al (1979)]. This subject is treated in detail in Chapter 5.

4.3 The Nucleation of InAs on (100) GaAs .

To obtain basic data, a series of undoped InAs epilayers were grown on semi-insulating (100) GaAs substrates (and on undoped GaAs buffer layers) using a fixed growth rate of $2.0 \pm 0.1 \mu\text{m/h}$ and a wide range of growth temperatures and As_4 :In flux ratios. Figure 4.1 illustrates the correlation between morphology, reconstruction and growth conditions. Five distinct growth regimes were identified. In overview, epilayers grown within the As_4 -rich, In-rich and In-accumulated regimes were severely defected, often being milky or even matt grey in appearance. These layers had, where measurable, poor electrical properties. Epilayers grown within the cross-hatched¹ and optimum regimes were mirror-shiny, but only those grown under optimum conditions exhibited high Hall mobilities. As shown in Figure 4.1, the boundary separating the cross-hatched and optimum growth regimes from the In-rich and In-accumulation regimes was delineated by a transition to a (4x2) surface reconstruction. A (1x1) or (2x4) reconstruction was obtained during growth within the optimum, cross-hatched and (slightly) arsenic rich regimes. No clear reconstruction boundary separated the optimum and X-hatch growth conditions from the As_4 -rich regime, and the dashed line included in Fig 4.1 is only intended as a guide for the eye. None-

¹ 'cross hatched' refers to the microscopic appearance of the epilayers grown in this regime, e.g. see Fig 4.5

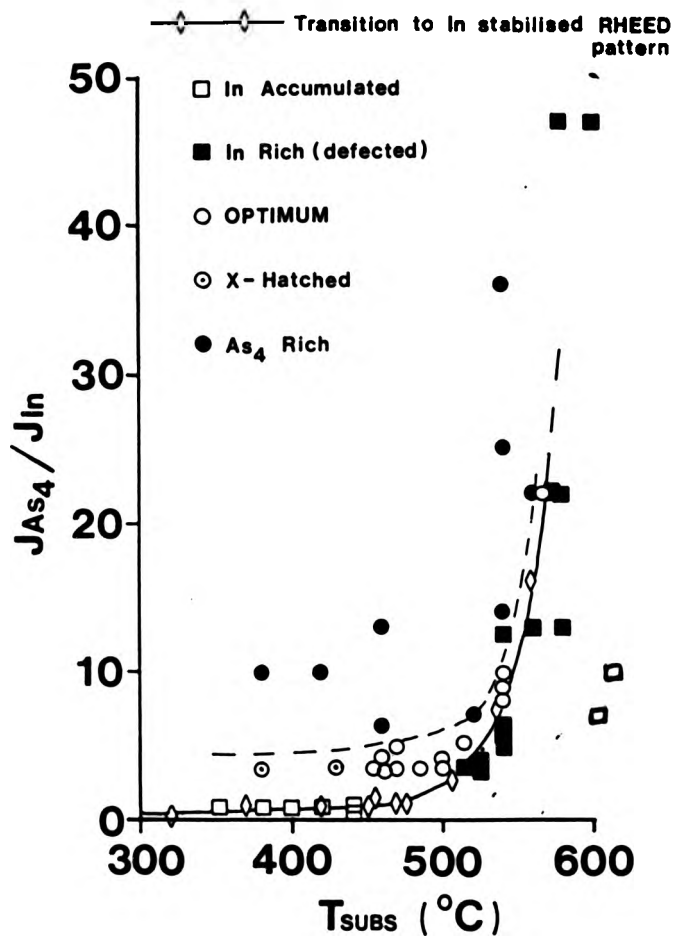


Fig 4.1 The effects of varying the substrate temperature and As₄:In flux ratio on the nucleation of InAs on (100) GaAs at a growth rate of 2 μm/h.

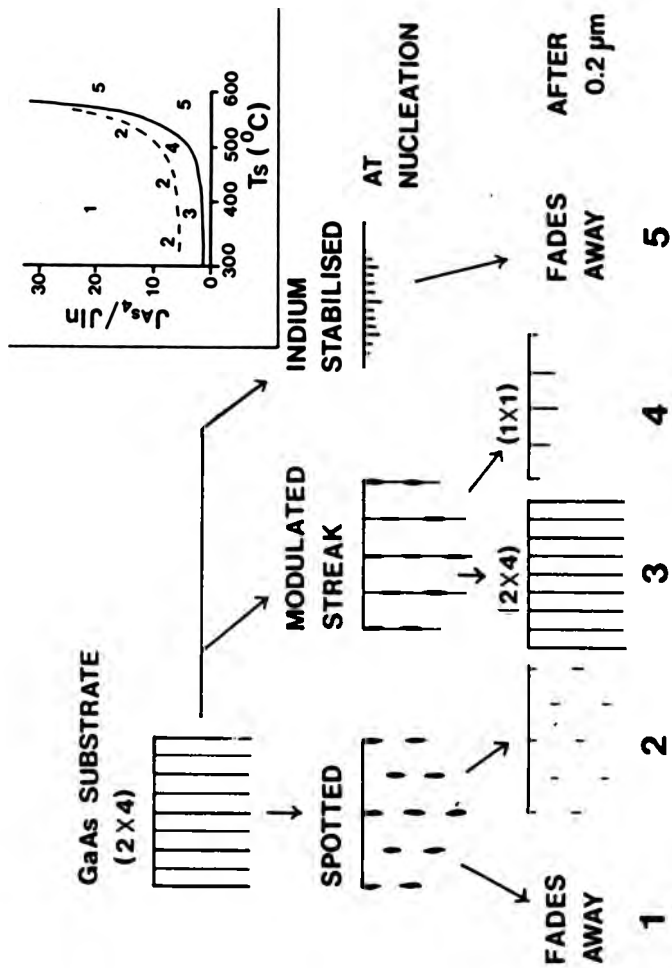


Fig 4.2 The development of the RHEED pattern in the [011] azimuth following the nucleation of InAs on (100) GaAs. Figure 4.1 is shown as an inset.

theless, as shown by Fig 4.2, it was usually possible to identify each growth condition from the development of the RHEED pattern immediately after nucleation. Growth under each regime will now be described in detail.

4.3 (i) Indium accumulation

Referring to Fig 4.1, indium accumulation occurred whenever $As_4:In$ flux ratios of less than 0.5:1 were used. Accumulation also occurred whenever growth temperatures in excess of $600^{\circ}C$ were used at $2 \mu m/h$, irrespective of the flux ratio. All accumulated layers were milky in appearance, due to the presence of indium droplets resulting from non-stoichiometric growth or sublimation. At nucleation, the (2×4) or $c(4 \times 4)/(2 \times 4)$ reconstruction of the GaAs substrate transformed to a rapidly fading (4×2) InAs pattern (Fig 4.2), as observed by Schaffer et al (1983).

4.3 (ii) Indium Rich Growth

NB: The terms 'indium rich' and 'arsenic rich' growth are used throughout this thesis for consistency with earlier reports [Schaffer et al (1983), Kubiak et al (1984a)]. These terms do not refer to the stoichiometry of the epilayers so described.

Indium rich growth occurred when using $As_4:In$ flux ratios greater than 0.5:1 at temperatures below those leading to accumulation,[†] but still high enough to result in the formation of a (4×2) InAs reconstruction immediately after nucleation (Figs 4.1, 4.2). All epilayers grown under these conditions were at best slightly milky in appearance, due to the presence of hillocks aligned with the $[011]$ direction (Fig 4.3a); similar defects have been observed on In-rich InAs by Yano et al (1977) and Kubiak et al (1984a). Referring back to Chapter 3 of this thesis, it will be seen

[†] $600^{\circ}C$ at $2 \mu m/h$

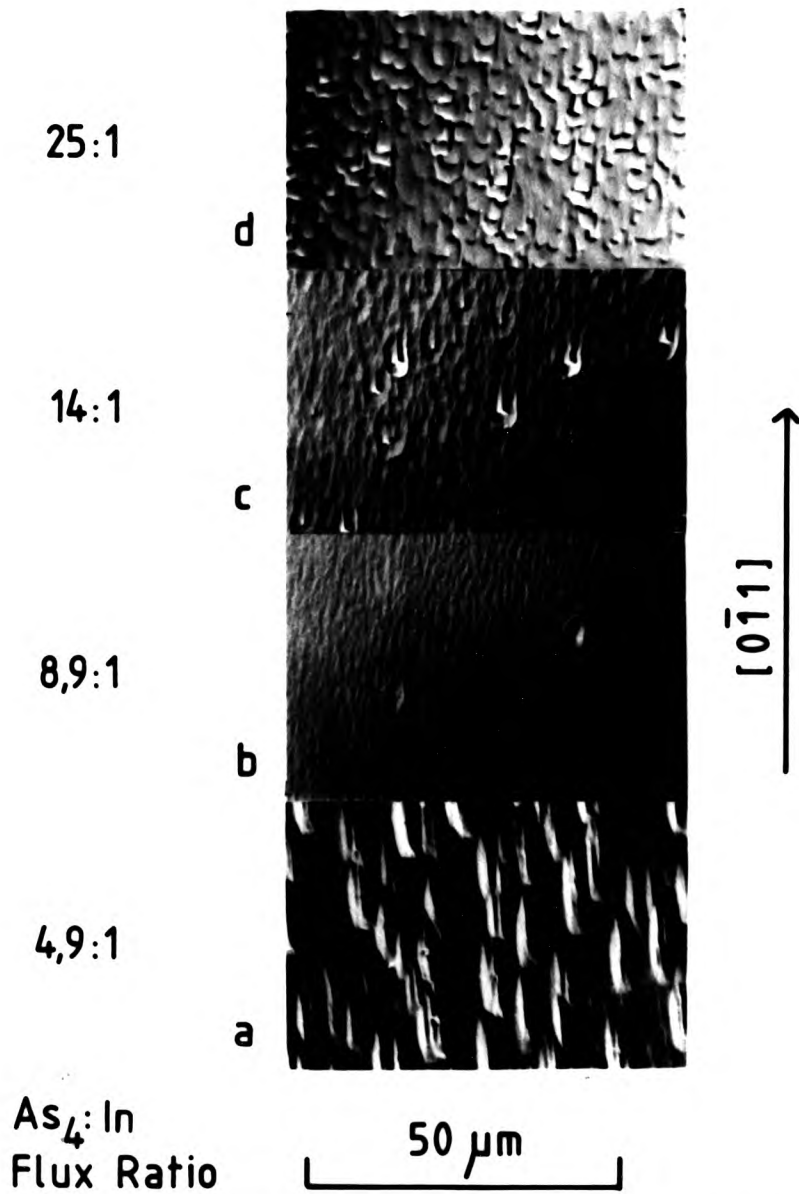


Fig 4.3 Normaski phase contrast micrographs of 2 μm thick InAs epilayers grown on (100) GaAs substrates at 2 $\mu m/h$ using a substrate temperature of 540°C: (a) In rich growth; (b) optimum conditions; (c) slightly As_4 rich growth; (d) severely As_4 rich conditions.

GaAs

InAs

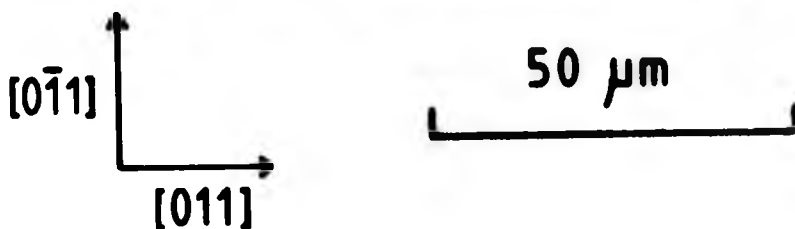


Fig 4.4 Normarski micrographs of (a) In-rich (100) InAs and (b) GaAs grown within the temporally unstable area of Region III of the (100) GaAs MBE phase diagram (Chapter 3). Both epilayers were $\sim 2 \mu\text{m}$ thick. Comparison of Figs 3.5 and 4.8 will show that the two growth conditions are equivalent.

that similar defects were present on GaAs grown within the temporally unstable area of Region III of the GaAs phase diagram (Figs 3.12, 4.4); in both cases, the defects resulted from growth at temperatures just in excess of T_{nc} at $JAs_4:JIn > 0.5:1$.

Unintentionally doped InAs grown under In-rich conditions was n-type with 300K Hall mobilities of between 4×10^3 and 1×10^4 $cm^2/V-s$ at $1 \times 10^{16} < N_D - N_A < 1 \times 10^{17} cm^{-3}$. The corresponding 77K mobilities ranged from 5×10^3 to 2×10^4 $cm^2/V-s$ (note that the properties of excessively defected layers have been excluded from these and subsequent assessments). It was not possible to find a combination of substrate temperature and $As_4:In$ flux ratio, within the range encompassed by Fig 4.1, which would allow the growth of substantially undefected InAs under a (4x2) reconstruction at a growth rate of $2 \mu m/h$.

4.3 (iii) Optimum Growth Conditions

The optimum growth regime yielded mirror-shiny and substantially undefected epilayers. As shown in Fig 4.1, these layers were grown at temperatures in the range $450-550^\circ C$ (at $2 \mu m/h$) using As_4 fluxes close to the minimum permitting stoichiometric growth. On commencing growth the streaked RHEED pattern of the GaAs substrate was preserved for a few seconds before transforming into bulk diffraction spots, indicating island nucleation. These spots elongated into bulk streaks over a period corresponding to between 150 and 350 Å of overgrowth (Fig 4.2). It was usual for bulk streaks to be retained throughout growth under optimum conditions, although a faint (2x1) reconstruction was sometimes visible. NB: It is possible to grow continuous coverages of strained but undислоated InAs on (100) GaAs substrates up to a critical thickness of about 50 Å [Houzay et al (1987), Munekata et al (1987)]. This accounts for the brief delay before the formation of bulk diffraction spots

at nucleation in the present experiments.

Figure 4.3b shows the morphology of a typical epilayer grown under optimum conditions. A slight background ripple is apparent: this was seen on all heteroepitaxial material and is believed to result from the large epilayer/substrate mismatch. The photograph also shows a few small defects, similar in appearance to the oval defects seen on MBE grown GaAs. This type of defect has not previously been reported on MBE grown InAs, and was only observed on optimum quality material. It is unlikely that the InAs ovals are vestigial In-rich defects as the latter were faceted, whereas the ovals were smooth and (for a given film thickness) somewhat smaller.

Typically, oval defect densities of between 8×10^2 and $3 \times 10^3 \text{ cm}^{-2}$ were obtained on InAs epilayers grown under optimum conditions at $2 \mu\text{m/h}$. This is a significant reduction on the oval defect densities of 1×10^3 to $1 \times 10^4 \text{ cm}^{-2}$ obtained on GaAs epilayers of similar thicknesses ($\approx 2 \mu\text{m}$) grown in parallel experiments. This may be related to the differing behaviour of the Ga and In suboxides in source charges. Prior et al (1984) have used thermodynamics to show that, at normal cell temperatures, the native oxide of In (In_2O_3) is almost all converted to In_2O via a reaction with the indium charge. In_2O is sufficiently volatile that (after normal outgassing procedures) oxygen contamination from the indium cell is unlikely to be a problem. Conversely, Ga_2O_3 and Ga_2O are persistent contaminants in MBE cell charges [Prior et al (1984)] and are frequently cited as a source of oval defects [Chai and Chow (1981), Kirchner et al (1981), Ito et al (1984)].

All unintentionally doped epilayers grown at $2 \mu\text{m/h}$ under optimum conditions were n-type. Maximum 77K Hall mobilities of $60 \times 10^3 \text{ cm}^2/\text{V-s}$ at $N_D - N_A \geq 5 \times 10^{15} \text{ cm}^{-3}$ were obtained from layers with thicknesses greater than $5 \mu\text{m}$. As shown in

Fig 4.1, optimum quality epilayers could be grown at temperatures in excess of 520°C so long as sufficient arsenic was supplied to stabilise the epilayer surface. No advantage was found in doing this, as there was no improvement in electrical properties under these conditions and the temperature range permitting optimised growth became excessively narrow.

4.3 (iv) Cross-Hatched Morphology

The use of minimised As₄ fluxes at lower substrate temperatures (e.g. 300-450°C at 2 μm/h) led to the growth of mirror-shiny epilayers under a clear (2x4) reconstruction (following a nucleation sequence similar to that seen under optimum conditions, described above and shown in Fig 4.2). These films generally, although not always, showed a cross-hatched morphology (Fig 4.5) reminiscent of that seen on InGaAs epilayers compressively mis-matched to InP substrates [Cheng et al (1981)]. Munekata et al (1987) have also reported cross-hatching on MBE-InAs grown at low substrate temperatures. The 300K mobilities of InAs epilayers (whether cross-hatched or not) grown under this regime were always lower than 1x10⁴ cm²/V-s at N_D-N_A>1x10¹⁶ cm⁻³. The 77K mobilities were always less than 25x10³ cm²/V-s. The MBE growth of InAs at low substrate temperatures has been investigated in detail by Meggitt et al (1978, 1979, 1980) and Grange et al (1979, 1980).

4.3 (v) Arsenic Rich Growth

Arsenic rich growth occurred at low substrate temperatures and/or high As₄ fluxes (Fig 4.1). As before, the streaked RHEED pattern of the GaAs substrate transformed to bulk spots almost immediately after nucleation (Fig 4.2), indicating island nucleation. Under extreme conditions (i.e. JAs₄:JIn>10:1 at 450°C) these spots faded rapidly, disappearing within the first few hundred Angstrom of

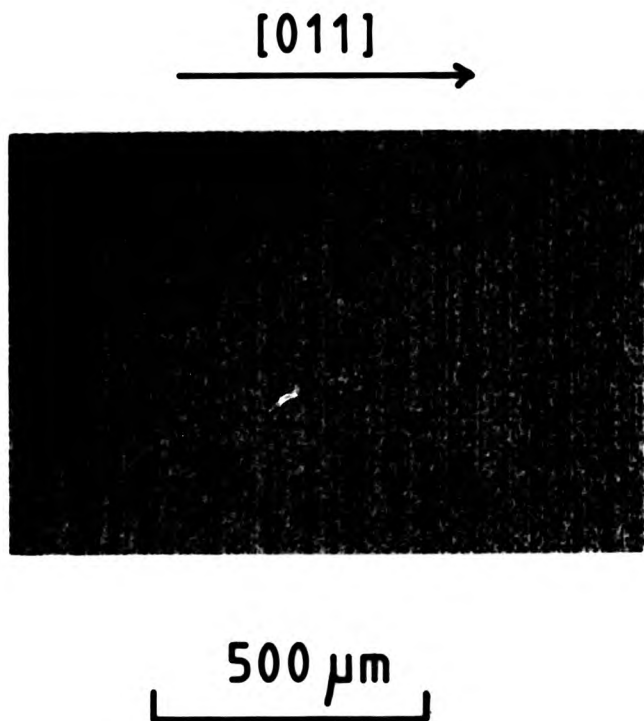


Fig 4.5 Cross-hatched morphology on a $2\mu\text{m}$ thick InAs epilayer. The grid pattern was most clearly visible at low magnifications.

overgrowth. Layers grown under these conditions were chalky in appearance, and were easily scraped from the substrate using a scalpel blade.

Under less extreme conditions (i.e. $\text{JAs}_4:\text{JIn}=6:1$ at 450°C) the RHEED diffraction spots formed at nucleation were preserved throughout growth (Fig 4.2; the spots were separated by spacings appropriate to the (2×1) or (1×1) reconstructions, according to the severity of the growth condition). Occasionally, under conditions close to those required for optimum or X-hatched growth, the RHEED spots coalesced into bulk streaks or a (2×4) reconstruction. Films grown under these conditions showed characteristic 'horseshoe' defects (Fig 4.3 c,d). SIMS [Kubiak et al (1984a)], Normanski and SEM (Fig 4.6) investigations have revealed these features to be asymmetrical C-shaped hillocks, surrounding irregularly shaped holes which extend to the epilayer/substrate interface. The density of horseshoe defects increased with increasing As_4 flux, decreased with increasing substrate temperature, and was independent of the oval defect density of any underlying GaAs buffer layer.

The electrical properties of As_4 rich epilayers were poor, with maximum 77K mobilities of about $40\times 10^3 \text{ cm}^2/\text{V-s}$ at $N_D - N_A = 1\times 10^{16} \text{ cm}^{-3}$ being obtained from lightly defected epilayers grown under near-optimum growth conditions (e.g. leading to a morphology similar to that shown in Fig 4.3c). The electron mobility decreased rapidly with increasing horseshoe defect density, so that a 77K mobility of $12\times 10^3 \text{ cm}^2/\text{V-s}$ at $8\times 10^{16} \text{ cm}^{-3}$ (as obtained from the layer shown in Fig 4.3d) should be considered more typical.

4.3 (vi) Effects of GaAs Buffer Layers

Within experimental error, it was found that the use of undoped GaAs buffer layers had no effect on the electrical



Fig 4.6 Scanning electron micrograph of 'horseshoe' defect on As_4 -rich heteroepitaxial InAs grown by MBE.

properties of InAs epilayers grown under the optimum, X-hatch, In-rich or As₄-rich conditions. This result conflicts with earlier reports [Meggitt (1979, 1980), Grange (1979, 1980)] that the use of GaAs buffer layers can result in increases of up to 25% in the Hall mobilities of InAs epilayers. However, the MBE systems used by Meggitt and Grange were not load-locked, and so had to be baked after every substrate exchange. This almost certainly caused the oxide caps on the substrates to become contaminated. In these circumstances, a GaAs buffer would serve to isolate the InAs epilayer from any residual contaminants left after in-situ thermal cleaning.

Referring to the present experiments, the use of undoped GaAs buffer layers was not found to alter the functional relationships shown in Fig 4.1.

4.4 Homoepitaxial Growth of InAs

The experiments described above could not distinguish between the non-optimum growth regimes intrinsic to InAs and those caused by nucleation problems in heteroepitaxy. To investigate this aspect of growth, InAs was deposited onto (100) InAs substrates and also onto good quality InAs buffer layers grown on (100) GaAs.

4.4 (i) Growth on InAs buffer layers

0.5 μm thick InAs buffer layers were nucleated and grown on (100) GaAs under optimum conditions in order to provide homoepitaxial 'substrates'. The mirror-like surfaces of these layers were not marred even when high arsenic fluxes were used during subsequent overgrowths. For example, specular material could be grown at As₄:In flux ratios as high as 40:1 when using substrate temperatures in the range 400°C to 500°C at a growth rate of 2 μm/h. Stable (2x4) or

(1x1) RHEED patterns were obtained under these conditions, according to the substrate temperature. Figure 4.1 shows that severely arsenic rich layers would have resulted from nucleation on (100) GaAs under the same conditions. The experiment was repeated at several growth rates in the range 1 $\mu\text{m/h}$ to 5 $\mu\text{m/h}$ with the same results. In contrast, it was found that no thickness of InAs buffer layer made undefected growth under a (4x2) reconstruction possible. Hancock and Kroemer (1984) and Sugiyama (1986) have also implied that arsenic rich growth is a nucleation condition which does not apply to homoepitaxy.

4.4 (ii) Growth on (100) InAs substrates

Additional results were obtained by growing InAs directly onto (100) InAs substrates. These results support the conclusions drawn above, although the poor surface finish of the InAs substrates used (obtained from MCP Electronic Materials Ltd.) impeded interpretation to some extent. Figures 4.7a and 4.7b show typical wafer surfaces 'as recieved'. Before use, the substrates were degreased in 111-trichloroethylene, acetone and methanol and etched for one to two minutes in either cold $30\text{H}_2\text{SO}_4:1\text{H}_2\text{O}_2:1\text{H}_2\text{O}$ or a weak (approx. 0.5%) solution of bromine in methanol [also used by Sugiyama (1986)]. Neither treatment noticeably worsened the surface roughness of the substrates (Figs 4.7c, 4.7d).

Whichever etch was used, the substrates cleaned up to give diffuse (1x1) bulk streaks at about 520°C under As_4 fluxes of between 1×10^{15} and $1 \times 10^{16} \text{ cm}^{-2} \text{ s}^{-1}$. A (2x4) reconstruction could sometimes be obtained by cooling below about 450°C after the substrate had cleaned up, although it was normal for the bulk streaks to be preserved. However, a weakly reconstructed surface could almost always be obtained following the deposition of a few tens of monolayers of InAs: the intensity of the RHEED pattern then

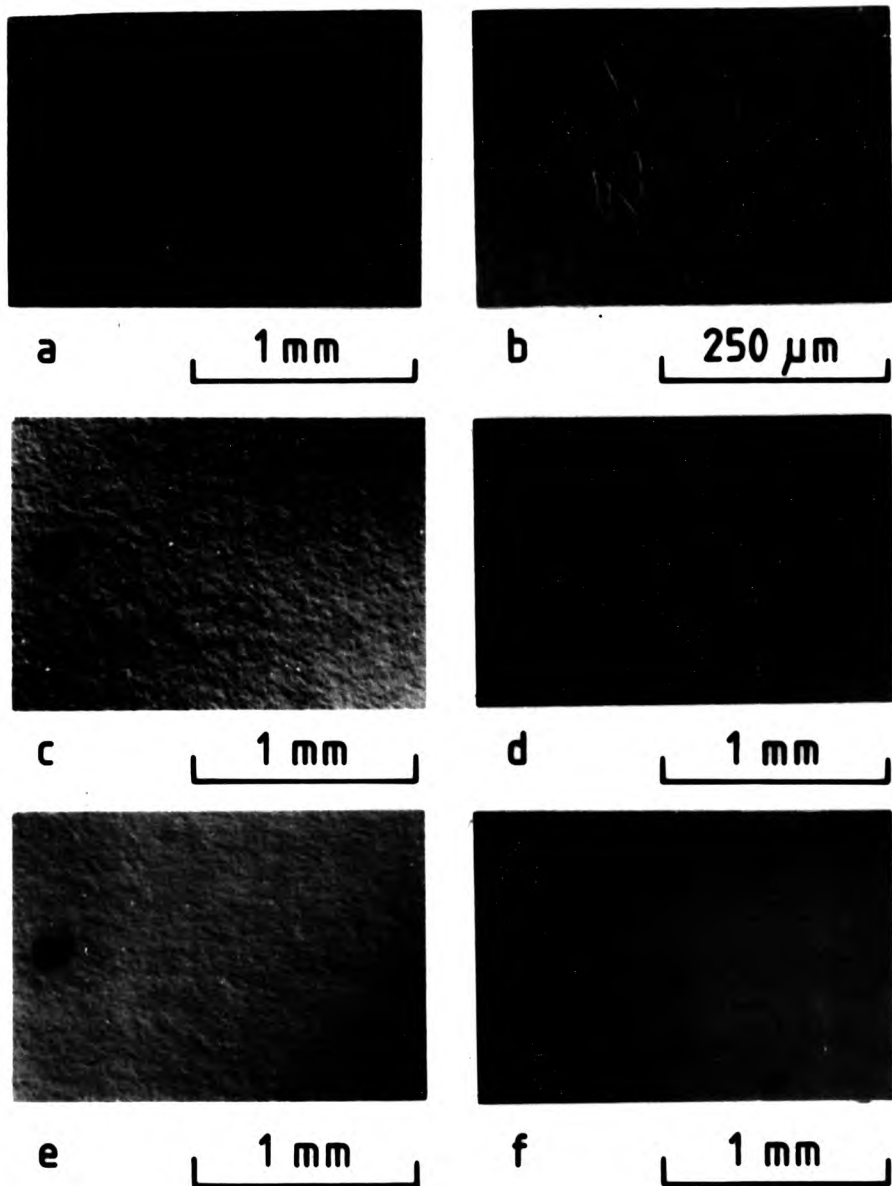


Fig 4.7 Homoepitaxial growth of InAs by MBE;
 (a,b) (100) InAs substrates as recieved
 (c) after etching in 0.5% bromine in methanol
 (d) after etching in $30\text{H}_2\text{SO}_4:1\text{H}_2\text{O}_2:1\text{H}_2\text{O}$
 (e) (c) after 1.2 μm of overgrowth
 (f) (d) after 1.2 μm of overgrowth

increased slowly with further deposition. Obviously, any information obtained from further growth on this buffer could equally well have been obtained from InAs grown on a GaAs substrate. More important is the fact that, outside of the In-accumulated and In-rich regimes indicated on Fig 4.1, the homoepitaxial nucleation of InAs was not noticeably affected by the $As_4:In$ flux ratio. Figures 4.7 e & f show the morphology of a 1.2 μm thick homoepitaxial layer nucleated at 450°C at a growth rate of 2 $\mu m/h$ and an $As_4:In$ flux ratio of $\approx 15:1$. Figure 4.1 shows that these conditions lie well inside the As_4 rich growth regime. Nevertheless, the surface of the epilayer reproduced the surface of the substrate (cf. Figs 4.7 a-f) and no arsenic rich growth features (as shown in Fig 4.3d) were noticeable. These results support the idea that 'arsenic rich growth' is not intrinsic to InAs, but a result of using non-optimum nucleation conditions in heteroepitaxy.

Some conclusions may be drawn about the mechanism by which excessive arsenic fluxes hamper homoepitaxial nucleation. As indicated in Sec 4.3 (iii), the growth of InAs on (100) GaAs proceeds by the coalescence of 3-D islands which result from the dislocation of an initially continuous 2-D overgrowth [this has been demonstrated using SEM, Meggitt (1979) and TEM, Houzay et al (1986)]. Assuming that the behaviour of In on InAs is essentially similar to that of Ga on GaAs, high surface populations of arsenic molecules may be expected to hinder the coalescence of these islands by severely limiting the diffusivity of the In adatoms [Neave et al (1985)]. Any discontinuities in the layer formed at this stage can reasonably be expected to halt the propagation of step edges during subsequent overgrowth, so forming holes through the epilayer. These may be manifest as the 'horseshoe' defects seen on As_4 -rich InAs [Kubiak et al (1984a), see also Sec 4.3 (v)].

The effects of high arsenic fluxes on homoepitaxial growth

are less significant, probably because layer-by-layer growth can commence at nucleation and no mechanism exists for the pinning of step edges. Nonetheless, the use of high group V fluxes should be avoided when growing InAs or any other III-V compound: as noted in Chapters 1 and 3, there is a consensus that most III-V compounds should be grown under minimised group III fluxes at as high a temperature as possible [Grange (1985)].

4.5 The MBE Surface Phase Diagram of (100) InAs

The experiments reported so far have identified the optimum conditions for nucleating InAs on (100) GaAs at a growth rate of 2 $\mu\text{m/h}$. The most practical way to extend this result to other growth rates is to note that optimised nucleation requires the use of substrate temperatures just below those which would result in In-rich growth (Fig 4.1). The upper limit of this range of temperatures is clearly marked by a transition between the (1x1) and (4x2) surface reconstructions, which is easy to map out using RHEED.

Schaffer et al (1983) were the first to specify the nucleation conditions of heteroepitaxial InAs with respect to a boundary between two surface reconstructions, and also the first to construct phase diagrams to show the existence regions of the major surface reconstructions of (100) InAs. Their phase diagrams employed the same axes as Fig 4.1 (i.e. $J_{\text{As}_4}/J_{\text{In}}$ versus growth temperature), but were mapped out by varying the growth rate at two fixed arsenic fluxes. This presentation is inconvenient, as most epitaxists use a fixed growth rate; furthermore, neither Schaffer's diagrams or Fig 4.1 are suitable for extrapolation. For this reason, an Arrhenius-type InAs MBE phase diagram (Fig 4.8) was constructed during the present study. As shown in Chapter 3, this type of diagram is easy to extrapolate to growth rates and/or arsenic fluxes other than those directly investigated.

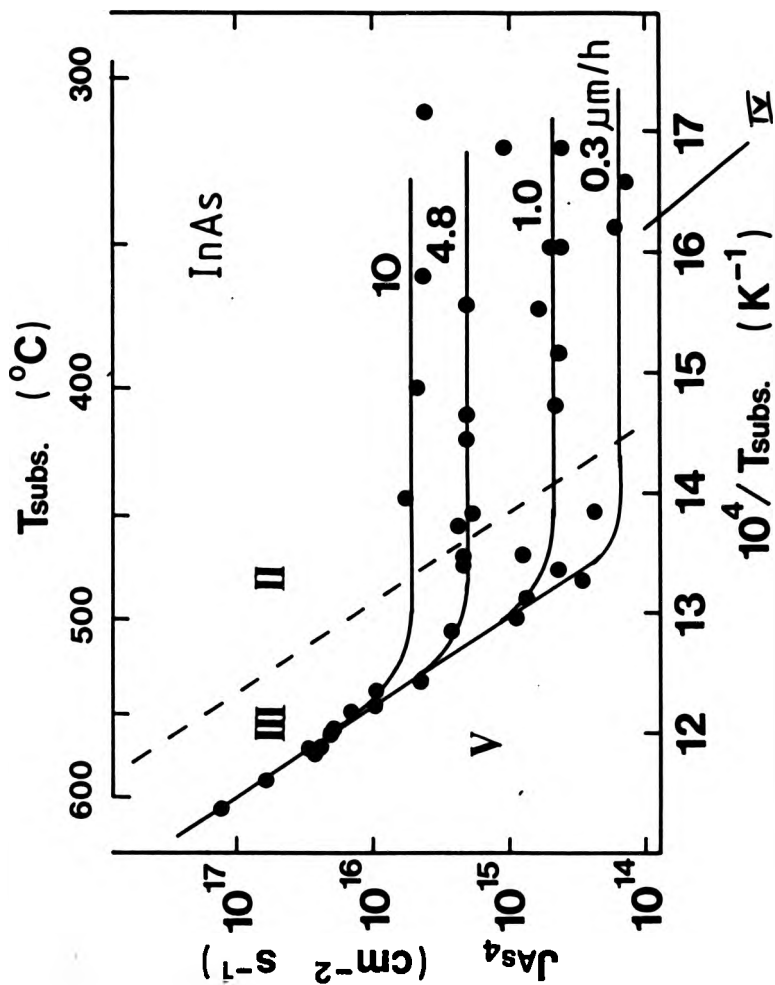


Fig 4.8 The MBE surface phase diagram of (100) InAs at growth rates (indicated beside each curve) of 0.3, 1.0, 4.8 and 10 $\mu\text{m/h}$.

The RHEED observations were made on undoped InAs buffer layers, of minimum thickness $0.5 \mu\text{m}$, nucleated under optimum conditions on (100) GaAs substrates. The experimental techniques employed were identical to those used when constructing the GaAs phase diagram described in Chapter 3. In brief, the reconstruction boundaries were mapped out at four fixed growth rates (0.3, 1.0, 4.8 and $10 \mu\text{m/h}$) by changing the As_4 flux at a series of fixed substrate temperatures and vice versa. The phase boundaries were approached from both directions (i.e. by both increasing and reducing the As_4 flux or substrate temperature) in order to check for hysteresis.

4.5 (i) The Surface Reconstructions of (100) InAs

The reconstructions seen in Regions II, III, IV of Fig. 4.8 correspond to those seen in corresponding regions of the MBE phase diagram of (100) GaAs, i.e.

Region II	(2x4)
Region III	(1x1) bulk streaks
Regions IV & V	(4x2)

The low-temperature composite (2x4)/c(4x4) reconstruction seen in Region I of the GaAs phase diagram was not sought on InAs in the experiments reported here; however Tsang and Chui (1986) have seen a c(4x4) reconstruction on InAs at (unspecified) low temperatures in the absence of an In flux. Schaffer et al (1983) have reported that (3x1) and (3x2) reconstructions can be seen on InAs at very low growth rates. These reconstructions were not seen when mapping out Fig 4.8 but, with reference to Schaffers' results, may be expected to occur in a narrow band of temperatures separating Regions III and V. As described in Sec 3.3 (ii), a (3x1) reconstruction is seen on (100) GaAs under equivalent conditions.

Closely similar (4x2) RHEED patterns were seen in Regions IV and V of the InAs phase diagram. Conversely, the patterns seen in Regions IV and V of the GaAs phase diagram (Fig 3.10) were easily distinguishable, although both corresponding to a (4x2)/c(2x8) periodicity. It is not felt that this indicates any fundamental difference in the behaviour of InAs and GaAs during MBE, as the surface of heteroepitaxial InAs was always slightly textured even if nucleated under optimal conditions (Fig 4.3b) and this will have reduced the definition of the InAs RHEED patterns. Nonetheless, the major phase transitions on (100) InAs (i.e. between the (2x4) and (1x1) or the (1x1) and (4x2) reconstructions) were always clearly defined.

4.5 (ii) The 'Nucleation Phase Diagram' of (100) InAs

It would be possible to construct a 'nucleation phase diagram' for (100) InAs/GaAs: this would involve re-drawing Figure 4.8 with added constraints to the usable range of As_4 fluxes at each growth rate. However, Fig 4.8 contains sufficient information for most purposes because, as previously noted, the optimum nucleation conditions simply follow the boundary between Regions III and V: i.e. for best results in heteroepitaxy the grower should nucleate under a minimised As_4 flux just within the elbow of the As_4 -to-In stabilisation curve appropriate to the growth rate.

4.5 (iii) Comparison with the phase diagram of (100) GaAs

The phase diagrams of (100) InAs (Fig 4.8) and (100) GaAs (Fig 3.5) are, although scaled differently, essentially similar. The similarity is not confined to the overall form of the phase diagram: the results presented above, and in Chapter 3, show that homoepitaxial epilayers of InAs and GaAs have similar morphologies provided that they are grown

within equivalent regions of their respective phase diagrams (i.e. under the same surface reconstructions). In particular;

- (i) Accumulations of In and Ga occurred on the surfaces of both InAs and GaAs whenever growth temperatures considerably in excess of T_{nc} or GpV:GpIII flux ratios of less than 0.5:1 were used. (4x2) surface reconstructions were seen in both cases, corresponding to growth in Regions IV and V.
- (ii) The defects seen on In-rich InAs epilayers were similar to those seen on GaAs epilayers grown in the temporally unstable area of Region III of the (100) GaAs phase diagram (Sec 3.4, Sec 4.3 (ii), see also Fig 4.4). Again, essentially identical growth conditions were involved: in both cases the GpV:GpIII flux ratio, although in excess of 0.5:1, was just insufficient to maintain an arsenic stable reconstruction at a high growth temperature.
- (iii) Mirror-shiny, substantially undefected homoepitaxial InAs and GaAs epilayers could be grown under the (2x4) and (1x1) surface reconstructions, i.e. within Regions II and III of their respective surface phase diagrams, but not under the (4x2) reconstruction occurring in Regions IV and V.

These results indicate that there are no significant differences between the MBE growth behaviour of (100) InAs and (100) GaAs. This conclusion is also supported by the results of modulated beam studies [Foxon and Joyce (1978)].

4.5 (iv) Activation energy of the Phase Boundaries

Figure 4.9 shows the activated boundary separating the (1x1) and (4x2) reconstructions. This data was replotted

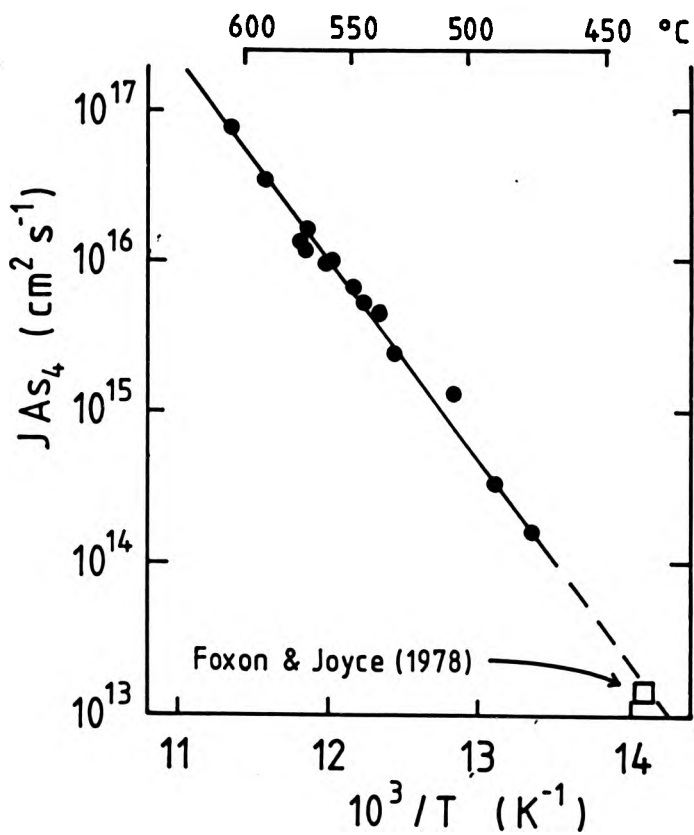


Fig 4.9 The activated phase boundary separating the (1x1) and (4x2) reconstructions on InAs. Note the excellent qualitative agreement with the result of Foxon and Joyce (1978).

from the InAs phase diagram, and includes measurements made at $JAs_4:JIn > 2:1$ at growth rates of 0.3, 1.0, 4.8 and 10 $\mu\text{m/h}$. The As_4 flux is, therefore, calibrated (with respect to the 0.5:1 minimum flux ratio) at four points within the range of fluxes investigated. The estimated position of the boundary is in good agreement with the measurements of Foxon and Joyce (1978).

The activation energy derived from Fig 4.9 is 2.6eV. In Chapter 3 it was argued that the slope of the activated phase boundaries on GaAs is determined by the energy required to free chemisorbed surface arsenic. The differing activation energies obtained from GaAs (3.9 eV, Sec 3.3 (iv)) and InAs (2.6 eV) are consistent with the relative bond strengths of the two compounds [Hilsun and Rose-Innes (1961)]. Nonetheless, 2.6 eV is considerably higher than previous estimates of the activation energy of the phase boundaries of InAs [e.g. 1.8 eV, Schaffer et al (1983) and 1.6 eV, Sugiyama (1986)]. Confidence in the new result can be justified,

- (i) because of the care taken to obtain reasonably accurate measurements of the substrate temperature in these experiments (e.g. see Sec 2.4), and
- (ii) because the estimates of the characteristic energy of the activated phase boundaries of GaAs, made using the same techniques and in the same apparatus, are in excellent agreement with independent estimates derived from related phenomena [Cho (1971), Goldstein et al (1976)].

As the techniques used to estimate the As_4 flux by Schaffer et al (1983) and Sugiyama (1986) were similar to those used for the work reported here, it is most likely that the earlier studies underestimated the activation energy because of the difficulties involved in measuring the substrate temperature.

4.6 Effects of varying the Arsenic Species

Thermally generated As_4 was used for all experiments reported in this thesis. It is unlikely that using As_2 would have had much affect on the overall form of the surface phase diagram which, as noted above, is largely determined by the thermal sublimation of chemisorbed arsenic. However, it is possible that the nucleation of InAs on GaAs may be affected by the arsenic species. Specifically, the longer surface lifetime and easier availability of arsenic atoms from As_2 [Foxon and Joyce (1981)] may result in shorter diffusion lengths for In adatoms. This would tend to exacerbate the problems of 'arsenic rich' nucleation [discussed at the end of Sec 4.6 (ii)]. There is insufficient experimental data to decide this question at present.

4.7 Critique of Previous InAs Growth Studies

The most important conclusion to be drawn from the results presented in this chapter is that, as far as may be implied from basic 'growth and assessment' studies, the chemistry and kinetics involved in the MBE of (100) InAs are identical to those of (100) GaAs: it is not possible to grow substantially undefected epilayers of either compound under any conditions leading to growth under a (4x2) reconstruction, and As_4 rich growth results from a nucleation problem in epitaxy rather than any intrinsic difficulty in growing InAs by MBE. It is, therefore, necessary to account for the earlier reports that good quality InAs epilayers could only be deposited onto GaAs by nucleation and/or growth under an indium stabilised (4x2) reconstruction.

Firstly, flux uniformity must be considered. Hancock and Kroemer (1984) reported that, when reducing the As_2 flux to approach the transition to indium stabilisation, the upper

portion of their substrate showed a (4x2) indium stabilised reconstruction whilst the lower portion was still arsenic stabilised, and that the transition region was less than 1mm wide. Given that the optimum nucleation condition lies close to this transition, it is difficult to accept that the morphology of rather limited areas of the epilayer could be accurately correlated with (glancing incidence) RHEED observations under these conditions. Conversely, there was no evidence of significant variations in the As₄:In flux ratio across the (typically) 1 cm x 2 cm substrates used for the experiments reported in this chapter: the defect density on epilayers grown under non-optimum conditions was uniform over this area, and no variation in the RHEED pattern across the epilayer was apparent when approaching phase boundaries.

The identification of the RHEED patterns seen during deposition must also be queried. Hancock and Kroemer (1984) only examined the reconstruction in the $[1\bar{1}0]$ azimuth of (001) substrates when performing their experiments on heteroepitaxy {this corresponds to examining the $[0\bar{1}1]$ azimuth of (100) substrates in the notation used throughout this thesis}. Schaffer et al (1983) also appear to have confined most of their observations to the $[0\bar{1}1]$ azimuth. It is believed that single azimuths were examined because the MBE systems used by these workers were not fitted with substrate rotation [H Kroemer, UCSB, priv. comm. (1986)]. It is unfortunate that the $[0\bar{1}1]$ azimuth was chosen because, as noted in Sec 4.3 (iii), an indistinct (1x2) reconstruction is sometimes seen under optimum growth conditions. It can, therefore be difficult to distinguish between Regions III and V in $[0\bar{1}1]$. This should be clear from the table below, which summarises the information in Fig 3.10 and Sec 4.3;

Region	Order of reconstruction	
	in [011]	in $[0\bar{1}1]$
II	2x	4x
III	1x	1x/2x
V	4x	2x

Clearly, an operator examining only the $[0\bar{1}1]$ azimuth, and expecting the (2x4) pattern to change to a (4x2) without an intermediate stage, could interpret the transition between Regions II and III as the onset of indium stabilised growth. As shown in this chapter, any epilayer nucleated under this (falsely identified) condition would be of good quality. The transition between the 4x and 1x/2x reconstructions occurring in the $[0\bar{1}1]$ azimuths of Regions II and III is particularly easy to see, compounding the problem: this may explain why Schaffer et al (1983) noted that the boundary between the As₄-rich and optimum growth conditions was clearly defined in their experiments, whereas that between the optimum and indium accumulation conditions was not. To ensure the correct identification of the various reconstructions, both major RHEED azimuths were always examined when performing the experiments reported in this thesis.

4.8 Summary and Discussion

Good quality InAs could only be nucleated on (100) GaAs by using the minimum As₄ flux permitting stoichiometric growth at a temperature just below that which would have caused the InAs to sublime non-congruently. All attempts to nucleate InAs under any other conditions produced morphologically or electrically inferior material: the characteristic defects occurring within four non-optimum nucleation regimes (In-accumulated, In-rich, cross-hatched and As₄-rich) have been described. Each regime could be identified by observing the development of the RHEED

pattern during the early stages of growth. The In-accumulated and In-rich growth conditions were shown to be directly equivalent to conditions affecting the growth of (100) GaAs by MBE. Cross-hatched and As₄-rich growth did not occur during the homoepitaxy of either InAs or GaAs, indicating that these conditions resulted from the large ($\approx 7\%$) lattice mismatch which is encountered when growing InAs on GaAs. Comparison of the surface phase diagrams of InAs and GaAs (Chapter 3) indicates that, contrary to some earlier reports, the MBE growth behaviour of these two compounds is identical.

Those heteroepitaxial layers nucleated under optimum conditions were mirror-shiny (despite a slight background ripple, only apparent when using a phase contrast microscope) and exhibited oval defects similar to those seen on GaAs. These defects, which have not been reported on MBE InAs before, were present at densities of between 8×10^2 and $3 \times 10^3 \text{ cm}^{-3}$. Oval defect densities of between 1×10^3 and $1 \times 10^4 \text{ cm}^{-3}$ were obtained on GaAs grown in parallel experiments. The difference in density is believed to have resulted from the differing behaviour of the group III suboxides in the In and Ga sources, as proposed by Prior et al (1984). All of the unintentionally doped InAs epilayers were n-type: those nucleated under optimum conditions had 77 K mobilities of $\approx 60 \times 10^3 \text{ cm}^2/\text{V-s}$ at $N_D - N_A \approx 2.5 \times 10^{15} \text{ cm}^{-3}$ regardless of the growth rate. However, the electrical characterisation of such layers is not entirely straightforward, as will be described in Chapter 5.

The requirements for optimised heteroepitaxial nucleation, a minimised As₄ flux and a high growth temperature, are also those which lead to layer-by-layer growth [Petroff et al (1984)]. Essentially similar conditions are required to nucleate other compressively mismatched layers, for example GaSb on GaAs [Lee et al (1986)]. It is probable that layer by layer growth (which requires the group III and group V adatoms to be freely mobile on the epilayer surface)

benefits the initial stages of heteroepitaxy by facilitating the coalescence of islands. It has been proposed that the problems of heteroepitaxy also affect homoepitaxial growth [Chang (1980, 1985)], albeit to a lesser extent. Systems with large mismatches, such as (100) InAs/GaAs, are therefore ideally suited for testing new growth techniques (e.g. superlattice buffer layers, etc). The present results support this idea, showing that the use of minimised group V fluxes and the highest practicable growth temperature [which is known to be desirable for the homoepitaxial growth of the majority of binary compounds, Grange (1985)] is essential for the nucleation of good quality InAs on (100) GaAs substrates.

CHAPTER 5

The Electrical Properties of Si, Sn and Unintentionally Doped InAs grown by Molecular Beam Epitaxy

Contents

Abstract (overleaf)

5.1 Introduction

5.2 Experimental: Sample Preparation and Hall Measurements

- (i) Electrical Isolation
- (ii) Hall Geometry
- (iii) Ohmic Contacts
- (iv) Hall Scattering Factor

5.3 Properties of Unintentionally Doped Epitaxial InAs

- (i) Characterisation of Lightly Doped Material
- (ii) Multi-layer Conduction Models
- (iii) Experimental: Depth Profiling
- (iv) Other Models
- (v) Discussion

5.4 Temperature Dependence of the Hall Properties

5.5 Majority Carrier Properties of Si and Sn doped InAs

- (i) Co-evaporation Doping of MBE-InAs
- (ii) Mobility versus Carrier Concentration
- (iii) Maximum Doping Levels Attainable in InAs

5.6 Summary and Conclusions

5.1 Introduction

The inherent difficulty of nucleating InAs on (100) GaAs has forced most MBE growth studies to concentrate on obtaining relatively undefected epilayers. In consequence, little information has been published on the doping of InAs during MBE growth [Yano et al (1977), Schaffer and Berg (1981) Kubiak et al (1984a)]. Recent interest in the use of MBE to prepare InAs based device structures (Sec 1.10) has highlighted this deficiency. As described in Chapter 1, it was considered useful; (i) to investigate the incorporation behaviour of Si and Sn in InAs; (ii) to investigate the growth of n^+ epilayers, as used for ohmic contacts and low resistivity buffer layers in microwave devices [Harris (1985)]; and (iii) to investigate the properties of n^- InAs grown by MBE, i.e. to allow a critical comparison to be made between the (present) capabilities of LPE, VPE and MBE.

5.2 Experimental: Sample Preparation and Hall Measurements

Care is required when performing Hall measurements on any semiconductor. The usual precautions include the use of cross-shaped or cloverleaf samples to reduce contact-area effects [van der Pauw (1958)]; ensuring good ohmic contacts to the epilayer [Putley (1960)]; making allowance for depletion effects [Chandra et al (1979)]; and including current and magnetic field reversals in the Hall measurement, e.g. to eliminate the effects of misalignment voltages and thermomagnetic effects [Putley (1960), Seeger (1982)].

Measurements on epitaxial InAs are further complicated by the effects of surface and interfacial conduction [Washburn et al (1979)]. In the case of lightly doped ($<5 \times 10^{16} \text{ cm}^{-3}$) material the combined sheet carrier density of the (electron accumulated) interfaces can exceed that of the

'bulk' epilayer. Specific problems arising from this situation will be discussed in the relevant sections of this chapter. However, it should be realised that some caution is necessary when comparing Hall properties between different InAs growth studies. For this reason the techniques used in the present study will be described in detail.

5.2 (i) Electrical Isolation of the Epilayers

All of the measurements reported in this chapter were made on InAs grown on semi-insulating GaAs substrates. Attempts to electrically isolate homoepitaxial layers by growing on substrates of the opposite carrier type failed because of excessive leakage through the p-n junction. To date, no data has been published on the electrical properties of junction isolated MBE-InAs, suggesting that other workers have encountered similar problems. However, Harrison and Houston (1986) have achieved junction isolation by using LPE to grow n^- InAs epilayers on p^+ InAs substrates. The doping levels of both epilayers (1×10^{16} – $5 \times 10^{18} \text{ cm}^{-3}$) and substrates ($5 \times 10^{17} \text{ cm}^{-3}$) were similar to those used in the experiments reported here. This may indicate that LPE-grown InAs homojunctions are currently of better quality than those grown by MBE: however, see also Sec 5.5 (ii) below.

5.2 (ii) Hall Geometry

The Hall samples were fabricated on cleaved squares of approximately 5 mm x 5 mm, upon which an etched cross was used to define an active area of between 1 mm² and 4 mm². The four radial 'arms' supporting the ohmic contacts were always aligned at 45° to the [011] direction (Fig 5.1). The same geometry was used for the measurements on GaAs epilayers reported in Chapter 3.

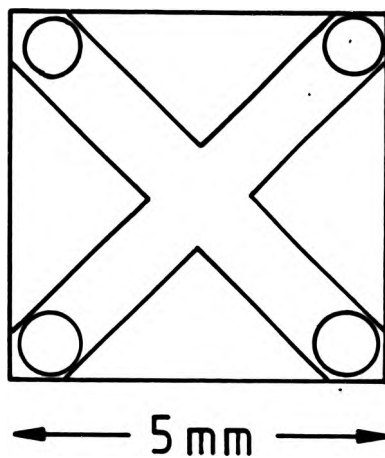


Fig 5.1 Geometry of the Hall Samples used for measurements on InAs and GaAs. The cross arms are at 45° to the $[011]$ direction.

5.2 (iii) Ohmic Contacts

Whilst it is not difficult to make ohmic contacts to n-type InAs, the treatments associated with contact alloying can influence the stability of the Hall properties. Specifically; (i) the Hall coefficients of both bulk and epitaxial samples tend to increase towards a stable value during storage [Dixon and Enright (1959), Edmond and Hilsun (1960), McCarthy (1967), Mizuno et al (1975)]; and (ii) this effect can be accelerated by thermal treatments. McCarthy (1967) reported that the Hall coefficients of his 'flash alloyed' VPE-grown InAs Hall samples stabilised over a period of two to three weeks at room temperature, but that the process only took 48 hours at 100°C. Significant changes were involved: the 77K Hall mobilities rose from $4.3-6.8 \times 10^4 \text{ cm}^2/\text{V-s}$ 'as grown' to $7.9-10.6 \times 10^4 \text{ cm}^2/\text{V-s}$ following storage or annealing. The (Hall) carrier concentration was also affected, decreasing from $0.56-3.3 \times 10^{16} \text{ cm}^{-3}$ to $0.18-0.81 \times 10^{16} \text{ cm}^{-3}$. Similarly, Kubiak (1983) reported that the Hall co-efficients of n^- ($\approx 5 \times 10^{16} \text{ cm}^{-3}$) MBE grown samples (which had been contacted by annealing on In and Sn contacts at 300-400°C in a reducing ambient) were still increasing after 100 hours, but stabilised after heating in air for 20 minutes at 250°C. 80% increases in the 300K Hall mobility and 30% decreases in the carrier concentration were observed.

This behaviour has been attributed to a thermally activated interaction between donor impurities [Cu, McCarthy (1967) and S, Mizuno et al (1975)] and lattice defects. However this explanation is inconsistent with the thermal history of most InAs samples, which are grown at temperatures in excess of 450°C. It is more probable that surface effects are responsible [Balagurov and Borkovskaya (1976), Millea and Silver (1978) Baglee et al (1982)]. This should be especially true of n^- epitaxial InAs, in which a significant fraction of the total carrier density can be confined within surface accumulation layers [Washburn et al

(1979)]. As annealing in air produces electrically stable Hall samples, whereas annealing in a reducing atmosphere does not, it is likely that passivation results from the formation of a stable surface oxide. For this reason all Hall samples used in the present study were contacted by annealing on In pellets for 20-30 minutes at 250°C in air. It was unnecessary to remove surface oxidation from the contact area prior to the application of the indium, and no difficulty was experienced in obtaining highly linear I-V characteristics at low doping levels (i.e. $N_D - N_A = 5 \times 10^{15} \text{ cm}^{-3}$). The Hall properties of samples prepared in this way have remained constant to within 5% over periods of up to two years, further validating the results reported by Kubiak (1983) and Kubiak et al (1984a).

5.2 (iv) Hall Scattering Factor

The Hall scattering factor (r_H) relates the Hall mobility to the carrier drift mobility ($r_H = \mu_{\text{drift}}/\mu_{\text{Hall}}$) and appears as a constant of proportionality in the Hall equation [Nag (1980), Seeger (1982)]

$$E_y/B_z J_x = R_H = r_H/ne$$

The magnitude of r_H is approximately unity and depends on the semiconductor and the dominant scattering mechanism. As no reliable value was available for InAs, r_H was assumed to be unity for all measurements reported in this thesis. Although this is a common assumption, r_H is sometimes taken to be 1.18 ($= 3\pi/8$), and care should be taken when comparing the results reported here with other studies. [$r_H = 3\pi/8$ when acoustic phonon scattering dominates, as is generally the case at room temperature, Seeger (1982)].

5.3 Properties of Unintentionally Doped Epitaxial InAs

This section describes how multi-layer conduction models

were used to interpret and deconvolute the Hall properties of unintentionally doped epilayers grown in CLPIV.

5.3 (i) Characterisation of Lightly Doped Material

Two problems are known to complicate the electrical characterisation of lightly-doped InAs grown on (100) GaAs substrates; the first results from bulk properties, but the second is specific to epitaxial material;

(i) The electron mobility of lightly doped InAs can be sufficiently high (at 77 K) to violate the simplifying assumption that $\mu B_H \ll 1$, used in the derivation of the low field Hall equation $E_y = R_H B_z J_x$ where $R_H \neq R_H(B_z)$ [Seeger (1982), Anderson and Apsley (1986)]. For example, a 77 K mobility of $60 \times 10^3 \text{ cm}^2/\text{V-s}$ and a typical Hall field (B_H) of 0.5 T, or $5 \times 10^{-5} \text{ cm}^{-2} \text{ V s}$, gives $\mu B_H = 3$. The overall effect is to cause the mobility calculated using $\mu = \sigma R_H$ to fall as B_z increases.

(ii) In addition to this bulk effect, the galvomagnetic properties of heteroepitaxial InAs can be strongly influenced by the effects of parallel conduction. Wieder (1974, 1977), Sites and Weider (1975), Washburn (1978) and Washburn et al (1979) have conducted detailed investigations into the properties of InAs grown on (100) GaAs by VPE, finding that conduction occurred through three layers; (a) an accumulation of low-mobility electrons confined to a quantum well at the free surface of the epilayer, (b) an extended accumulation of low mobility electrons at the epilayer/substrate interface and (c) a layer of material with bulk-like electrical properties separating the accumulated interfaces. MBE grown InAs has shown the same structure [Grange et al (1979, 1980), Kubiak et al (1983, 1984a)].

A third effect which may cause Hall measurements to underestimate carrier mobilities in n^- InAs is the formation of Landau levels [Seeger (1982)], e.g. as a result of applying B_H . This mechanism was proposed by Kamakura et al (1975) to account for decreases in the 77 K Hall mobility of a bulk-grown single crystal sample of n-type ($1.7 \times 10^{16} \text{ cm}^{-3}$) InAs as B_H was raised above 0.2 T. Unfortunately the geometry of this sample was not clearly described, and it is unclear whether interface effects may have been significant. However, comparable temperatures, carrier concentrations and magnetic fields are frequently met in the characterisation of MBE grown material.

Figure 5.2 illustrates the extent to which these mechanisms affect Hall measurements on MBE grown InAs. The diagram shows the variation in the 77 K Hall mobility with B_H obtained from four unintentionally doped InAs epilayers of different thicknesses grown in CLPIV. These epilayers were nucleated on (100) GaAs substrates under near optimum conditions (as defined in Chapter 4). The carrier concentration of the 4.1 μm thick epilayer was $8 \times 10^{15} \text{ cm}^{-3}$ n-type at 77 K. The magnetic field was varied from between 0.1 and 0.6 T, covering the range commonly used for non-critical Hall measurements. Two observations are of interest here: (a) the 77 K Hall mobility obtained from the 4.1 μm layer at a field of 0.6 T was only about two thirds of the mobility at 0.1 T, and (b) that, at a given B_H , the Hall mobility decreased rapidly with decreasing layer thickness. These results indicate that it can be highly misleading to attempt to characterise lightly doped heteroepitaxial InAs with a single Hall measurement [Washburn et al (1979)].

5.3 (ii) Multi-layer Conduction Models

It is pertinent to consider how the bulk and interfacial properties of InAs epilayers may be derived from Hall

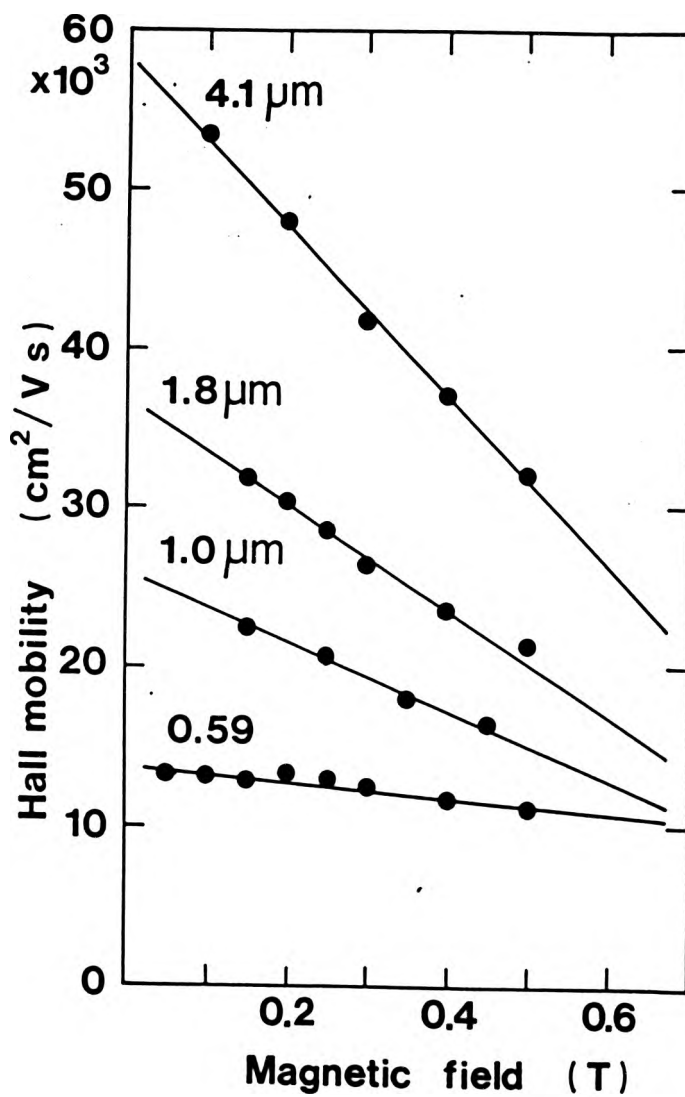


Fig 5.2 The variation of Hall mobility with B_x of four unintentionally doped InAs epilayers of different thicknesses nucleated under identical conditions.

measurements. Figure 5.3 introduces the two layer model of Nedoluha and Koch (1952). This model considers the epilayer to consist of two homogeneous slabs of semiconductor which are joined at the edges by zero resistance loops (e.g. the ohmic contacts of the Hall samples). When the model is applied to InAs [Weider (1974), Washburn (1979), Grange (1980), Kubiak et al (1983, 1984a)] it is assumed that one layer has a bulk-like conductivity (σ_b) and Hall coefficient (R_b). The other layer is assigned the properties σ_i and R_i appropriate to an 'interfacial layer', which combines the properties of the free surface and the epilayer/substrate heterojunction. If the epilayer lies in the x-y plane, the Hall current I_H is applied in the x-direction and a homogeneous magnetic field B is applied in the z-direction (as shown in Fig 5.3), then the electric fields across the bulk-like layer are given by

$$E_x = J_{bx}/\sigma_b - R_b J_{by} B \quad 5.1$$

and

$$E_y = J_{by}/\sigma_b + R_b J_{bx} B \quad 5.2$$

Similar equations may be written for the interfacial layer;

$$E_x = J_{ix}/\sigma_i - R_i J_{iy} B \quad 5.3$$

$$E_y = J_{iy}/\sigma_i + R_i J_{ix} B \quad 5.4$$

Note that E_x and E_y must be the same across the bulk and interfacial layers because of the physical connection at their edges. Two further constraints are that the total current in the x-direction must equal the sum of the x currents in the layers, i.e.

$$J_x d_m = (J_{bx} d_b + J_{ix} d_i) \quad 5.5$$

similarly,

$$J_y d_m = (J_{by} d_b + J_{iy} d_i) \quad 5.6$$

Where $d_m = d_b + d_i$, i.e. the total thickness of the epilayer. The subscript 'm' is used here, and in subsequent expressions, to denote a directly measurable quantity. Under

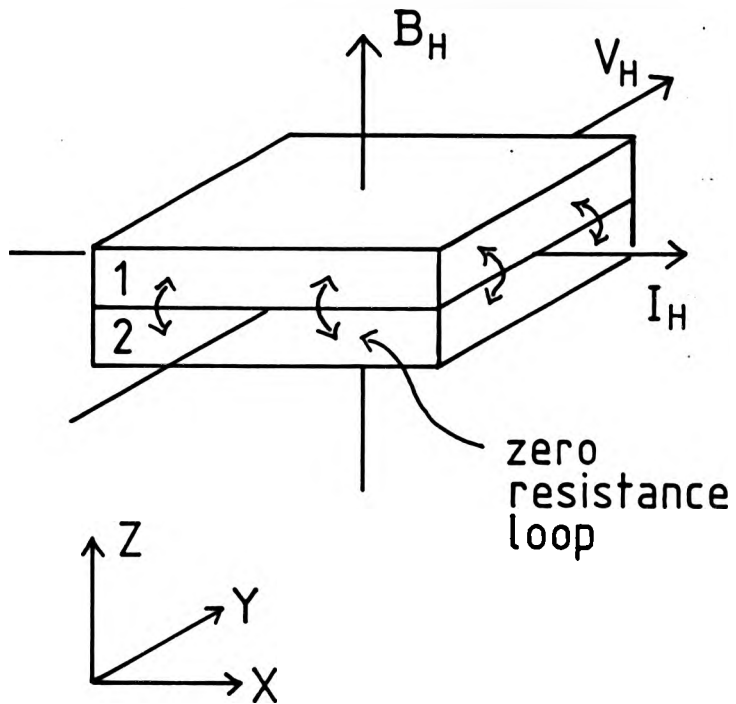


Fig 5.3 The two layer conduction model of Nedoluha and Koch (1952) - definition of parameters

normal conditions no current is drawn from the Hall voltage probes and J_y is zero. However, this does not preclude the possibility of circulating currents (i.e. in which $J_{by}d_b = -J_{iy}d_i$; the magnetic field dependence does, in part, derive from such currents). If these restrictions are applied to equations 5.1 to 5.6 it is possible to write the constants of proportionality between (J_x and E_x) and (E_y and E_x) in terms of the fixed parameters (σ_b , σ_i , R_b , R_i , d_b , d_i and B). The Hall properties of the epilayer as a whole may then be obtained by substitution into $\sigma = J_x/E_x$ and $R_H = E_y/B_2 J_x$. If unipolar conduction is assumed, $\sigma = ne\mu$ may then be used to obtain [Weider (1974)]

$$\sigma_m d_m = (\sigma_b d_b + \sigma_i d_i) \quad 5.7$$

(σ_m is measured in the absence of a magnetic field), and

$$R_m(B) = \{\mu_b \sigma_b d_b + \mu_i \sigma_i d_i + \mu_b \mu_i \Pi B^2\} / \{(\sigma_b d_b + \sigma_i d_i)^2 + \Pi^2 B^2\} \quad 5.8$$

where

$$\Pi = (\mu_i \sigma_b d_b + \mu_b \sigma_i d_i) \quad 5.9$$

The magnetoresistance of the two-layer system is

$$\Delta\rho/\rho = \{(\mu_b - \mu_i)^2 d_b \sigma_b d_i \sigma_i B^2\} / \{(d_b \sigma_b + d_i \sigma_i)^2 + \Pi B^2\} \quad 5.10$$

If required, the model may be generalised by considering the epilayer to consist of a larger number of layers [Washburn (1978)]. However, this increases the complexity of the analysis and, as shown by Weider (1974), Grange (1980), Kubiak (1983), and Kubiak et al (1984a), the two layer model adequately describes the Hall properties of InAs grown on GaAs substrates. The derivation given *considers only* the magnetic field dependence of the Hall properties deriving from the composite structure of the epilayer, but normal magnetoresistance can be handled by equations 5.1 to 5.10 by replacing σ_b with $\sigma_b(B)$, R_b with

$R_b(B)$, and so on.

The application of equations 5.7 to 5.10 either requires some material parameters to be assumed or measurements to be made at low and high (≈ 8 T) magnetic fields [Wieder (1974), Washburn (1978)]. Such large fields are not commonly available: for this reason, several authors have introduced simplifying approximations into the derivation outlined above. The most common of these is that $I_{by}d_b/\sigma_b \ll R_b I_{bx}B$ (and $I_{iy}d_i/\sigma_i \ll R_i I_{ix}B$), i.e. that the voltage drop due to the circulating currents in the y-direction is much smaller than the Hall voltage. This assumption is included, although not stated, in the analyses developed by Petritz (1958), Kubiak et al (1984a) & Stewart et al (1986). Equations 5.7 - 5.9 then reduce to;

$$\sigma_m d_m = \sigma_b d_b + \sigma_i d_i \quad 5.11$$

$$R_m \sigma_m^2 d_m = R_b \sigma_b^2 d_b + R_i \sigma_i^2 d_i \quad 5.12$$

where $d_m = d_b + d_i$ as before. These equations still assume that some interaction between the layers needs to be taken into account, e.g. by requiring that E_x and E_y must be the same across both the bulk and interfacial layers; in effect this means that one Hall voltage may back off the other. As a consequence $R_m = R_m(B)$ and $\sigma_m = \sigma_m(B)$ even though no 'B' term appears in 5.11 and 5.12 [Washburn (1978)]. It is useful to re-write 5.11 and 5.12 in the form of linear equations,

$$\sigma_m = \sigma_b + \Gamma/d_m \quad 5.13$$

$$R_m \sigma_m^2 = R_b \sigma_b^2 + \Phi/d_m \quad 5.14$$

where Γ and Φ are constants (for layers grown under identical conditions) defined by;

$$\Gamma = d_i(\sigma_i - \sigma_b) \quad 5.15$$

$$\Phi = d_i(R_i \sigma_i^2 - R_b \sigma_b^2) \quad 5.16$$

Hence (for example) σ_b may be obtained from the intercept

of a plot of conductivity versus reciprocal epilayer thickness. The equations may also be used to check the validity of the simplifying assumptions.

5.3 (iii) Experimental: Depth Profiling

Two techniques were used to obtain electrical profiles of epilayers grown in CLPIV. In the first the substrate shutter was advanced in stages across the epilayer during growth. This produced up to four layers of different thickness nucleated under identical conditions. The small number of thickness steps available in a single growth meant that this technique was best suited to the analysis of relatively thin layers [e.g. see Kubiak et al (1984a)]. The technique of etch profiling was found to be more useful for deriving the properties of the bulk-like region of thick epilayers.

Etch profiling involves the sequential thinning and measurement of the active region of a Hall sample. Meggitt (1979) and Grange et al (1979, 1980) have previously reported the profiling of InAs in this manner, and 'Hall and strip' measurements are becoming a routine means of assessment for GaAs/AlGaAs compounds [Stewart et al (1986)]. In the present experiments, etch profiling was used to analyse an unintentionally doped 23.4 μm thick epilayer grown on SI GaAs under near-optimum conditions (Chapter 4).

Experimental: The Hall sample was mounted on a paxolin strip and thin wires were soldered to the ohmic contacts. Everything but the active region of the Hall sample was then coated in black wax. A scrap of n^- InAs was mounted beside the Hall sample before each etch stage. This scrap was partially covered by tape, allowing the thickness of material removed to be measured using a 'Talystep' stylus profiler. The etch used was cold $30\text{H}_2\text{SO}_4:\text{H}_2\text{O}:\text{H}_2\text{O}_2$, which removed InAs at about 0.08 $\mu\text{m}/\text{min}$. The conductivity and

Hall co-efficient were measured at four magnetic fields (0.3, 0.65, 1.0 and 1.4 T) at each thickness so that the field dependence of the derived properties μ_b and σ_b could be investigated. Fig 5.4 shows the 300 K and 77 K Hall properties of the epilayer (measured as a function of B_H) 'as grown'. The layer had the properties $\mu=46 \times 10^3 \text{ cm}^2/\text{V-s}$ and $N_D - N_A = 5.9 \times 10^{15} \text{ cm}^{-3}$ at 77 K and $B_H = 0.3 \text{ T}$.

Conductivity versus d_m : The 300 K and 77 K conductivities measured at various thicknesses ' d_m ' are shown in Fig 5.5. σ_m is a linear function of $1/d_m$ at both temperatures. This relationship was predicted by Eqtn 15.13, and indicates that the two layer conduction model is applicable to the data. The values $\sigma_b(300 \text{ K}) = 6.44 \pm 0.85 \Omega^{-1} \text{ cm}^{-1}$ and $\sigma_b(77 \text{ K}) = 23.46 \pm 3.10 \Omega^{-1} \text{ cm}^{-1}$ were obtained from the intercepts of the σ versus $1/d$ plots. The estimates of error on these parameters were based, via linear regression, on the scatter on the data. The possibility of systematic error is discussed in Sec 5.3 (vi).

300 K Properties of the Bulk-Like Layer: The variation of $R_m(300 \text{ K})$ with thickness at $B_H = 0.3, 0.65, 1.0$ and 1.4 T is shown in Fig 5.6. This data was used, with the conductivity data from Fig 5.5, to calculate $R_m \sigma_m^2$ at several thicknesses. $R_m \sigma_m^2$ was then plotted against $1/d_m$ for each value of B_H (Fig 5.7). As predicted by Eqtn 5.14, the plots were linear with intercepts at $R_b \sigma_b^2 = 1.60 \pm 0.32 \times 10^5 \text{ A cm s}$ (at 0.3 T) and $R_b \sigma_b^2 = 1.93 \pm 0.21 \times 10^5 \text{ A cm s}$ (at 0.65, 1.0 and 1.4 T). The mobility ($R_b \sigma_b$) and carrier concentration ($1/R_b e$) of the bulk-like layer were calculated from $R_b \sigma_b^2$ using $\sigma_b(300 \text{ K}) = 6.44 \Omega^{-1} \text{ cm}^{-1}$, yielding

$$\begin{aligned} \mu_b(300 \text{ K}) &= (24.8 \pm 7.1) \times 10^3 \text{ cm}^2/\text{V-s} && \text{with } B_H \\ n_b(300 \text{ K}) &= (1.64 \pm 0.62) \times 10^{15} \text{ cm}^{-3} && = 0.3 \text{ T} \\ \text{and} \\ \mu_b(300 \text{ K}) &= (30.0 \pm 8.3) \times 10^3 \text{ cm}^2/\text{V-s} && \text{with } B_H \\ n_b(300 \text{ K}) &= (1.34 \pm 0.43) \times 10^{15} \text{ cm}^{-3} && = 0.65, 1.0 \text{ \& } 1.4 \text{ T} \end{aligned}$$

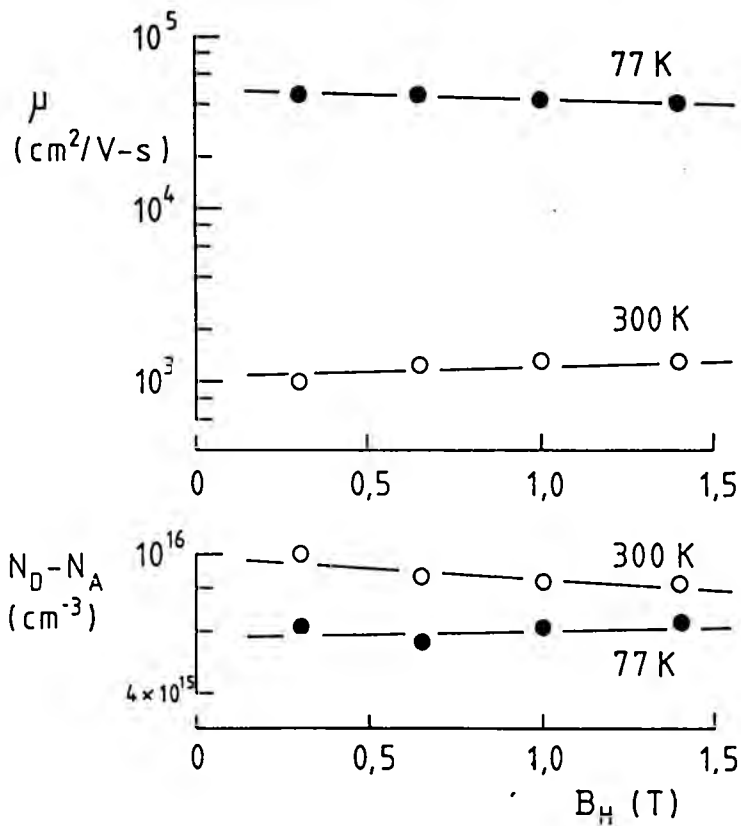


Fig 5.4 B_H dependence of the directly measured 300 K and 77 K Hall properties of the unintentionally doped 23.4 μm epilayer which was further analysed by etch profiling.

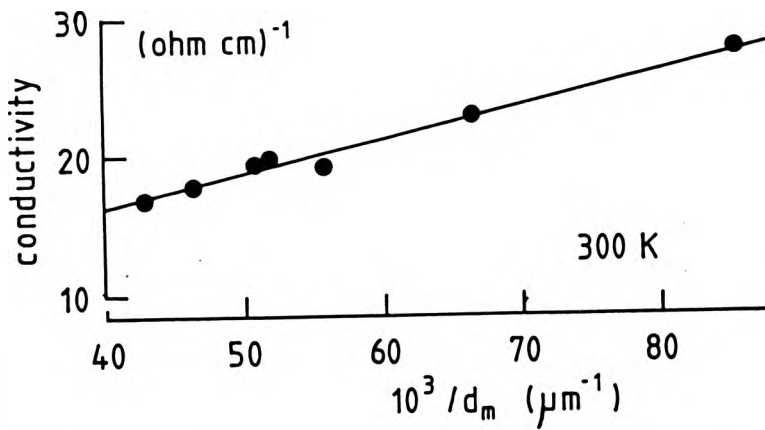
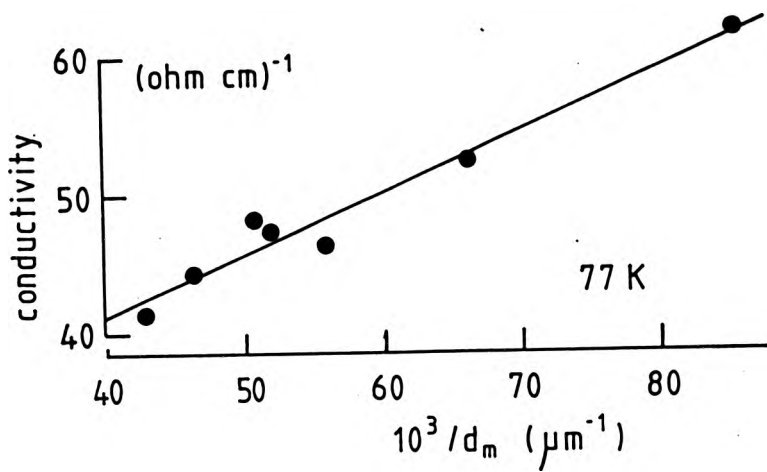


Fig 5.5 Etch Profile: the variation of conductivity with (reciprocal) InAs layer thickness at 300 K and 77 K.

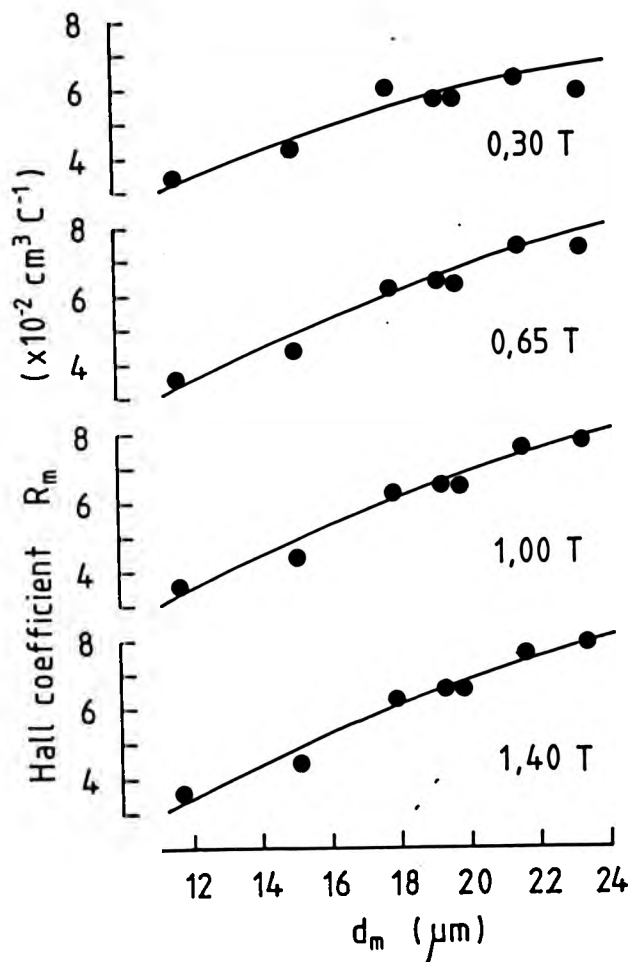


Fig 5.6 Etch Profile: The variation of the 300 K Hall co-efficient with thickness at $B_H=0.3, 0.65, 1.0$ and 1.4 T.

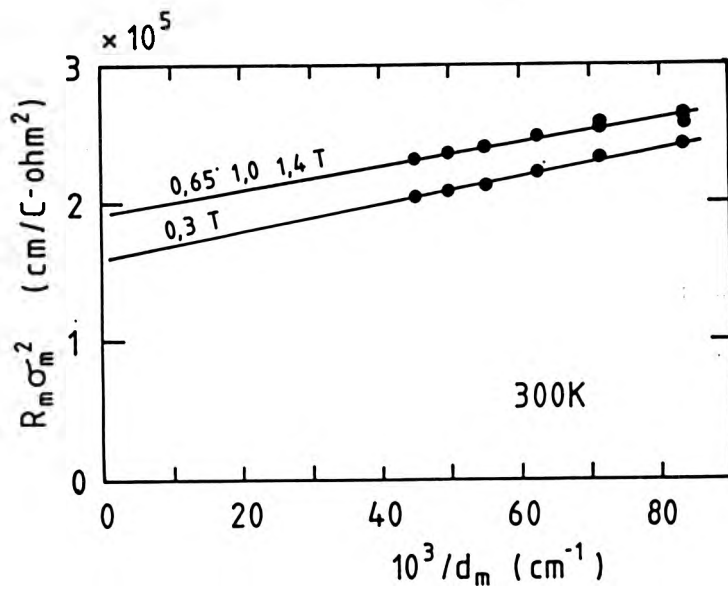


Fig 5.7 $R_m \sigma_m^{-2}$ versus $1/d_m$ at 300 K. The intercept at $1/d_m = 0$ gives $R_m \sigma_m^{-2}$, the properties of the bulk-like layer.

It is not clear why the 0.3 T bulk mobility is about 20% lower than that derived for the higher fields. However, the discrepancy probably lies within experimental error. The estimated carrier concentration of the bulk-like layer is lower than that obtained from measurements on the whole epilayer ($>5 \times 10^{15} \text{ cm}^{-3}$): this is reasonable, as the latter would include contributions from the accumulated interfaces. The mobilities derived for the bulk-like region lie close to the values obtained from bulk InAs at similar doping levels [Schillman (1956)]. NB: the properties of the bulk-like region derived from this, and subsequent, analyses are summarised in Table 5.1 and compared with other workers results in Table 5.2.

Multi-layer Analysis: A second way to derive the properties of the bulk layer is to consider the epilayer to be split up into many homogeneous slabs, with the k^{th} slab having the properties σ_k , R_k and d_k . Under the simplifications already described, equations 5.11 and 5.12 may then be rewritten [Petritz (1958)],

$$\sigma_m = (e/d_m) \times (\sum n_k \mu_k d_k) \quad 5.17$$

$$R_m = (e/\sigma_m^2 d_m) \times (\sum n_k \mu_k^2 d_k) \quad 5.18$$

where the summation is carried out over the total number of slabs forming the epilayer. If the Hall properties of two otherwise identical samples of different thickness are measured, the average values of the carrier concentration and Hall mobility (n_k and μ_k) occurring within the 'extra' material in the thicker layer may be calculated using [Washburn et al (1979)],

$$\langle n_k \mu_k \rangle = \Delta(\sigma_m d_m) / (e \Delta d_m) \quad 5.19$$

$$\langle n_k \mu_k^2 \rangle = \Delta(R_m d_m \sigma_m^2) / (e \Delta d_m) \quad 5.20$$

where Δd_m is the change in thickness between the two layers, and so on. Provided that the epilayers under consideration are thicker than the combined widths of the

two electron accumulated interfaces, the properties n_k and μ_k pertain to material in the bulk-like layer. The accuracy of this analysis does not rely on long extrapolations.

Figure 5.8 shows the thickness dependence of $\mu_k(300\text{ K})$ and $n_k(300\text{ K})$ calculated from the curves fitted to the conductivity (Fig 5.5) and 1 T Hall data (Fig 5.6). The parameters are plotted at the mid-point of each incremental step. The mobilities and carrier concentrations obtained from direct measurements at $B_H=1.0\text{ T}$ are included for comparison. As expected, a constant mobility was derived over the thicknesses examined [these were in excess of $12\mu\text{m}$; the combined width of the accumulated interfaces is $\approx 0.5\mu\text{m}$ in $n^- \text{InAs}$, Kubiak et al (1984a)]. This mobility, $(29.9 \pm 0.46) \times 10^3\text{ cm}^2/\text{V-s}$, and the corresponding carrier concentration, $(1.34 \pm 0.20) \times 10^{15}\text{ cm}^{-3}$, are in good agreement with the estimates derived from the two layer model.

77 K Properties of Bulk-Like Layer: The techniques described above were also applied to the 77 K data. The 77 K Hall co-efficients at 0.3, 0.65, 1.0 and 1.4 T are shown as a function of layer thickness in Fig 5.9. Considering first the two layer model, the product $R_m\sigma_m^2$ is plotted as a function of $1/d_m$ for each B_H in Fig 5.10. It is noticeable that $R_m\sigma_m^2$ is almost independent of the layer thickness at 77 K so that, according to Eqtn 5.18, $d_i(R_i\sigma_i^2 - R_b\sigma_b^2)/d_m \ll R_b\sigma_b^2$. Conversely, $R_m\sigma_m^2$ increased noticeably with $1/d_m$ at 300 K (Fig 5.7), indicating that $R_i\sigma_i^2 (=n_i\mu_i^2)$ was appreciably greater than $R_b\sigma_b^2 (=n_b\mu_b^2)$ at room temperature. It is probable that balance between $n_i\mu_i^2$ and $n_b\mu_b^2$ was altered by the rapid increase in μ_b and the freezeout of interfacial carriers (see Sec 5.4) with falling temperature, so that $n_b\mu_b^2 \gg n_i\mu_i^2$ at 77 K. In this case the slope of $R_m\sigma_m^2$ against $1/d_m$ reduces to $d_iR_b\sigma_b^2$ and, taking $d_i \approx 0.5\mu\text{m}$ as estimated by Kubiak et al (1984a), Eqtn 5.14 indicates that $R_m\sigma_m^2$ would only differ from $R_b\sigma_b^2$ by about 2% in a 23 μm layer.

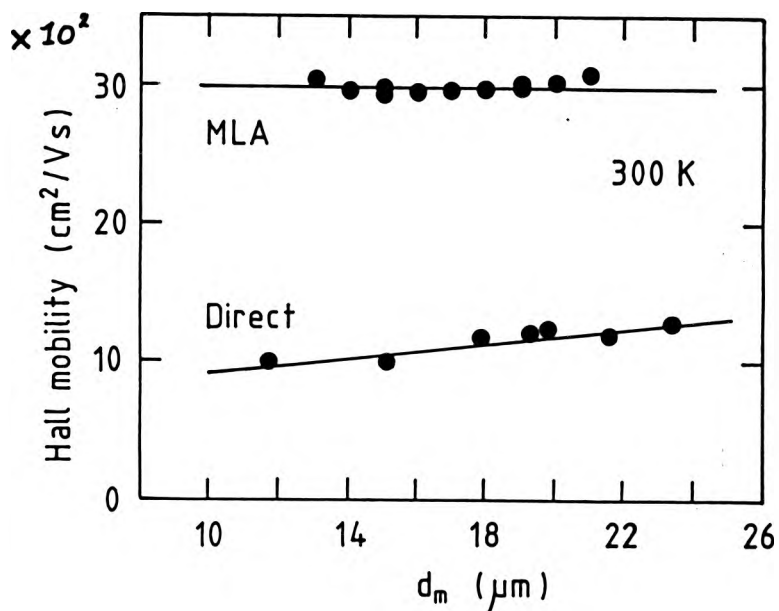


Fig 5.8 The average value of the 300 K Hall mobility at various points across the 23.4 μm epilayer, calculated using the multi-layer analysis (MLA). The Hall parameters measured at $B_H=1.0$ T during etch profiling (Direct) are included for comparison.

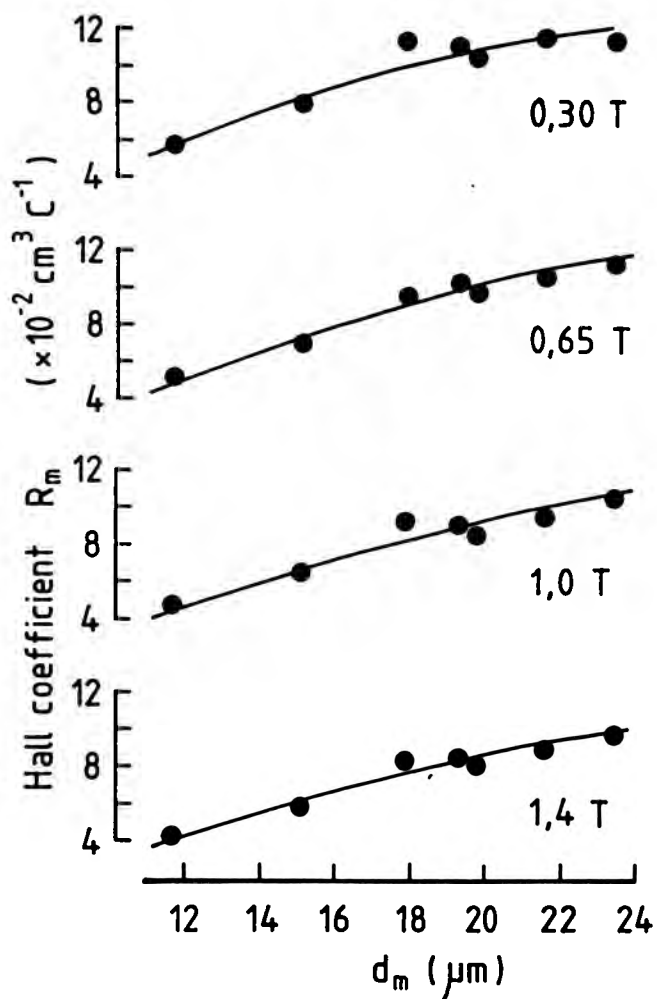


Fig 5.9 Etch Profile: The variation of the 77 K Hall coefficient with layer thickness at 0.3, 0.65, 1.0 and 1.4 T.

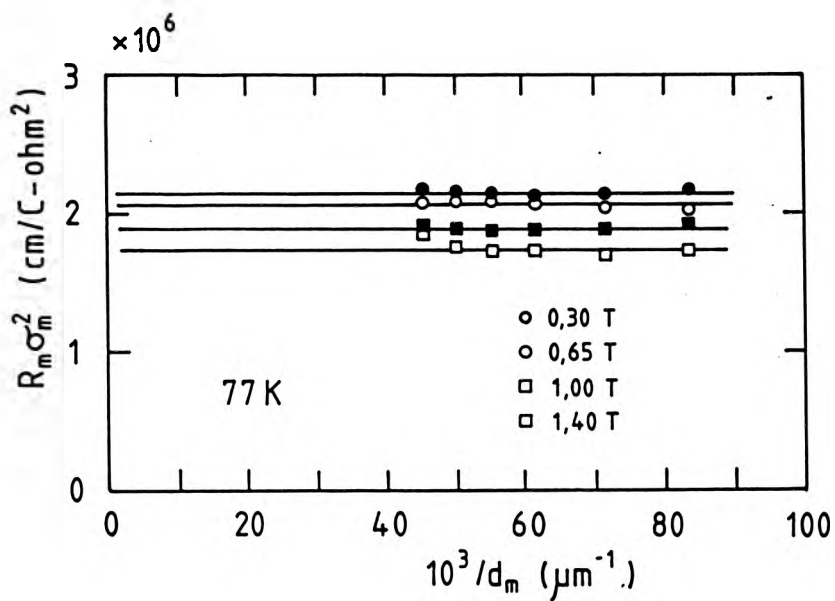


Fig 5.10 $R_m \sigma_m^2$ versus $1/d_m$ at 77 K. The intercept at $1/d_m = 0$ gives $R_m \sigma_m^2$, the properties of the bulk-like layer.

A second feature apparent in Fig 5.10 is that $R_b \sigma_D^2$ (the property of the bulk-like layer) is a weak function of B_H at 77 K. The electron mobilities corresponding to each (thickness independent) value calculated using $\sigma_D(77\text{ K})=23.46 \text{ } \Omega^{-1} \text{ cm}^{-1}$ (from Fig 5.5) are listed in Table 5.1 and plotted as a function of B_H in Fig 5.11. The mobility variation is comparable to that seen by Kamakura et al (1975) in bulk n^- InAs samples at similar magnetic fields (see inset to Fig 5.11). Referring to the MBE data, it should be noted that the dimensionless product $\mu_D B_H$ increases from 2.7 at 0.3 T to 10 at 1.4 T. As previously mentioned, this violates the simplifying assumption that $\mu B \ll 1$ which makes R_H independent of B_H in the derivation of the Hall equations [Nag (1980), Seeger (1982)]. It is, then, not surprising that $R_b=R_b(B)$ in the present case. The formation of Landau levels, as discussed by Kamakura et al (1975), may also have influenced the results.

The multilayer analysis was also applied to the 77 K data. Fig 5.12 shows μ_D at $B_H=0.3, 0.65, 1.0$ and 1.4 T calculated from the data in Figs 5.5 and 5.9 by using Eqtns 5.19 and 5.20. Within the scatter on the data, the mobilities calculated at 0.65 T and 1.4 T are independent of film thickness and comparable with the estimates derived from the two layer model. Conversely, the values of μ_D calculated at 0.3 and 1.0 T increase slightly with the layer thickness. This is not believed to be a genuine trend as (i) the deviation involved is comparable with the scatter on the data and (ii) because the average mobilities obtained at 0.3, 0.65, 1.0 and 1.4 T are comparable with the averages obtained from the two layer analysis, showing a similar decrease in μ_D with increasing B_H (Fig 5.11).

5.3 (iv) Other Models of Conduction

Aina et al (1986) analysed parallel conduction through a 2DEG in GaAs and its n^+ AlGaAs cladding layer. These

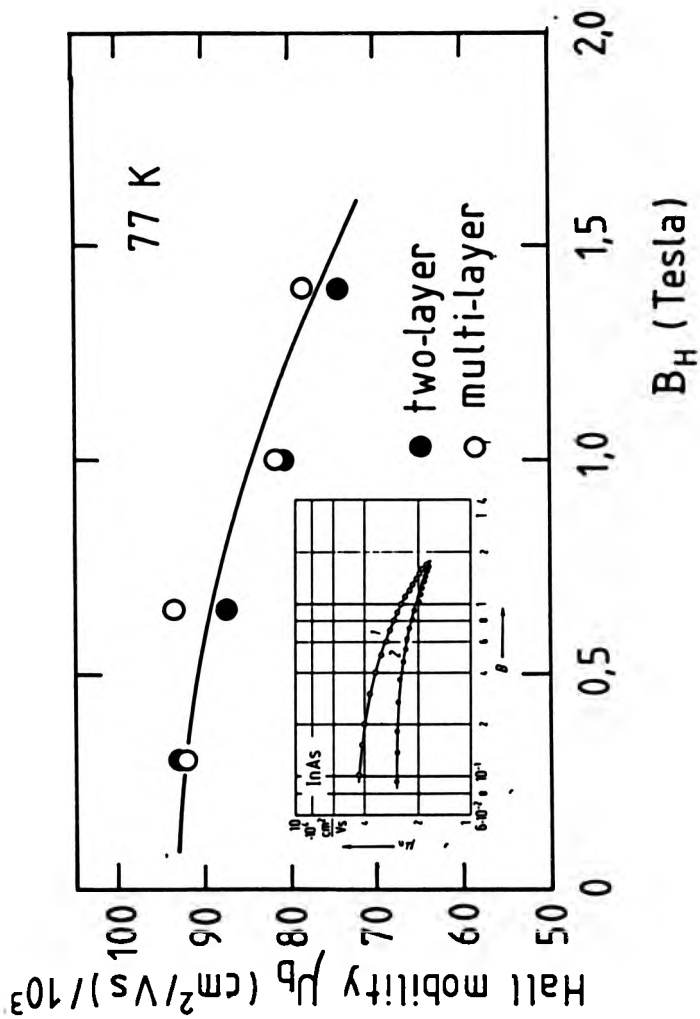


Fig 5.11 The magnetic field dependence of the 77 K mobilities of the bulk-like layer derived via the two layer (filled circles) and multi layer (open circles) analyses. The inset shows the properties of bulk n⁻ InAs measured by by Kamakura et al (1975).

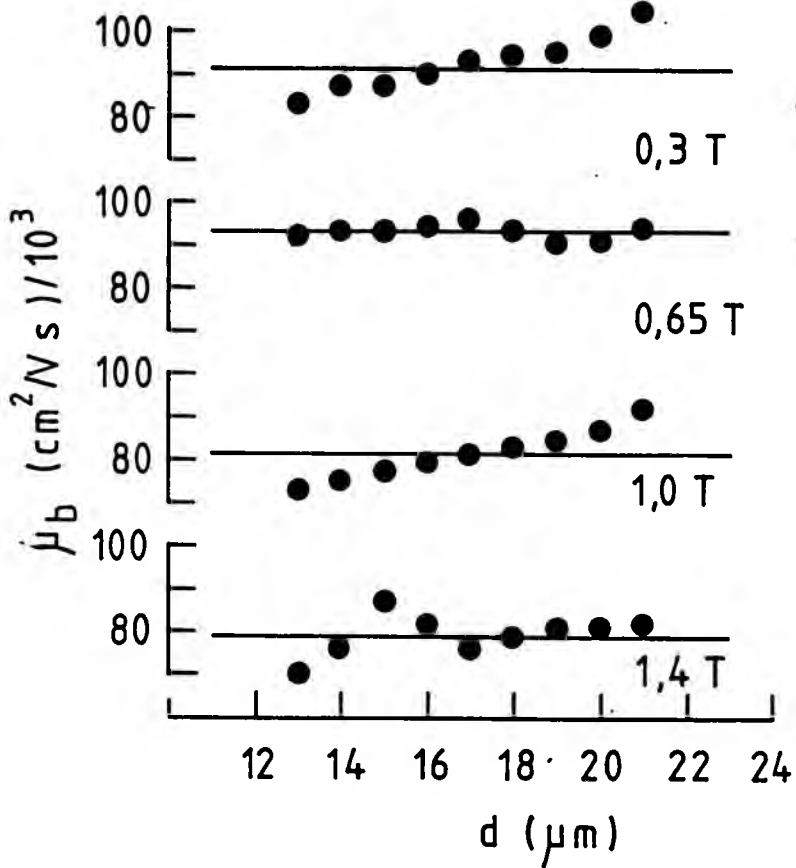


Fig 5.12 The average value of the 77 K Hall mobility and carrier concentration at various points across the 23.4 μm epilayer, calculated from the data in Figs 5.5 and 5.9 using the multi-layer analysis (Eqtns 5.19 and 5.20).

workers assumed that the Hall co-efficient of the composite layer would behave similarly to that of a homogeneous semiconductor exhibiting unipolar conduction by two sets of carriers of different mobility [cf. light and heavy hole conduction in p-type Ge, Willardson et al (1954)]. If applied to 'light and heavy electrons', the theory does predict that R_H will fall, and eventually saturate, with increasing magnetic field. However, only an approximate fit could be made to the InAs Hall data.

5.3 (v) Discussion

The results of the analyses presented above are summarised in Table 5.1. For comparison, the directly measured Hall properties were, at 0.3 T, $\mu(300\text{ K})=11 \times 10^3\text{ cm}^2/\text{V-s}$, $n(300)=9 \times 10^{15}\text{ cm}^{-3}$, $\mu(77\text{ K})=46 \times 10^3\text{ cm}^2/\text{V-s}$ and $n(77\text{ K})=5.9 \times 10^{15}\text{ cm}^{-3}$ (see also Fig 5.4). These values significantly underestimate the mobility and overestimate the carrier concentration of the bulk-like region of the epilayer. This is reasonable, given the influence of the accumulated interfaces. Table 5.2 compares the results of several workers who have examined the electrical properties of InAs on (100) GaAs. Three points are immediately apparent;

- (i) All workers have found that the ratio, μ_b/μ , of the bulk-region mobility to the directly measured mobility is ≈ 3.2 at 300 K and ≈ 1.9 at 77 K. As shown by the data of Washburn et al (1979), this observation is not confined to the highest mobility layers.
- (ii) Similarly, all workers have found the ratio n/n_b to be ≈ 2.7 at 77 K. The situation is less clear at 300 K because of the lack of data for comparison.
- (iii) The comments above apply to both MBE and VPE grown material.

Table 5.1: The 300 K and 77 K properties of the bulk-like region of a 23.4 μm thick unintentionally doped InAs epilayer grown in CLPIV

B_H	μ_b (two layer analysis)	μ_b (multi layer analysis)	n_b (two layer analysis)	n_b (multi layer analysis)
(T)	($\text{cm}^2/\text{V-s}$) $\times 10^{-4}$	($\text{cm}^2/\text{V-s}$) $\times 10^{-4}$	(cm^{-3}) $\times 10^{-15}$	(cm^{-3}) $\times 10^{-15}$
300 K Data				
0.30	24.8 \pm 7.1		1.64 \pm 0.62	
0.65				
1.00	30.0 \pm 8.3	29.9 \pm 0.46	1.34 \pm 0.43	1.34 \pm 0.15
1.40				
77 K Data				
0.30	91.6 \pm 9.8	91.7 \pm 8.6	1.60 \pm 0.46	1.61 \pm 0.37
0.65	87.8 \pm 9.6	93.3 \pm 2.9	1.67 \pm 0.43	1.57 \pm 0.11
1.00	80.7 \pm 8.9	81.7 \pm 6.2	1.81 \pm 0.52	1.80 \pm 0.36
1.40	74.1 \pm 7.9	78.6 \pm 5.9	1.98 \pm 0.57	1.87 \pm 0.16

Table 5.2: Directly measured Hall properties compared with the properties derived for the bulk-like regions of InAs epilayers grown on (100) GaAs by MBE and VPE

	Growth Technique	Layer Thickness ^a (μm)	Directly Measured Properties		Derived Properties		μ_b/μ
			μ ($\text{cm}^2/\text{V-s}$)	N_D-N_A (cm^{-3})	μ_b ($\text{cm}^2/\text{V-s}$)	$(N_D-N_A)_b$ (cm^{-3})	
300 K Properties							
Grange et al (1979) ^b	MBE	1	8.3×10^3	6.4×10^{16}	30×10^3	2.1×10^{15}	3.61
This study ^b	MBE	23	11×10^3	9.0×10^{15}	30×10^3	1.3×10^{15}	2.73
77 K Properties							
Washburn (1978) ^c	VPE	15	60×10^3	3×10^{15}	120×10^3	1.2×10^{15}	2.03
Washburn et al (1979) ^d	VPE	15	21×10^3	2×10^{16}	35×10^3	9.0×10^{15}	1.67
This study ^b	MBE	23	46×10^3	6×10^{15}	90×10^3	1.7×10^{15}	1.96

^a Thickness of layer at which the directly measured properties were obtained.

^b Depth profile by chemical etch.

^c μ_b , n_b estimated from 'best fit' to Eqtns 5.7 & 5.8 at high and low magnetic fields.

^d Depth profile by argon ion milling.

The good agreement of μ_b/μ and n/n_b between these studies is to be expected as essentially the same model was used in all of the analyses (the linear plots derived from Eqtns 5.13 and 5.14 are evidence for the validity of the model). As a general point, it should be noted that any etching or milling technique will modify the front surface of the epilayer. This may lead to sequential changes in the measured electrical properties (i.e. because of increasing surface roughening) if several layers of material are removed. This would obviously give spurious results in the present application. The 77 K data in Table 5.2 is particularly useful because three separate techniques were used to estimate the properties of the bulk-like region of the layer; profiling by argon ion milling [Washburn et al (1978, 1979)], etch profiling (this study) and fitting parameters to Eqtns 5.7 and 5.8 [Washburn et al (1979)]. Although the latter analysis did not involve etching or milling, the results obtained were comparable to (and lend confidence to) those obtained by physical profiling.

5.4 Temperature Dependence of the Hall Properties

Figure 5.13 shows the temperature variation of the Hall properties of a 34 μm thick unintentionally doped n-type epilayer grown in CLPIV. The data shown in the diagram was measured at $B_H=0.3$ T. The parameters measured at other fields were qualitatively similar, and it was found that

$$\begin{array}{lll} \mu = AT^{-1.46} & \text{for} & 100 \text{ K} < T < 300 \text{ K} \\ \text{and } \mu = BT^{0.85} & \text{for} & 10 \text{ K} < T < 50 \text{ K} \end{array}$$

where A and B are fixed parameters at a given magnetic field. The overall behavior of both μ and n is similar to that seen in lightly doped GaAs (e.g. see Fig 3.4).

Referring to the InAs data, $N_D - N_A$ fell from $1.1 \times 10^{16} \text{ cm}^{-3}$ to $6.2 \times 10^{15} \text{ cm}^{-3}$ (0.3 T data) as the temperature was

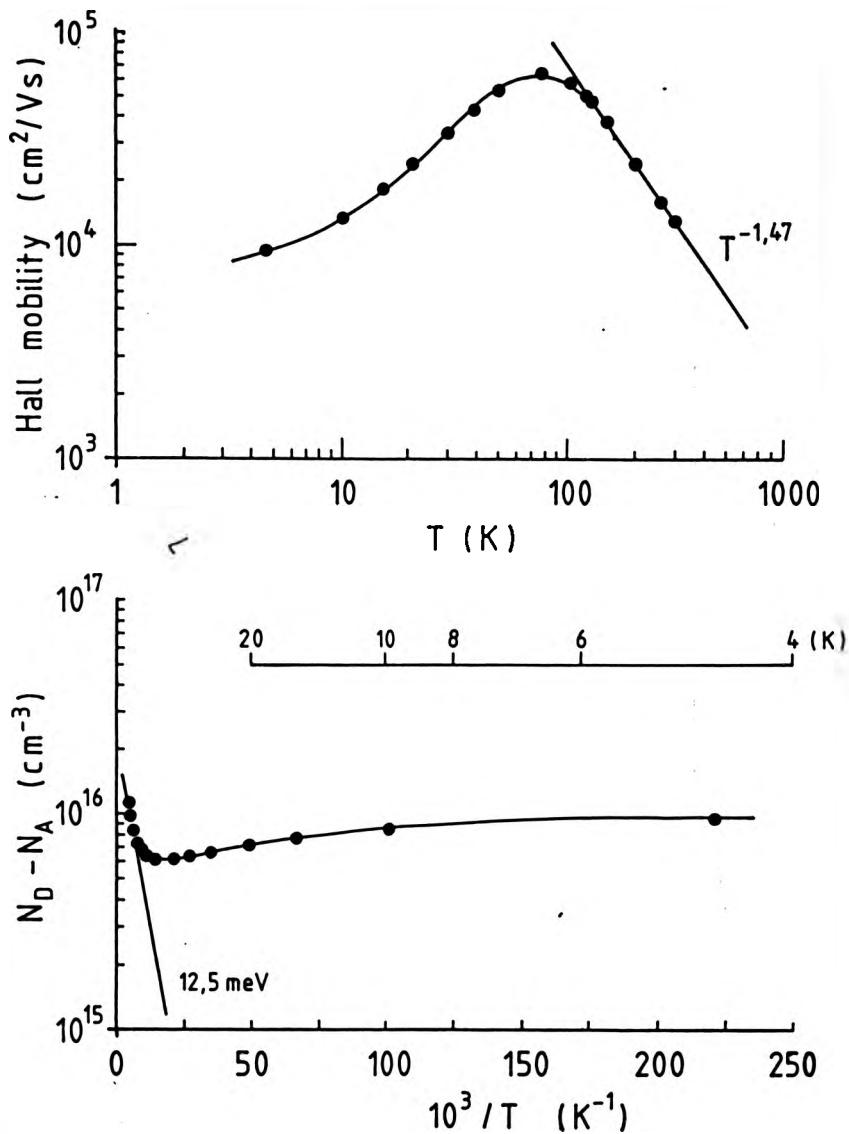


Fig 5.13 The temperature dependence of the Hall properties of a thick (34 μm) unintentionally doped InAs epilayer grown in CLPIV.

reduced from 300 K to 77 K. Similar behaviour was associated with the freezeout of shallow (Sn) donors in GaAs [Sec 3.2(ii)]. However, the activation energy obtained from the InAs data is 12.5 meV. This is much larger than the ionisation energy of hydrogen-like donors in InAs, which freezeout measurements on Si, Ge, Sn, S, Se and Te doped melt grown InAs indicate to be about 5 meV [Schillmann (1956)]¹. The carriers in question are not intrinsic as 12.2 meV is less than one tenth of $E_g/2$ [180 meV at 300 K, Landolt-Bornstein (1982)]. Furthermore, Casey (1962) has calculated the intrinsic carrier concentration of InAs at 300 K to be $2 \times 10^{14} \text{ cm}^{-3}$. It is possible that Fig 5.13 shows (i) the freezeout of defect-related carriers at the epilayer/substrate interface, or (ii) the freezeout of a deep donor. The first of these possibilities is supported by the observation that the carrier concentration derived for the bulk-like region of the epilayer analysed in Sec 5.3 increased by a factor of 1.3 between 300 K and 77 K [Table 5.1; the actual variation could be smaller if the estimates of $N_D - N_A$ were affected by variations in τ_H between 300 K and 77 K, Anderson and Apsley (1986)].

The cessation of carrier freezeout in InAs (starting at ≈ 100 K in Fig 5.13) may be attributable to the onset of hopping conduction as described in Sec 3.2 (ii). However, the ground state wavefunctions of hydrogen-like donors in InAs begin to overlap at $N_D = 2 \times 10^{16} \text{ cm}^{-3}$ (calculated using $m^*/m = 0.028$ and $\epsilon = 12.5$ in Eqtns 3.1 and 3.2). It is, therefore, possible that impurity band conduction contributes to low temperature transport even in lightly doped InAs [Harrison and Houston (1986)]. There is also the possibility that the low mobility electrons in the 2DEG at the free

¹ An ionisation energy of 2.4 meV can be estimated by using $\epsilon = 12.5$ and $m^*/m = 0.028$ in $E_i = 13.6 m^*/m \epsilon^2$.

surface of the InAs epilayer do not freeze out. However, the basic similarity between Fig 5.13 and the GaAs data shown in Fig 3.4 implies that the same mechanism causes the cessation of freezeout in both compounds, and it is difficult to see how a 2DEG would arise in homoepitaxial GaAs.

It is believed that the Hall mobility was limited by acoustic deformation (phonon) scattering at the higher temperatures investigated (100 K to 300 K). This would lead to a $T^{-3/2}$ temperature dependence in a semiconductor with spherical E-k surfaces [Nag (1980), Seeger (1982)]. However Hilsam and Rose-Innes (1961) indicate that the phonon limited mobility in bulk InAs is proportional to T^{-x} with $1.2 < x < 1.5$. The $T^{-1.47}$ temperature dependence observed in the MBE grown samples (Fig 5.13) lies within this range and is identical to that previously obtained from measurements made on bulk [Madelung (1964), Wagini (1965)] and VPE [Weider (1974)] grown InAs.

5.5 Majority Carrier Properties of Si and Sn doped InAs

As shown in Sec 5.3, the Hall properties of lightly doped layers are significantly affected by field and thickness effects. The parameters used for all measurements reported below were $B_H = 0.3$ T and $I_H = 1.0$ mA. No evidence of Joule heating (e.g. as manifested by a short term drift in the Hall voltages) was noticed at any of the doping levels investigated.

5.5 (i) Co-evaporation Doping of MBE-InAs

Figure 5.14 shows the dependence of the 300 K Hall carrier concentration in InAs and GaAs on the Si cell temperature. The data is normalised to a growth rate of $1.0 \mu\text{m/hr}$ and the GaAs doping levels have been corrected for the

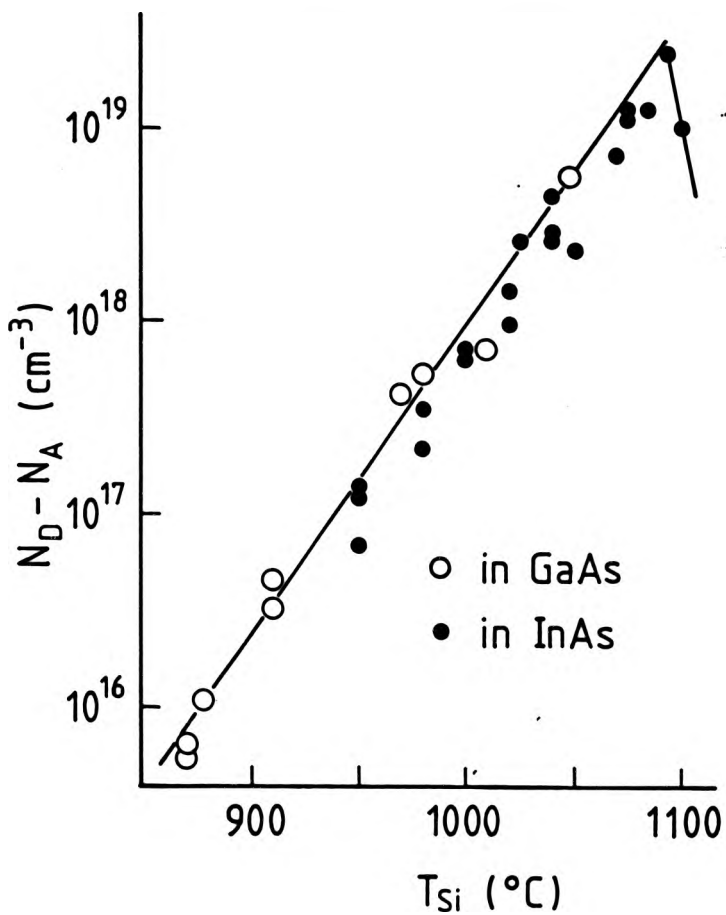


Fig 5.14 The dependence of the 300 K Hall carrier concentration in InAs and GaAs on the Si cell temperature, normalised to a growth rate of $1 \mu\text{m/h}$ and corrected for the different lattice spacings of the two compounds.

different atomic density of InAs and GaAs. A similar doping efficiency is apparent in InAs and GaAs at carrier concentrations of between 7×10^{16} and $2 \times 10^{19} \text{ cm}^{-3}$. This indicates that Si has a unity sticking co-efficient and exhibits 100% electrically active incorporation in MBE grown InAs, as these properties have previously been demonstrated for Si in MBE grown GaAs [Cho and Arthur (1975), Chai et al (1981), Mendez et al (1983), Hiyamizu et al (1981), Sacks and Shen (1985)]. The peak carrier concentration in Fig 5.14 is not equal to the maximum attainable doping level in InAs because the data was normalised from a number of growth rates within the range 0.9 to 3.6 $\mu\text{m/h}$. Peak doping levels are discussed in Sec 5.5(iii).

5.5 (ii) Mobility versus Carrier Concentration

Figures 5.15 and 5.16 show the the 300 K and 77 K Hall mobilities of Si, Sn and unintentionally doped InAs epilayers grown in CLPIV as a function of the (Hall) carrier concentration. Representative data from other studies is included for comparison. The solid line in Fig 5.15 (300 K data) is fitted to the extensive bulk doping data of von Schillmann (1956). At doping levels below $1 \times 10^{19} \text{ cm}^{-3}$ this line is closely fitted by the semi-empirical expression [Hilsum (1974)],

$$\mu = \mu_0 / \{1 + (N/N_0)^n\} \quad 5.21$$

with $\mu_0 = 2.8 \times 10^4 \text{ cm}^2/\text{V-s}$, $N_0 = 5 \times 10^{17} \text{ cm}^{-3}$ and $n=0.5$. NB: the Hall mobilities reported by von Schillmann (1956) were based on a Hall factor (r_H) of $3\pi/8$. These mobilities were re-calculated on the basis of a Hall factor of unity before inclusion in Fig 5.15 to allow direct comparison with the MBE results. The solid line in Fig 5.16 (77 K data) was not derived from bulk data but was fitted to Eqtn 5.21 with $\mu_0 = 1 \times 10^5 \text{ cm}^2/\text{V-s}$, $N_0 = 2 \times 10^{16} \text{ cm}^{-3}$, and $n=0.5$ to provide an approximate datum for the purposes of comparison. However,

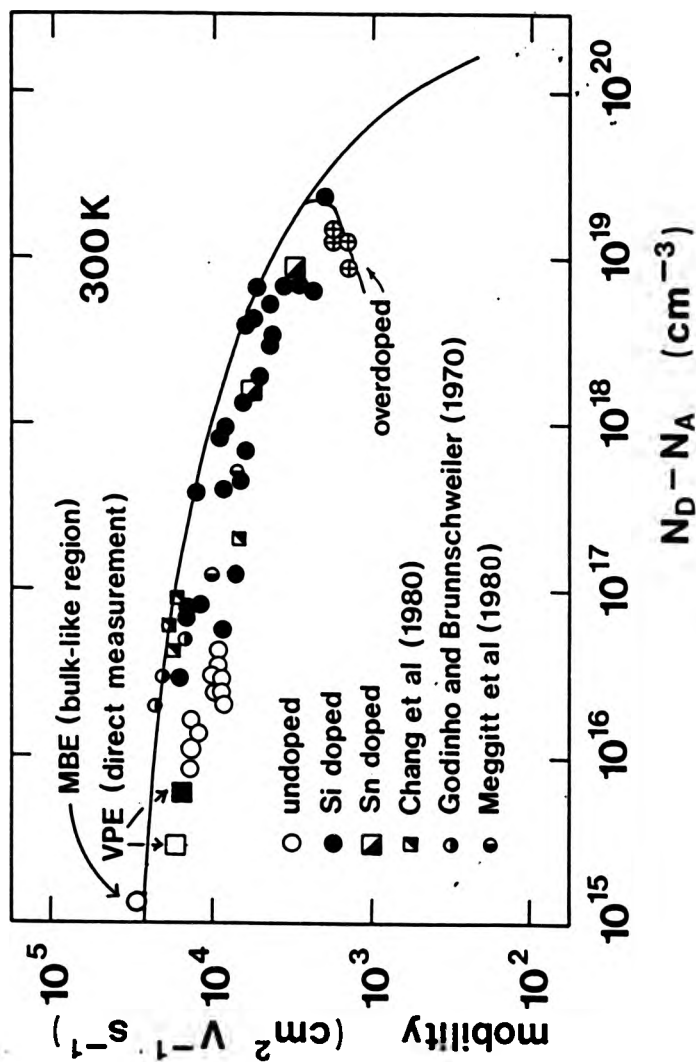


Fig 5.15 The 300 K Hall mobilities of InAs epilayers grown in CLPIV as a function of the (Hall) carrier concentration. The solid line is fitted to the extensive bulk doping data of Schillmann (1956). Representative data is included from other MBE and VPE [open box, Weider (1974); filled box, McCarthy (1967)] growth studies.

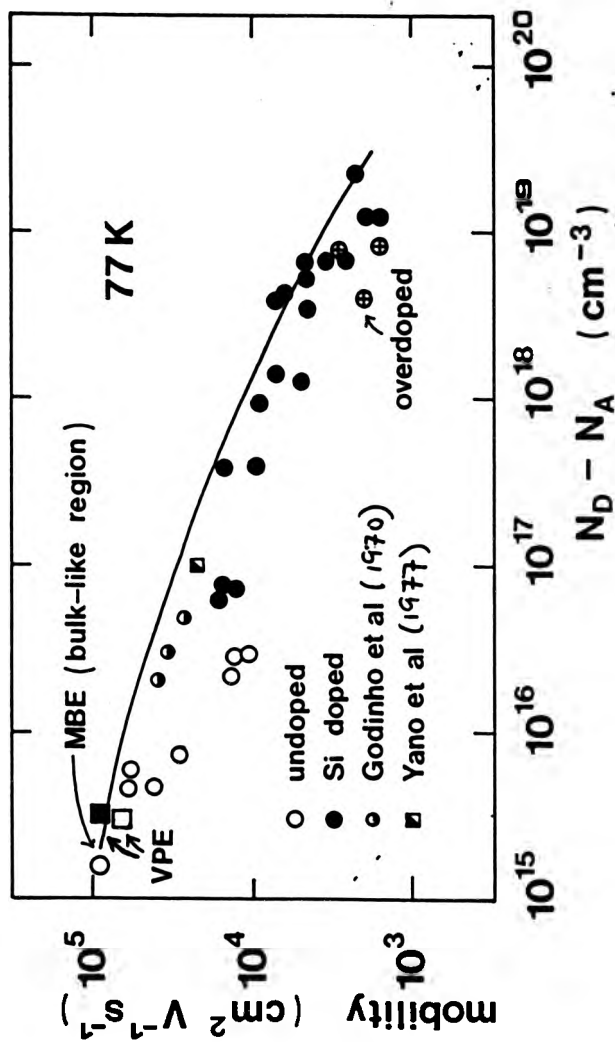


Fig 5.16 77 K Hall mobilities of InAs epilayers grown in CLPIV as a function of the (Hall) carrier concentration. Representative MBE and VPE [open box, Washburn (1978); filled box, McCarthy (1967)] data is shown for comparison.

this line is a reasonable fit to the upper limit of the 77 K VPE data of McCarthy (1967), which covers carrier concentrations of between $2 \times 10^{15} \text{ cm}^{-3}$ and $4 \times 10^{17} \text{ cm}^{-3}$.

Harrison and Houston (1986) have calculated 77K mobility versus carrier concentration curves for InAs at compensation ratios of 1 and 0.5. Their calculations included the effects degeneracy as well as polar-optical and ionised impurity scattering. The mobilities predicted for uncompensated material at doping levels of between $1 \times 10^{17} \text{ cm}^{-3}$ and $1 \times 10^{18} \text{ cm}^{-3}$ are approximately 30% higher than those obtained from epilayers grown in CLPIV. Harrison and Houston (1986) also present mobility data on intentionally doped (Sn and Te) n-type InAs grown by LPE. The mobilities claimed for these layers are in agreement with the theoretical calculations. *Two possible explanations are,*

- (i) A non-unity Hall scattering factor (r_H) may have been assumed when analysing the Hall data. An assumption that $r_H = 3\pi/8$ would account for more than half of the discrepancy.
- (ii) Harrison and Houston measured the properties of junction isolated homolayers. It is possible that the epilayers were not completely isolated from the p^+ substrates, or that electrical inhomogenities had occurred by some other means. As demonstrated in Sec 5.3, this could have been checked by performing Hall measurements at several magnetic fields. A particular cause for concern is that the temperature variation of the Hall mobility of the n^- LPE samples was very weak compared to that shown in Fig 5.13.

Returning to the MBE results, certain features are common to both Fig 5.15 and Fig 5.16. Most noticeably, there is appreciable spread on the data. This can be attributed to two factors;

(i) Several of the epilayers doped to $1 \times 10^{17} \text{ cm}^{-3}$ or higher were nucleated under slightly non-optimum conditions (these layers were grown during the optimization exercises reported in Chapter 4). The unintentional doping level in these layers would, in general, be considerably lower than the intentional doping level and would not be expected to affect the results. However, these layers were moderately defected (Fig 4.3) possibly leading to increased carrier scattering [Many et al (1965)].

(ii) Although all epilayers having doping levels below $1 \times 10^{17} \text{ cm}^{-3}$ and included in Figs 5.15 and 5.16 were nucleated under optimum conditions, interfacial conduction will have reduced the mobilities measured at these doping levels as described in Sec 5.3.

Referring to Fig 5.15, it is apparent that the 300 K mobilities of the unintentionally doped epilayers grown in CLPIV lay slightly below those of the Si doped epilayers grown to similar carrier concentrations ($1 \times 10^{16} < N_D - N_A < 1 \times 10^{17} \text{ cm}^{-3}$). This implies that the undoped layers were more compensated, although it is difficult to see how n^- doping could reduce the net acceptor density. Despite this, Figs 5.15 and 5.16 show that the Hall mobilities of n^- InAs epilayers grown in CLPIV were comparable with those obtained from VPE-grown material at similar carrier concentrations. It will also be seen that the mobilities derived for the bulk-like region of the 23.4 μm epilayer (see Sec 5.3) were appropriate to the carrier concentration.

It was not possible to use PL techniques to identify the residual donor in the InAs epilayers as this material is not yet characterised and, in any case, it is expected that the donors would be too shallow to permit easy identification. It seems probable that many of the

electrons at the epilayer/substrate interface are defect-derived (see also 5.4 above). The origin of the donors in the bulk-like layer is less certain. It is possible that carbon, the predominant acceptor in the GaAs grown in CLPIV, incorporates as a donor in InAs. This would explain; (i) the correlation between the almost constant background acceptor level of the n⁻ GaAs epilayers [$\approx 1.5 \times 10^{15} \text{ cm}^{-3}$, Sec 3.2 (ii)] and the residual donor level in InAs [also $\approx 1.5 \times 10^{15} \text{ cm}^{-3}$, Table 5.1]; (ii) why relatively high residual doping levels tended to be reported in previous MBE growth studies [Table 4.1: Grange (1980), Kubiak (1983) and Croydon (1985) all indicate that carbon incorporation has been a problem in home-built MBE systems]; and (iii) why the residual doping level tends to decrease with increasing growth temperature [Table 4.1], assuming that the carbon (compound?) is volatile on InAs at normal growth temperatures. Unfortunately, no data is available on the electrical behaviour of C in InAs to support or refute this suggestion.

Without disregarding the problems discussed above, the 300 K bulk Hall data (Fig 5.15) accurately delineates the upper limit of the mobilities measured on epilayers grown in this and other MBE studies, indicating that good quality intentionally doped InAs epilayers can be grown by MBE.

5.5 (iii) Maximum Doping Levels Attainable in InAs

Referring to Fig 5.15, a peak in the 300K Si doping level was attained at a carrier concentration of $2.4 \times 10^{19} \text{ cm}^{-3}$. Any attempt to dope at higher levels, e.g. by increasing the temperature of the Si cell, resulted in decreases in the carrier concentration and Hall mobility. The same phenomenon is noticeable in the 77K data (Fig 5.16). Overdoped layers had roughened surfaces, and occasionally showed accumulations of metallic droplets. Similar behaviour has been reported at high doping levels in Si

doped MBE GaAs [Chai et al (1981)] and InGaAs [Kubiak et al (1984b)]. Whichever host material is considered, the decrease in carrier concentration and mobility beyond the peak suggests the onset of compensation. Two basic mechanisms have been suggested; (i) autocompensation, caused by the incorporation of Si on the As sub-lattice, and (ii) compensation caused by the incorporation of nitrogen generated by the decomposition of the PBN components of the Si source at high temperatures [Sachs and Shen (1985), Leroux et al (1986)]. With regard to (i), Chai et al (1981) have suggested that, in GaAs, the strain associated with the insertion of the relatively small Si⁺ ion eventually leads to incorporation into the arsenic sublattice and that, if Si⁺ ions are present on adjacent lattice sites, precipitation of the dopant ensues because of the high Si-Si bond strength.

It is also possible that atomic size effects influence the maximum attainable carrier concentrations [size effects in MBE are discussed more fully by Patel et al (1987)]. Figure 5.17 shows that (as far as can be seen from the available data) the peak Si and Sn derived carrier concentrations attainable in InGaAs increase linearly with increasing In mole fraction. The average atomic radii of the lattice and dopant atoms are [Dean (1985)];

Species	Atomic Radius (Å)	
	Neutral	1 ⁺
Ga	1.25	
As	1.21	
In	1.60	
Si	1.17	0.65
Sn	1.40	0.82

A dopant atom thermally accommodated with the epilayer surface will possess an energy $=kT$, i.e. 0.08 eV at 600°C. This energy is small compared to the first ionisation

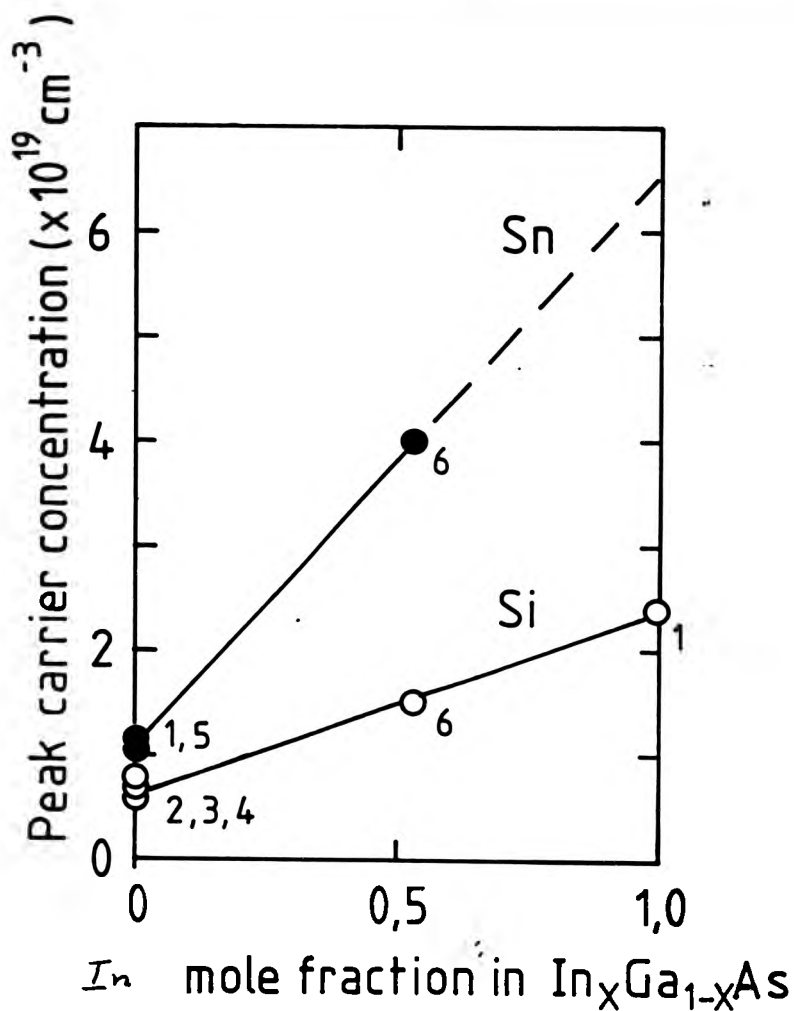


Fig 5.17 Peak carrier concentrations attainable in InGaAs as a function of the In mole fraction. References (1) This study, (2) Chai et al (1981), (3) Akimoto et al (1983), (4) Neave et al (1983), Appl. Phys. A 32, 195, (5) Harris et al (1982), (6) Kubiak et al (1984b).

potentials of both Si (8.15 eV) and Sn (7.34 eV) [Kaye and Laby (1975)] and so the dopants may be expected to remain as neutral atoms until after incorporation. If the compound being doped is GaAs, in which both matrix species are closely similar in size, it is reasonable to assume that other factors determine the sublattice upon which the greater number of dopant atoms incorporate. If, however, the matrix atoms differ appreciably in size, as is the case with InAs, it is possible that the dopant atoms would be forced to incorporate as substitutes for the matrix atom closest to their own size. As Sn atoms are comparable in size to the In atom, this effect would oppose their incorporation on the As sublattice and so, conceivably, delay the onset of compensation at high doping levels. It would not be unreasonable to expect an approximately linear variation in the maximum attainable carrier concentration for intermediate compositions, as shown in Fig 5.17. (NB: Harrison and Houston (1986) have reported an upper doping limit of $\approx 2 \times 10^{18} \text{ cm}^{-3}$ in LPE InAs. This limit was determined by the solubility of Sn in the melt, a factor which does not affect MBE growth).

The highest Si-derived carrier concentration reported in bulk-grown InAs is $1 \times 10^{20} \text{ cm}^{-3}$ [von Schillmann (1956)], or approximately four times greater than the peak level attained in the MBE experiments reported here. This behaviour differs from that of GaAs, in which the highest attainable electron concentration ($\approx 8 \times 10^{18} \text{ cm}^{-3}$) appears to be almost independent of the the dopant and growth technique [bulk or epitaxial, Wright (1985)]. It is difficult to suggest an explanation for this observation in terms of size effects.

Resistivity is often of more interest than carrier mobility in the applications of heavily doped epitaxial material (low resistivity buffer layers, etc). Figure 5.18 shows the variation in resistivity with (Hall) carrier concentration of the n-type InAs epilayers grown in CLPIV. The solid line

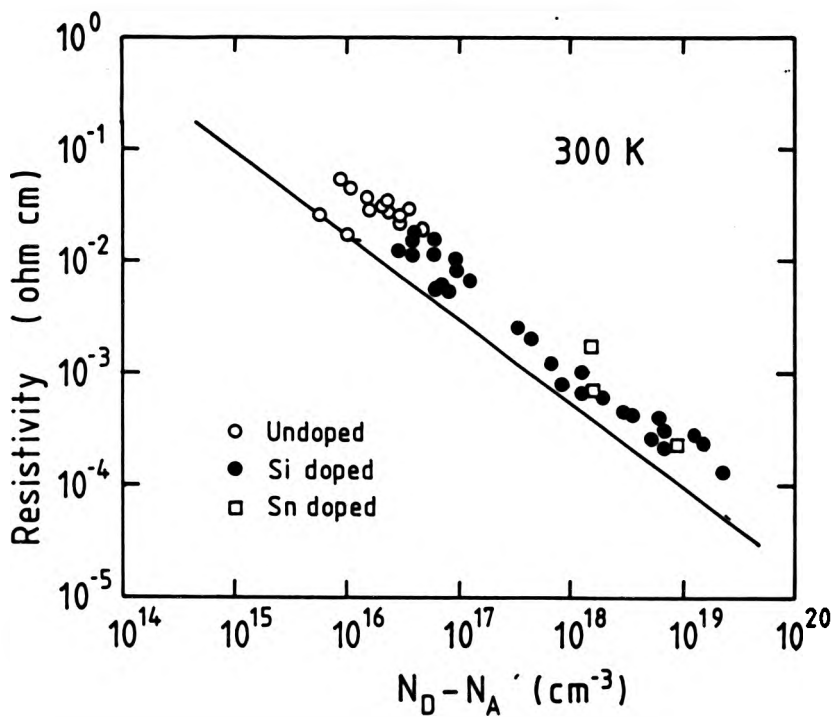


Fig 5.19 The resistivity of the n-type InAs epilayers grown in CLPIV as a function of the (Hall) carrier concentration. The solid line is fitted to the bulk doping data of Schillmann (1956).

delimiting the lower boundary of the resistivities is fitted to bulk doping data [von Schillmann (1956)] and is described by the expression

$$\rho = [4.55 \times 10^{13} / N]^{0.75} \text{ } \Omega \text{ cm}$$

where N is the free carrier concentration in cm^{-3} . The lowest resistivity MBE grown material was obtained by doping to the highest attainable carrier concentration; no reduction in resistivity was obtained by overdoping. A resistivity of $1.3 \times 10^{-4} \text{ } \Omega \text{ cm}$ was obtained at the peak Si doping level ($2.4 \times 10^{19} \text{ cm}^{-3}$). Figure 5.18 shows that a resistivity of about $5.5 \times 10^{-5} \text{ } \Omega \text{ cm}$ would be expected from bulk material at the same carrier concentration, so there is some potential for improvement. However, greater reductions in the resistivity of MBE grown InAs may be possible through the use of Sn as a dopant; resistivities down to $2.4 \times 10^{-5} \text{ } \Omega \text{ cm}$ would be accessible if, as is suggested by Fig 5.17, carrier concentrations of up to $6.5 \times 10^{19} \text{ cm}^{-3}$ could be attained. For comparison, the lower limit to the resistivity of Si doped GaAs grown by MBE has been reported to be $4.75 \times 10^{-4} \text{ } \Omega \text{ cm}$ [Sachs and Shen (1985)].

5.6 Summary and Conclusions

The co-evaporation doping of InAs with Si and Sn was investigated. Both impurities exhibited controllable doping behaviour and 100% electrically active incorporation at concentrations above $1 \times 10^{16} \text{ cm}^{-3}$. The maximum carrier concentration available using Si was $2.3 \times 10^{19} \text{ cm}^{-3}$. The significance of atomic size effects in determining the peak carrier concentration were discussed. The Hall mobilities of epilayers doped in excess of $5 \times 10^{16} \text{ cm}^{-3}$ were comparable to those obtained from bulk-grown InAs. At lower doping levels the Hall properties were found to be strongly dependent on the layer thickness and magnetic field (B_H). Analysis of the data indicated that, at low doping levels, conduction took place through two layers; an accumulation

of low mobility electrons at an 'interfacial region', believed to be a composite of the free surface and the epilayer/substrate interfaces; and a region of 'bulk-like' material remote from the interfaces. Chemical etch profiling was used to derive a weakly B_H dependent 77 K mobility of $\approx 90 \times 10^3$ $\text{cm}^2/\text{V-s}$ at $N_D - N_A = 1.5 \times 10^{15}$ cm^{-3} for the bulk-like region of a thick unintentionally doped layer. This figure is comparable to the best mobilities obtained from VPE and bulk grown material at similar doping levels. The electron mobility of the bulk-like layer was found to be ≈ 2.7 times larger than the directly measured mobility at 300 K and 2.0 times larger at 77 K. Similar ratios have previously been derived from both MBE and VPE grown material by a variety of techniques (including profiling by chemical etch and argon ion milling, and the fitting of theoretical expressions to experimental data).

In conclusion, the electrical properties of doped and undoped InAs epilayers grown on (100) GaAs by MBE have been shown to compare favorably with those of heteroepitaxial layers grown by rival epitaxial techniques. Although the effects of carbon incorporation in MBE InAs are unclear, it is apparent that good quality InAs could be grown without undue difficulty in a system which yielded (by the standards of mid-1980's commercial systems) GaAs quite highly compensated with carbon.

Results and Proposals

The work reported in this thesis clearly demonstrates that system design, good operating procedures and the optimisation of growth conditions are of equal importance in determining the quality of the materials grown in MBE experiments. The quality of the GaAs grown in the course of this project was limited by carbon incorporation, believed to have resulted from the use of graphite crucibles in the high temperature sources. It would be necessary to alleviate this problem before high quality GaAs/AlGaAs device structures could be grown. This may only require the substitution of PBN crucibles: however, it is not felt that chasing high mobilities in GaAs would be original or useful as an objective for further study.

The growth of InAs based compounds for device purposes would be more productive and follows naturally from the content of this thesis. There is currently a need for optoelectronic emitters and detectors operating at wavelengths in the range 2-4 μm , e.g. to exploit the low loss and dispersion windows predicted for long-haul fluoride glass optical fibers [Tran et al (1986)]. As described in Chapter 1, several InAs-based compounds are available to access these wavelengths. In many cases only a small fraction of a third element need be added to the binary. For example, $\text{InAs}_{0.91}\text{Sb}_{0.09}$ is lattice matched to GaSb and has been found useful for the active layers of both laser emitters [van der Zeil et al (1986)] and photodetectors [Bubulac et al (1980)]. It is not unreasonable to expect that the optimum growth conditions for this ternary should be little different for those identified for InAs in the present study. If so, it should be possible to realise an actual device structure at an early stage of a future project. Such a study could profitably be extended to include an investigation of the growth and doping of the Sb

rich alloys of In, Ga, Al and As, as required for cladding and confinement layers [van der Zell et al (1986)]. It would be particularly interesting to determine the extent to which MBE may be used to grow within the equilibrium miscibility gaps of these compounds [Stringfellow (1983)]. It may also be necessary to grow strained-layer superlattices [Hughes (1987)].

The performance of the MBE system constructed during the present study should be adequate¹ for the tasks outlined above as, despite the carbon background, the best InAs grown in this system was of comparable quality to LPE and VPE grown material. Furthermore, the close control of the growth conditions available when using this system would be a considerable advantage whether investigating new materials systems or attempting to reproduce device characteristics.

¹ after the provision of Al and Sb sources and alternative dopants.

References

- Aina L, Mattingly M and Pande K (1986), Appl. Phys. Lett. 49, 865
- Anderson D A, Apsley N, Davies P and Giles P L (1985), J. Appl. Phys. 58, 3059
- Anderson D A and Apsley N (1986), Semicon. Sci. Technol. 1, 187
- Andrews D A, Kong M Y, Heckingbottom R and Davies G J (1984), J. Appl. Phys. 55, 841
- Akatsu Y, Ohno H and Hasegawa H (1987), J. Crystal Growth 81, 319
- Akimoto K, Dohsen M, Arai M and Watanabe N (1984), Appl. Phys. Lett. 45, 922
- Arthur J R (1973), Surf. Sci. 43, 449
- Ashcroft N W and Mermin D N (1976), 'Solid State Physics', Holt-Saunders, New York
- Bachrach R Z, Bauer R S, Chiaradia P and Hansson G V (1981), J. Vac. Sci. Technol. 19, 335
- Bachrach R Z and Kruszor B S (1981), J. Vac. Sci. Technol. 18, 756
- Bachrach R Z and Bringans R D (1983), J. Vac. Sci. Technol. B1, 142
- Baglee D A, Ferry D K, Wilmsen C W and Weider H H (1982), J. Vac. Sci. Technol. 17, 1032
- Balagurov L A and Borkovskaya O Y (1976), Sov. J. Phys. Semicon. 10, 659
- Ballingall J M and Wood C E C (1982), Appl. Phys. Lett. 41, 947
- Ballingall J M and Wood C E C (1983), J. Vac. Sci. Technol. B1, 162
- Bandy S, Nishimoto C, Hyder S and Hooper C (1981), Appl. Phys. Lett. 38, 817
- Barnard J A, Ohno H, Wood C E C, Eastman L F (1980), IEEE Electron Device Lett. EDL-1, 174
- Barnes P A and Cho A Y (1979), Appl. Phys. Lett. 33, 651
- Bauer E (1969) in 'Techniques of Metals Research', R Bunshan Ed., 3, 501

- Bean J C and Dingle R (1979), *Appl. Phys. Lett.* 35, 925
- Benchimol J L (1987), CNET, Priv. Comm.
- Blakemore J S (1959), *Phil. Mag.* 4, 560
- Blood P, Roberts J S and Stagg J P (1982), *J. Appl. Phys.* 53, 3145
- Briones F and Collins D M (1982), *J. Electron. Mat.* 11, 847
- Briones F, Golmayo D, Gonzalez L and De Miguel J L (1985), *Jap. J. Appl. Phys.* 24, L478
- Bubulac L O, Andrews A M, Gertner E R and Chueng D T (1980), *Appl. Phys. Lett.* 36, 734
- Calawa A R (1978), *Appl. Phys. Lett.* 33, 1020
- Caldwell P J, Laidig W D, Lin Y F, Peng C K, Magee T J and Leung C (1985), *J. Appl. Phys.* 57, 984
- Casey H C and Panish M B (1978), 'Heterostructure Lasers', Academic Press, New York
- Chai Y G and Chow R (1981), *Appl. Phys. Lett.* 38, 796
- Chai Y G, Chow R and Wood C E C (1981), *Appl. Phys. Lett.* 39, 800
- Chai Y G, Pao Y-C and Hierl T (1985), *Appl. Phys. Lett.* 47, 1327
- Chandra A, Wood C E C, Woodward D W and Eastman L F (1979), *Solid State Electron.* 22, 645
- Chang C-A, Serrano C M, Chang L L and Esaki L (1980) *Appl. Phys. Lett.* 37, 538
- Chang C-A (1982), *J. Vac. Sci. Technol.* 21, 663
- Chang C-A, Mendez E E, Chang L L and Esaki L (1984), *Surf. Sci.* 142, 598
- Chang C-A (1985), Chapter 9 in 'Proceedings of the NATO ASI on MBE and Heterostructures' (Erice, Italy 1983), Nijhoff, Netherlands
- Chang L L, Esaki L, Howard W E and Ludeke R (1973), *J. Vac. Sci. Technol.* 10, 11
- Chang L L and Esaki L (1980), *Surf. Sci.* 98, 70
- Chang L L (1983), *J. Vac. Sci. Technol.* B1, 120
- Chattopadhyay D and Quisser J J (1981), *Rev. Mod. Phys.* 53, 745

- Cheng K Y, Cho A Y, Wagner W R, Bonner W A (1981), J. Appl. Phys. 52, 1015
- Cheung D T, Andrews A M, Gertner E R, Williams G M, Clarke J E, Pasko J G and Longo J T (1977), Appl. Phys. Lett. 30, 587
- Chiu T H, Zyskind J L and Tsang W T (1987), J. Electronic Materials 16, 57
- Cho A Y (1970), J. Appl. Phys. 41, 2780
- Cho A Y (1971a), J. Appl. Phys. 42, 2074
- Cho A Y (1971b), J. Vac. Sci. Technol. 8, S31
- Cho A Y and Hiyashi I (1971), J. Appl. Phys. 42, 4422
- Cho A Y (1975), J. Appl. Phys. 46, 1733
- Cho A Y and Arthur J R (1975), Prog. in Solid State Chem. 10, 157
- Cho A Y and Ballamy W C (1975), J. Appl. Phys. 46, 783
- Cho A Y (1976), J. Appl. Phys. 47, 2841
- Cho A Y and Reinhart F K (1982), Appl. Phys. Lett. 21, 355
- Cho A Y (1983), Thin Solid Films 100, 291
- Covington D W and Meeks E L (1979), J. Vac. Sci. Technol. 16, 847
- Covington D W, Litton C W, Reynolds D C, Almassey R J and McCoy G L (1979), Inst. Phys. Conf. Ser. 45, 171
- Cronin G R, Conrad R W and Borrello S R (1966) J. Electrochem. Soc. 113, 1336
- Croydon W F (1985), PhD Thesis CNAAC, City of London Polytechnic
- Croydon W F, Dowsett M G, King R M and Parker E H C (1985), J. Vac. Sci. Technol. B3, 604
- Dahr S, Hong W-P, Bhattaycharya P K, Nashimoto Y and Juang F-Y (1986), IEEE Trans. Electron Dev. ED-33, 698
- Dapkus P D (1984), J. Crystal Growth 68, 345
- Davies G J, Andrews D A and Heckingbottom R (1981), J. Appl. Phys. 52, 7214
- Davies G J and Andrews D A (1984), Vacuum 34, 543

- Davies G J and Williams D (1985), in 'The Technology and Physics of Molecular Beam Epitaxy', E. H. C. Parker, Ed., Plenum, New York, pp 15-44
- Dean J A (1985) Ed., 'Lange's Handbook of Chemistry', 13th Ed., McGraw-Hill, New York
- DeBarr A E (1962), 'Automatic Control', IoP/Chapman and Hall, London
- Dingle R, Weisbuch C, Stormer H L, Morkoc H and Cho A Y (1982), Appl. Phys. Lett. 40, 507
- Dixon J R and Enright D P (1959), J. Appl. Phys. 30, 1462
- Dobson P J, Neave J H and Joyce B A (1982), Surf. Sci. 119, L339
- Dobson P J, Norton N G, Neave J H and Joyce B A (1983), Vacuum 33, 10
- Dorrity I A, Grange J D and Wickenden D K (1985), in 'Gallium Arsenide; materials, devices and circuits', M J Howes and D V Morgan Eds., Wiley-Interscience pp 95-117
- Drathen P, Ranke W and Jacobi K (1978), Surf. Sci. 77, L126
- Drummond T J, Morkoc H and Cho A Y (1982a), J. Crystal Growth 56, 449
- Drummond T J, Lyons W G, Fischer R, Thorne R E, Morkoc H, Hopkins G C and Evans C A (1982b), J. Vac. Sci. Technol. 21, 957
- Duggan G, Dawson P, Foxon C T and Hooft G W (1984), J. Physique 43, C5/129
- Eastman L F (1983), J. Vac. Sci. Technol. B1, 131
- Edmond J T and Hilsum C (1960), J. Appl. Phys. 31, 1300
- Erickson L P, Carpenter G L, Seibel D D, Palmberg P W, Pearah P, Kopp W and Morkoc H (1985), J. Vac. Sci. Technol. B3, 536
- Esaki L and McGroddy J C (1975), IBM Tech. Disclosure Bull. A 3108
- Esaki L, Chang L L and Mendez E E (1981), Jpn. J. Appl. Phys. 20, L259
- Farrow R F C (1975), J. Phys. D 8, L87
- Farrow R F C and Williams G M (1978), Thin Solid Films 55, 303

- Fischer R, Klem J, Drummond T J, Thorne R E, Kopp W, Morkoc H and Cho A Y (1983), *J. Appl. Phys.* 54, 2508
- Foxon C T, Harvey J A and Joyce B A (1973), *J. Phys. Chem. Solids* 34, 1693
- Foxon C T and Joyce B A (1975), *Surf. Sci.* 50, 434
- Foxon C T and Joyce B A (1977), *Surf. Sci.* 64, 293
- Foxon C T and Joyce B A (1978), *J. Crystal Growth* 44, 75
- Foxon C T, Joyce B A and Norris M T (1980), *J. Crystal Growth* 49, 132
- Foxon C T and Joyce B A (1981), Chapter 1 in 'Current Topics in Materials Science', Vol 7, E. Kaldis Ed., North-Holland 1981
- Foxon C T (1983), *J. Vac. Sci. Technol.* B1, 293
- Foxon C T, Philips Research Laboratories, Priv. Comm. (1987)
- Freller H (1979), *Thin Solid Films* 58, 49
- Fritzsche H and Lark-Horovitz K (1955), *Phys. Rev.* 98, 1532
- Fynn G W and Powell W J A (1979), 'The Cutting and Polishing of Electro-Optic Materials', Adam Hilger, London
- Goldstein B, Szostack D J and Ban V S (1976), *Surf. Sci.* 57, 733
- Godinho N and Brunnschweiler A (1970), *Solid State Electron.* 13, 47
- Gossard A C (1984), *IEEE ED-31*, 1667
- Gotoh H, Sasamoto K, Kuroda S, Yamatomo T, Tamamura K, Fukushima M and Kimata M (1981), *Jap. J. Apl. Phys.* 20, L893
- Grange J D, Parker E H C and King R M (1979), *J. Phys. D* 12, 1601
- Grange J. D. (1980), PhD Thesis CNAA, City of London Polytechnic
- Grange J. D. (1982), *Vacuum* 32, 447
- Grange J. D. (1985), in 'The Technology and Physics of Molecular Beam Epitaxy', E. H. C. Parker, Ed., Plenum, New York, pp 47-58
- Grunthaner F J, Yen M Y, Fernandez R, Lee T C, Madhukar A and Lewis B F (1985), *Appl. Phys. Lett.* 46, 983

- Gunther K G (1958), *Z. Naturforsch.* 13a, 1081
- Gunther K G (1961) in 'Compound Semiconductors' Vol 1, R R Willardson and H L Goering Eds., Reinhold, New York
- Hancock B R and Kroemer H (1984), *J. Appl. Phys.* 55, 4239
- Harris J J, Joyce B A and Dobson P J (1981), *Surf. Sci.* 103, L90
- Harris J J, Joyce B A, Gowers J P and Neave J H (1982), *Appl. Phys. A* 28, 63
- Harris J J, Philips Research Laboratories, Priv. Comm. (1984)
- Harris J J, Ashenford D A, Foxon C T, Dobson P and Joyce B A (1984), *Appl. Phys. A*, 33, 87
- Harris J J (1985) in 'The Technology and Physics of Molecular Beam Epitaxy', E. H. C. Parker, Ed., Plenum, New York, pp 425-460
- Harrison and Houston (1986), *J. Crystal Growth* 78, 257
- Heckingbottom R, Davies G J and Prior K A (1983), *Surf. Sci.* 132, 375
- Heckingbottom R (1985), *J. Vac. Sci. Technol.* B3, 572
- Heiblum M, Mendez E E and Osterling L (1983a), *J. Appl. Phys.* 54, 6982
- Heiblum M, Wang W I, Osterling L E and Deline V (1983b), *J. Appl. Phys.* 54, 6751
- Heinecke H, Werner K, Weyers M, Luth L and Balk P (1987), *J. Crystal Growth* 81, 270
- Herman M A (1982), *Vacuum* 32, 555
- Hilsum C (1974), *Electron. Lett.* 10, 259
- Hilsum C and Rose-Innes A C (1961), 'Semiconducting III-V Compounds', Pergamon, London
- Hiyamizu H, Nanbu K, Fujii T, Sakura T, Hashimoto H and Ryuzano O (1980), *J. Electrochem Soc.* 127, 1562
- Hiyamizu H, Fujii T, Nanbu K and Hashimoto H (1981), *J. Crystal Growth* 51, 149
- Hiyamizu H, Fujii T, Muto S, Inata T, Nakata Y, Sugiyama Y and Sasa A (1987), *J. Crystal Growth* 81, 349
- Honig R E and Kramer D A (1969), *R C A Review* 30, 285
- Howson (1968), *Brit. J. Appl. Phys. Ser. 2*, 1, 15 & 939

- Howson (1970), *J. Phys. D* 3, 584
- Houzay F, Guille C, Moison J M, Henoc P and Barthe F (1987), *J. Crystal Growth* 81, 67
- Hrostowski H J, Morin F J, Geballe T H and Wheatley G H (1955), *Phys. Rev.* 100, 1672
- Hughes R C (1987), *Optical Engineering* 26, 249
- Hwang J C M, Temkin H, Brennan T M and Frahm R E (1983), *Appl. Phys. Lett.* 42, 66
- Ilegems M (1977), *J. Appl. Phys.* 48, 1278
- Ilegems M and Dingle R (1975), *Inst. Phys. Conf. Ser.* 24, 1
- Ilegems M (1985) in 'The Technology and Physics of Molecular Beam Epitaxy', E. H. C. Parker, Ed., Plenum, New York, pp 83-138
- Ishizaka A, Nagakawa K and Shiraki Y (1982), 2nd Int. Symposium in MBE and Related Clean Surface Techniques, Tokyo
- Ito T, Shinohara M and Imamura Y (1984), *Jap. J. Appl. Phys.* 23, L524
- Janson M (1983), *J. Electrochem. Soc.* April 1983, 960
- Jensen E W (1973), *Solid State Technol.* 16, 49
- Johnson J E (1966), *J. Appl. Phys.* 37, 2188
- Joyce B A (1974), *Rep. Prog. Phys.* 37, 367
- Joyce B A (1985), Chapter 2 in 'Proceedings of the NATO ASI on MBE and Heterostructures' (Erice, Italy 1983), Nijhoff, Netherlands
- Kasano H (1978), *J. Appl. Phys.* 49, 4746
- Kawamura Y, Asahi H, Ikeda M and Okamoto H (1981), *J. Appl. Phys.* 52, 3445
- Kamakura K, Akashi T and Tsuzuki M (1975), *J. Phys. Soc. Japan* 38, 1383
- Kaye G W C and Laby T H (1973), 'Tables of Physical and Chemical Constants' 14th Ed., Longman, London
- Kerr T M, Peacock D C, Holmes S J and Wood C E C (1987) *J. Crystal Growth* 81, 175
- Kilgore B F and Roberts R W (1963), *Review Sci. Instr.* 34, 11

- Kimura K, Horiguchi S, Kamon K, Shimazu M, Mashita M, Mihara M and Ishii M (19870, *J. Crystal Growth* 81, 276
- Kirchener P D, Woodall J M, Freeout J L and Pettit G D (1981), *Appl. Phys. Lett.* 38, 427; also *J. Vac. Sci. Technol.* 19, (1981), 604
- Kirkpatrick C G, Chen R T, Holmes D E and Elliot K R (1985), in 'Gallium Arsenide Materials, Devices and Circuits', Ed. M J Howes and D V Morgan, Wiley-Interscience, New York
- Kojima T, Kawai N J, Nakagawa T, Ota K, Sakamoto T and Kawashima M (1985), *Appl. Phys. Lett.* 47, 286
- Kowalczyk S P, Schaffer W J, Kraut E A and Grant R W (1982), *J. Vac. Sci. Technol.* 20, 705
- Krusor B S and Bachrach R Z (1983), *J. Vac. Sci. Technol.* B1, 138
- Kubiak R A, Driscoll P and Parker E H C (1982), *J. Vac. Sci. Technol.* 20, 252
- Kubiak R A (1983), PhD Thesis CNAAC, City of London Polytechnic
- Kubiak R A A and Parker E H C (1984), *Appl. Phys. A* 35, 75
- Kubiak R A A, Parker E H C, Newstead S and Harris J J (1984a), *Appl. Phys. A* 35, 61
- Kubiak R A A, Harris J J and Dawson P (1984b), *J. Appl. Phys.* 55, 598
- Kubiak R A A, Parker E H C and Iyer S S (1986), Chapter 2 in 'Silicon MBE', E Casper and J C Bean Eds., in press
- Kunig H E (1968), *Solid State Electronics* 11, 335
- Kunig H E (1970), *J. Vac. Sci. Technol.* 7, 100
- Kunzel H, Knecht J, Jung H, Wuntzel K and Ploog K (1982), *Appl. Phys. A* 28, 167
- Kuphal E (1981), *J. Crystal Growth* 54, 117
- Lambert M, Bonnevie D and Huet D: 2nd European Workshop on MBE, University of Sussex, March 1983
- Landolt-Bornstein (1982), 'Group III: Crystal and Solid State Physics' Vol 17, Ed. K H Hellwege, Springer, Berlin-Heidelberg
- Larsen P K, Neave J H and Joyce B A (1981), *J. Phys. C* 14, 167

- Laurence G, Simondet F and Saget P (1979), Appl. Phys. 19, 63
- Lee M, Nicholas D J, Singer K E and Hamilton B (1986), J. Appl. Phys. 59, 2895
- Leong W Y (1985), PhD Thesis CNAAC, City of London Polytechnic
- Lewis B (1971), Thin Solid Films 7, 179
- Lewis B F, Lee T C, Grunthaler F J, Madhukar A, Fernandez R and Maserjian J (1984), J. Vac. Sci. Technol. B2, 419
- Leroux M, Leymarie J, Beye A C, Contour J P, Neu G, Massies J, Gilbert P and Verie C (1986), presented at 4th. Int. Conf. MBE, York
- Littlejohn M A, Hauser J R, Glisson T H, Ferry D K and Harrison J W (1978), Solid State Electron. 21, 107
- Liu S-M and Das M B (1987), J. Crystal Growth 81, 359
- Lovett D R (1977), 'Semimetals and Narrow-Gap Semiconductors', 1st Edn., Pion, London
- Ludeke R (1978), IBM J. Res. Dev. 22, 304
- Ludeke R, King R M and Parker E H C (1985), in 'The Technology and Physics of Molecular Beam Epitaxy', E. H. C. Parker, Ed., Plenum, New York, pp 555-623
- Ludowise M J (1985), J. Appl. Phys. 58, R31
- Madelung O (1964), 'Physics of III-V Compounds' Wiley, New York
- Maissel L I and Glang R (1970), 'Handbook of Thin Film Technology', McGraw-Hill, New York
- Many A, Goldstein Y and Grover N B (1967), 'Semiconductor Surfaces' North-Holland, Amsterdam
- Massies J, Etienne P and Linh N T (1976), Rev. Tech. Thomson CSF 8, 5
- Massies J, Etienne P, Dezaly F and Linh N T (1980), Surface Science 99, 121
- Massies J, Rochette J P, Etienne P, Delescluse P, Huber A M and Chevrier J (1983), J. Crystal Growth 64, 101
- Massies J and Contour J P (1985a), J. Appl. Phys. 58, 806

- Massies J and Contour J P (1985b), Appl. Phys. Lett. 46, 1150
- McCarthy J P (1967), Solid State Electron. 10, 649
- McClintock and Wilson (1987), J. Crystal Growth 81, 177
- McLevige W V, Vaidyanathan K V, Streetman V G, Ilegems M, Comas J and Lew L P (1978), Appl. Phys. Lett. 33, 127
- Meggitt B T, Parker E H C and King R M (1978), Appl. Phys. Lett. 33, 528
- Meggitt B T (1979), PhD Thesis CNAAC, City of London Polytechnic
- Meggitt B T, Parker E H C, King R M and Grange J D (1980), J. Crystal Growth 50, 538
- Mendez E E, Heiblum M, Fischer R, Klem J, Thorpe R E and Morkoc H (1983), J. Appl. Phys. 54, 4202
- Mendez E E, Chang L L, Chang C-A, Alexander L F and Esaki L (1984), 215
- Metze G M, Stall R A, Wood C E C and Eastman L F (1980), Appl. Phys. Lett. 37, 165
- Metze G M, Calawa A R and Mavriodes J G (1983), J. Vac. Sci. Technol. B1, 166
- Milea M F and Silver A H (1978) J. Vac. Sci. Technol. 15, 1362
- Miller D L, Zehr S W and Harris J S (1982), J. Appl. Phys. 53, 744
- Miller D L (1985), Appl. Phys. Lett. 47, 1309
- Missous M and Singer K (1986) in 'GaAs and related Compounds'
- Mizuno O, Watanabe H and Shinoda D (1975), Jap. J. Appl. Phys 14, 184
- Monch W (1985), Chapter 4 in 'Proceedings of the NATO ASI on MBE and Heterostructures', Erice, Italy (1983), Nijhof, Netherlands
- Morkoc H and Cho A Y (1979), J. Appl. Phys. 50, 6413
- Morkoc H (1985), Solid State Technol., August, 32
- Munekata H, Chang L L, Woronick S C and Kao Y H (1987), J. Crystal Growth 81, 237

- Murotani T, Shimano T and Mitsui (1978), J. Crystal Growth 45, 302
- Nag (1980) 'Electron Transport in Compound Semiconductors', Springer Series in Solid State Sciences, Vol 11
- Naganuma M and Takahashi K (1975), Appl. Phys. Lett. 27, 342
- Nakajima O, Nagata K, Ito H, Ishibashi T and Sugeta T (1985), Jpn. J. Appl. Phys. 24, 1368
- Neave J H and Joyce B A (1978a), J. Crystal Growth 43, 204
- Neave J H and Joyce B A (1978b), J. Crystal Growth 44, 387
- Neave J H, Blood P and Joyce B A (1980), Appl. Phys. Lett. 36, 311
- Neave J H, Joyce B A and Dobson P J and Norton N (1983), Appl. Phys. A31, 1
- Neave J H, Joyce B A and Dobson P J (1984), Appl. Phys. A33, 184
- Neave J H, Dobson P J, Joyce B A and Zhang J (1985), Appl. Phys. Lett. 47, 100
- Nedoluha A and Koch K M (1952), Z. Phys. 132, 608
- Newstead S M, Kubiak R A A and Parker E H C (1984), J. Vac. Sci. Technol. A2, 1603
- Newstead S M, Kubiak R A A and Parker E H C (1987), J. Crystal Growth 81, 49
- Nishi S, Inomata H, Akiyama M and Kaminishi K (1985), Jap. J. Appl. Phys. 24, L391
- Noad J P and SpringThorpe A J (1980), J. Electronic Mat. 9, 601
- O'Hanlon J F (1983), J. Vac. Sci. Technol. A1, 228
- Osaka J, Hyuga F and Watanabe K (1985), Appl. Phys. Lett. 47, 1307
- Osbourne G C (1982), J. Appl. Phys. 53, 1586
- Palmtree S C, Lee B R and Hwang J C M (1984), J. Electrochem. Soc. 131, 3028
- Pao Y-C, Liu D, Lee W S and Harris J S (1986) Appl. Phys. Lett. 48, 1291
- Pankove J I (1975), 'Optical Processes in Semiconductors', Dover, New York

- Parker E H C, Kubiak R A, King R M and Grange J D (1981),
J. Phys. D 14, 1853
- Patel G, Kubiak R A A and Newstead S M (1987), in
preparation
- Panish M B, Sumski S and Hayashi I (1971), Met. Trans. 2,
795
- Panish M B (1980), J. Electrochem Soc. 127, 2729
- Pearson G L and Bardeen J (1948), Phys. Rev. 73, 1256A
- Petroff P M, Gossard A C and Weigmann W (1984), Appl. Phys.
Lett. 45, 620
- Ploog K (1980), in 'Crystals; Growth, Properties and
Applications', F C Freyhardt Ed., Springer,
Heidelberg
- Poth H, Bruch H, Heyen M and Balk P (1979), J. Appl. Phys.
49, 285
- Praseuth J P, Goldstein L, Hènoc P, Primot J and Danan G
(1987), J. Appl. Phys. 61, 215
- Prior K A, Davies G J and Heckingbottom R (1984), J.
Crystal Growth 66, 55
- Pruyton M (1975), 'Surface Physics', Clarendon Press,
Oxford
- Putley E H (1960), 'The Hall Effect and Related Phenomena',
Butterworth, London
- Rezazadeh A, GEC Hirst Research Centre, Priv. Comm. (1987)
- Rhode D L and Knight S (1971), Phys. Rev. B3, 2534
- Robinson J W and Ilegems M (1978), Rev. Sci. Inst. 49, 205
- Rockett A, Drummond T J, Greene J E and Morkoc H (1982), J.
Appl. Phys. 53, 7085
- Sachs R and Shen H (1985), Appl. Phys. Lett. 47, 374
- Sai-Balasz G A, Tsu R and Esaki L (1977), Appl. Phys. Lett.
30, 651
- Schaffer W J (1980), Rockwell International Science Centre
Report No. AFWAL-TR-81-1018 (1980)
- Schaffer W J and Berg A L (1981), unpublished work
(Rockwell Contract No. F33615-80-C-1052)
- Schaffer W J, Lind M D, Kowalczyk S P and Grant R W (1983),
J. Vac. Sci. Technol. B1, 688

- Schillmann Von E (1956), Z. Naturforschg. 11a, 463
- Schklovskii B I and Efros A L (1984), 'Electronic Properties of Doped Semiconductors', Vol. 45, Springer Series in Solid State Sciences
- Seeger K (1982), 'Semiconductor Physics', Vol. 40, Springer Series in Solid State Sciences
- Shinohara M, Ito T, Yamada K and Imamura Y (1985), Jap. J. Appl. Phys. 24, L711
- Sites J R and Weider H H (October 1975), CRC Crit. Rev. in Solid State Sciences, 385
- Solomon P M and Morkoc H (1984), IEEE J. ED-31, 1015
- SpringThorpe A J and Mandeville P (1986), J. Vac. Sci. Technol. B4, 853
- SpringThorpe A J, Ingreys S J, Emmerstorfer B, Mandeville P and Moore W T (1987), Appl. Phys. Lett. 50, 77
- Stall R A, Wood C E C, Kirchner P D and Eastman L F (1980), Electron. Lett. 16, 171
- Stewart C P, Blight S R and Nicholls R E (1986), GEC J. Res. 4, 229
- Stringfellow G B (1983), J. Crystal Growth 65, 1983
- Sugiyama K (1986), J. Crystal Growth 75, 435
- Suzuki Y, Seki M, Horikoshi Y, Okamoto H (1984), Jap. J. Appl. Phys. 23, 164
- Sze S M (1981), 'Physics of Semiconductor Devices', 2/Ed, Wiley-Interscience, New York
- Tegayadi O, Sun Y L, Klem J, Fischer R, Klein M V and Morkoc H (1983), Solid State Comm. 46, 251
- Tran D C, Levin K H, Burk M J, Fisher C F and Brower D (1986), 'Infra-red Optical Materials and Fibers IV' SPIE Vol. 618, 48
- Tsang W T (1982), J. Crystal Growth 56, 464
- Tsang W T (1984) Appl. Phys. Lett. 45, 1234
- Tsang W T (1985) in 'The Technology and Physics of Molecular Beam Epitaxy', Plenum, New York, pp 467-550
- Tsang W T and Chui T H, unpublished work, priv. comm. (1986)
- Tsang W T (1987), J. Crystal Growth 81, 261
- Tsui D C and Gossard A C (1981), Appl. Phys. Lett. 38, 551

- Tuck B (1975), *J. Mater. Sci.* 10, 321
- van der Pauw L J (1958), *Philips Res. Rep.* 13, 1
- van der Ziel J P, Chiu T H and Tsang W T (1986), *Appl. Phys. Lett.* 48, 315
- Van Hove J M and Cohen P I (1982), *J. Vac. Sci. Technol.* 29, 726
- Van Hove J M, Cohen P I and Lent C S (1983), *J. Vac. Sci. Technol.* A1, 546
- Van Hove J M, Pukite P R, Whaley G H, Nowchack A M and Cohen P I (1985), *J. Vac. Sci. Technol.* B3, 1116
- Van Hove J M and Cohen P I (1987), *J. Crystal Growth* 81, 13
- Vasquez R P, Lewis B F and Grunthaler F J (1983), *Appl. Phys. Lett.* 42, 293
- Vechten J A (1977), *J. Vac. Sci. Technol.* 14, 992
- Walukiewicz W, Lagowski J and Gatos H C (1982), *J. Appl. Phys.* 53, 769
- Wagini H (1965), *Z. Naturforsch.* A20, 921
- Washburn H A (1978), PhD Thesis, Colorado State University
- Washburn H A, Sites J R and Weider H H (1979), *J. Appl. Phys.* 50, 4872
- Weider H H (1974), *Appl. Phys. Lett.* 25, 206
- Weider H H (1977), *Thin Solid Films* 41, 185
- Weimann G (1979), *Phys. Status Solidi A* 53, K173
- Weimann G (1985), *J. Vac. Sci. Technol.* B3, 514
- Weng S-L, Webb C, Chai Y G and Bandy S G (1985), *Appl. Phys. Lett.* 47, 391
- Weng S-L (1986), *Appl. Phys. Lett.* 49, 345
- Werner K, Heinecke H, weyers M, Luth H and Balk P (1987), *J. Crystal Growth* 81, 281
- Weston G F (1984a), *Vacuum* 34, 619
- Weston G F (1984b), *Phys. Technol.* 15, 37
- Wheeler W R (1972), *Physics Today*, August, 52
- Wicks G, Wang W I, Wood C E C, Eastman L F and Rathbun L (1981), *J. Appl. Phys.* 52, 5792

- Wieder H H (1974), Appl. Phys. Lett. 25, 206
- Weider H H (1977), Thin Solid Films 41, 185
- Wiemann G (1979), Phys. Stat. Sol. A 35, K173
- Wiley J D (1975), in 'Semiconductors and Semimetals', 10,
91, R K Willardson and A C Beer Eds., Academic,
New York
- Willardson R, Harman Y and Beer A (1954), Phys. Rev. 96,
1512
- Williams R S, Paine B M, Schaffer W J and Kowalczyk S P
(1982), J. Vac. Sci. Technol. 21, 386
- Wolf C M and Stillman G E (1975), Appl. Phys. Lett. 27, 564
- Wood C E C (1978), Appl. Phys. Lett. 33, 770
- Wood C E C and Joyce B A (1978), J. Appl. Phys. 49, 4854
- Wood C E C, Woodcock J and Harris J J (1979), IOP Conf.
Ser. 45, 28
- Wood C E C, Rathbun L, Ohno H and DeSimone D (1981), J.
Crystal Growth 51, 299
- Wood C E C, DeSimone D, Singer K and Wicks G W (1982), J.
Appl. Phys. 53, 4230
- Wood C E C, Singer K, Ohashi T, Dawson L R and Noreika A J
(1983a), J. Appl. Phys. 54, 2732
- Wood C E C, Stanley C R, Wicks G W and Esi M B (1983b), J.
Appl. Phys. 54, 1868
- Wood C E C (1985) in 'The Technology and Physics of
Molecular Beam Epitaxy', E. H. C. Parker, Ed.,
Plenum, New York, pp 61-81
- Wood E A (1964), J. Appl. Phys. 35, 1306
- Woodall J M, Freeouf J L, Pettit G D, Jackson T and
Kirchener J (1981), J. Vac. Sci. Technol. 19, 626
- Wright D R (1985), in 'Gall-ium Arsenide; materials,
devices and circuits', M J Howes and D V Morgan
Eds., Wiley-Interscience
- Wright S L, Marks R F, Tiwari S, Jackson T N and Baratte H
(1986a), Appl. Phys. Lett. 49, 1545
- Wright S L, Marks R F and Wang W I (1986b), J. Vac. Sci.
Technol. B4, 505

Yano M, Nogami M, Matshusima Y and Kimita M (1977), Jap. J. Appl. Phys. 16, 2131

Yao T (1983), Jap. J. Appl. Phys. 22, L680

Yen M Y, Levine B F, Bethea C G, Choi K K and Cho A Y (1987), Appl. Phys. Lett. 50, 927

SHOP NOTES

These are "how-to-do-it" papers. They should be written and illustrated so that the reader may easily follow whatever instruction or advice is being given.

The use of sliding metal electrical contacts in UHV

S. M. Newstead, R. A. A. Kubick, and E. H. C. Parker

Department of Physics, City of London Polytechnic, 31 Jewry Street, London EC3N 2EY, United Kingdom

(Received 31 May 1984; accepted 4 August 1984)

A simple and versatile method of contacting to sliding stainless steel rods is described. Compact linear motions are made possible, in which the supports of a component also act as electrical feeds. Problems associated with insulated flexible connectors are thus eliminated. The contacts have worked reliably in a III-V MBE system environment.

PACS numbers: 07.30.Kf, 73.40.Ns, 81.15. - z

Providing electrical connections to a moving component (e.g., substrate manipulator or ionization gauge flux monitor) is a frequent requirement within UHV systems. Flexible conductors, insulated with alumina or silica beads, are often used for this purpose. A problem which has been experienced with this arrangement is a tendency for the insulating beads to fracture and abrade against each other, with subsequent contamination of other components in the UHV system (the possible contamination of evaporation sources is of particular concern). Insulated flexible conductors can also be inconveniently bulky. This article describes a simple, compact, and contamination free sliding metal contact for use with linear drives in which rods supporting the moving component also act as electrical connections. The contacts are especially well suited for use with magnetically coupled drives. The combination allows the construction of a long linear motion with electrical feeds without the expense of a bellows seal.

Figure 1 shows one pair of contacts. 0.4 mm thick, 6 mm wide hard rolled phosphor bronze spring strips press firmly onto 1/8 in. o.d. stainless steel rods at an angle of 15°. The strips are isolated from a conical stainless steel support/terminal block by ceramic collars. Flats milled along the sides of the cone allow positive location of the insulators. A fixed

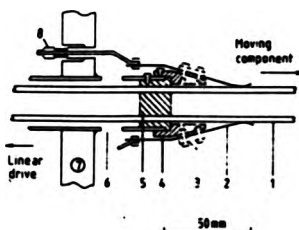


FIG. 1. Sliding metal electrical contacts: (1) stainless steel rod; (2) phosphor bronze strip; (3) ceramic resistor; (4) stainless steel support; (5) PTFE bearing; (6) pumping hole; (7) "Conflat" flange; (8) electrical feedthrough.

PTFE (Teflon) bearing located underneath the terminal block insulates the rods and ensures that they are correctly positioned with respect to the contacting strips. The sliding rods require a second constraint to keep them parallel which can be located at either end of the linear drive according to convenience. The drive may be applied through one or more of the rods, provided that they remain insulated from one another. The only critical point in construction is that the clearance holes through the PTFE bearing should be about 5% larger than the diameter of the stainless steel rods, as PTFE has a high temperature coefficient of expansion and also tends to deform during the first few bakeouts at 200 °C.¹

Contacts to five parallel rods have been used in the construction of a movable ionization gauge flux monitor, a component of 400 l s⁻¹ ion pumped bakable UHV system used for III-V MBE. Despite moving the gauge fairly rapidly (~5 cm s⁻¹) no problems have been experienced with cold welding (phosphor bronze/stainless steel bearings are used commercially in UHV). Momentary pressure bursts, consisting mainly of H₂ and CO, are limited to ~3 × 10⁻¹⁰ mbar above a background pressure of 5 × 10⁻¹⁰ mbar. No difficulty is experienced in passing a 2 A filament current and it is notable that the contacts are reliable for the nanoampere collector current of the ionization gauge even after exposure to arsenic ambients; the background pressure indicated by the monitor tracks the pressure indicated by the main system ionization gauge down to the x-ray limit of the movable gauge (~1 × 10⁻⁹ mbar).

Sliding metal electrical contacts have also been used in conjunction with rotary motions. We have employed a tantalum wire spring as an electrical contact to a rotating molybdenum disk and found similar reliability and contamination-free performance to that described above.

Acknowledgments: Helpful suggestions and technical assistance from V. B. Manning, G. J. C. Burton, and the staff of the Polytechnic workshops are gratefully acknowledged.

¹A. Roth, *Vacuum Sealing Techniques*, 1st ed (Pergamon, London, 1960), pp. 323 and following.

ON THE PRACTICAL APPLICATIONS OF MBE SURFACE PHASE DIAGRAMS *

S.M. NEWSTEAD

GEC Hirst Research Centre, East Lane, Wembley, Middlesex HA9 7PP, UK

R.A.A. KUBIAK

VG Semicon Ltd., Imberhorne Lane, East Grinstead, Sussex RH19 1XZ, UK

and

E.H.C. PARKER

University of Warwick, Coventry CV4 7AL, UK

This paper reports detailed surface phase diagrams for (100) GaAs and (100) InAs. In the case of GaAs, growth rates from 0.07 to 3.0 $\mu\text{m/h}$, As_4 :Ga flux ratios from 0.25:1 to 100:1 and growth temperatures from 300°C to 800°C were used, covering the whole range of growth conditions of practical use in MBE. Results on the nucleation of the (100) InAs/GaAs heterojunction are also presented. The correlation between material properties, surface reconstruction and growth conditions is discussed for both GaAs and homo- and heteroepitaxial InAs. The emphasis of the paper is on the practical application of the results as an aid to optimising (and reproducing) MBE growth conditions with reasonable efficiency.

1. Introduction

Many workers [1-14] have realised the value of specifying MBE growth conditions against a system-independent phenomenon, such as surface reconstruction, in order to improve reproducibility [5-7,11] and facilitate the comparison of results between laboratories [7,13]. Perhaps the most reproducible way of specifying a growth condition is to use the boundary between two surface reconstructions as a reference point [6,13]. The availability of a surface phase diagram, showing the existence regions of the reconstructions supported by a growing surface as a function of the substrate temperature and growth fluxes, is obviously helpful in this application.

Several complete and partial phase diagrams have been reported for (100) GaAs [1,3-10]. These

diagrams are in substantial agreement on the ordering of the various reconstructions but there is a considerable spread in the reported positions of the phase boundaries, probably due to the recognised difficulties involved in measuring the substrate temperature [13] and arsenic flux [6,7,14] in practical growth systems. Also, as far as we are aware, no published phase diagram shows the effects of varying the growth rate.

In this paper we report a detailed phase diagram for (100) GaAs, discuss the nucleation of the (100) InAs/GaAs heterojunction and describe the similarities between the phase diagrams of GaAs and InAs. The effects of varying the growth rate are clearly shown for both compounds. Care was taken to obtain accurate and reproducible estimates of the substrate temperature and growth fluxes when mapping out the diagrams. The correlation between basic material properties, surface reconstruction and the MBE growth conditions is also reported.

* This work was undertaken whilst the authors were at the Department of Physics of the City of London Polytechnic.

2. Experimental

The experiments were performed in a research-orientated MBE system, CLP1V, designed and built in-house. The substrate heater was designed to allow a reproducible measurement of the growth temperature whilst remaining compatible with load-locked operation (fig. 1). Substrates were transferred into the growth chamber soldered to a Mo plate with 6N indium. This transfer plate was then soldered to a second Mo plate forming one end of the heater assembly. The substrate thermocouple was permanently mounted in a 1.2 mm diameter hole passing through the fixed plate. Calibration against the sharply defined phase boundaries on (100) GaAs under static conditions [6,13] indicates that the temperatures reported here were reproducible to within $\pm 5^\circ\text{C}$. The absolute accuracy of measurement was also reasonable; the In solder fixing the transfer block was found to melt at indicated temperatures within the range $160\text{--}185^\circ\text{C}$ (cf. the MP of In, 157°C) and GaAs clean-up (oxide desorption) temperatures of $590\text{--}600^\circ\text{C}$ were normally adequate.

The As_2 flux was estimated from the arsenic overpressure measured using a fixed ionisation gauge mounted close to the growth region (but not directly exposed to any growth flux). The overpressure was calibrated by finding the boundary between the (2×4) As and the (4×2) Ga stabilised reconstructions whilst depositing GaAs onto (100) buffer layers at growth temperatures in the range $450\text{--}500^\circ\text{C}$. The As_2 :Ga flux ratio at this boundary is known to be $0.5:1$ [15]. Similar tech-

niques have been successfully used by other workers [6,11,16]. Periodic checks were made on the absolute intensities of the Ga and In fluxes by growing stepped films.

The GaAs RHEED studies were performed on freshly grown undoped buffer layers. The substrates used were generally $1\text{ cm} \times 2\text{ cm}$ pieces cleaved from 2 inch wafers (ICI undoped GaAs, (100) on-axis). There was no indication that the ratio of the growth fluxes varied significantly across this small area. 5 keV RHEED was used for the majority of observations.

3. The surface phase diagram of (100) GaAs

Fig. 2 is the surface phase diagram of (100) GaAs growing at $0.65\ \mu\text{m/h}$. The reconstructions seen during growth were:

- Region I mixed $(2 \times 4)/c(4 \times 4)$,
- Region II (2×4) ,
- Region III (1×1) bulk streaks,
- Region IV (4×2) ,
- Region V $c(8 \times 2)$

No additional reconstructions were seen under static conditions. A clear $c(4 \times 4)$ pattern was only seen under large As_2 fluxes in Region I. The pattern seen under practical growth conditions (i.e. $J_{\text{As}_2}:J_{\text{Ga}} < 50:1$) was a composite of the (2×4) and $c(4 \times 4)$ RHEED patterns. A clear $c(4 \times 4)$ reconstruction could always be obtained under

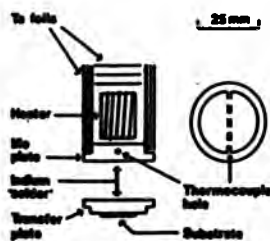


Fig. 1. Schematic illustration of the substrate heater.

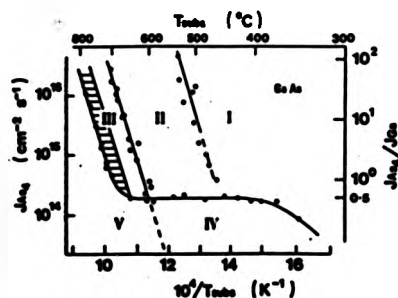


Fig. 2. The MBE surface phase diagram of (100) GaAs for a fixed growth rate of $0.65\ \mu\text{m/h}$.

static conditions. Our identification of the (8×2) and (4×2) reconstructions as occurring in separate regions is tentative, although consistent with the results of Cho [2].

Several workers have reported a (3×1) reconstruction under As_2 [3,4,17] and As_4 [5] fluxes, even quoting this reconstruction as optimum for the growth of material with maximum photoluminescent efficiency [17]. The fact that we, in common with others [6,8,10], did not see a (3×1) reconstruction implies that it may only be visible with a critically adjusted RHEED geometry (see also Panish [4]). With reference to published data [3-5,17], the (3×1) reconstruction may be expected to occur between the (2×4) and (1×1) reconstructions, i.e. within Region III of the phase diagram reported here.

The phase boundaries were mapped out by varying T_s at a fixed As_4 flux or vice versa. Hysteresis was not seen at any boundary implying that, within the timescale of the experiments, the reconstructed surfaces remained in equilibrium with the growth fluxes. Note, however that epilayers grown in the shaded area of Region III (fig. 2) were temporally unstable, showing (1×1) bulk streaks at nucleation but becoming $(4 \times 2)/(8 \times 2)$ gallium stabilised within the first few minutes of growth.

Referring to fig 2, a fixed $As_4:Ga$ flux ratio (assumed to be 0.5:1 as previously described) was found to be just sufficient to maintain an arsenic stabilised reconstruction over a wide range of temperatures (400-635°C), indicating the range of applicability of the Foxon/Joyce growth model [15,18] at this growth rate. At temperatures below 400°C the transition to a gallium stabilised reconstruction occurred at flux ratios below 0.5:1 and at temperatures below about 320°C the arsenic stabilised pattern became "frozen in" and no change to gallium stabilisation could be induced, the RHEED pattern becoming slightly spotty and fading away as the As_4 flux was reduced. We cannot offer a full explanation of this phenomenon but note that some apparent differences in the surface interaction chemistry of $As_4-Ga-(100)GaAs$ above and below 330°C have been attributed to the formation of an intrinsic population of Ga atoms at the higher tempera-

tures due to the desorption of As_2 [18].

Several of the reconstructions are separated by a series of parallel boundaries (between I and II, II and III, III and V). These boundaries are characterised by an activation energy of 3.9 eV. Within experimental error, the same activation energy has previously been obtained from independent observations of some of the phase boundaries reported here [4], from the time taken to evaporate a surface layer of arsenic from MBE grown (100) GaAs [1] and from the vapour pressure of As_2 over GaAs [19]. This suggests that the basic mechanism determining the slope of the boundaries can be associated with the evaporation of chemisorbed arsenic from the epilayer surface (3.9 eV is comparable with chemical bond strengths).

4. Variation of growth rate

Fig. 3 is the superposition of the (100) GaAs surface phase diagrams for five fixed growth rates in the range 0.07-3.0 $\mu m/h$. The activated phase boundaries are common to all growth rates. The low temperature deviation from the minimum flux ratio occurs at lower temperatures for lower growth rates; this may be related to surface lifetime phenomena. It is apparent that there is an upper limit to the growth rate of GaAs under the (2×4)

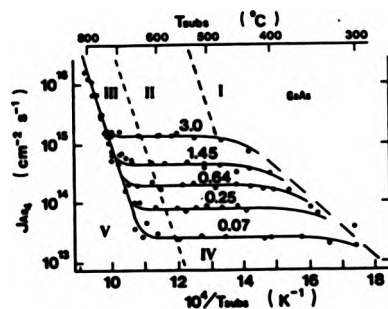


Fig. 3. The superposition of the (100) GaAs surface phase diagrams for five fixed growth rates in the range 0.07-3.0 $\mu m/h$.

reconstruction. Even allowing for the use of a generous flux ratio this limit is in excess of 60 $\mu\text{m}/\text{h}$ and is unlikely to be restrictive in practice.

5. GaAs epilayer properties

In summary: all epilayers grown in Regions IV and V of the phase diagram were spoiled by surface accumulations of Ga. Epilayers grown in Region I were typically mirror shiny and (with the exception of the common oval defect) substantially undefected but had poor electrical properties, often being highly resistive even if doped at $1 \times 10^{17} \text{cm}^{-3}$ with Si or Sn. Epilayers grown in the temporally unstable area of Region III were marred by large hillock features very similar in appearance to those which we have reported on (100) InAs grown under a similar metal-rich regime (ref. [20] and section 6). The electron mobilities of Si and Sn doped epilayers grown in Region II and the temporally stable area of Region III lay close to Poth's 77 K μ versus n curve [21] at carrier concentrations above about $5 \times 10^{15} \text{cm}^{-3}$. Unintentionally doped material was typically $2 \times 10^{15} \text{cm}^{-3}$ p-type. Typical oval defect defect densities of about $1 \times 10^3 \text{cm}^{-2}$ were obtained when using a fresh gallium charge, rising to about $1 \times 10^4 \text{cm}^{-2}$ at the end of an extended growth series.

6. The nucleation of InAs onto (100) GaAs

The (100) InAs/GaAs heterojunction is difficult to nucleate because of the large ($\sim 7\%$) lattice mis-match between the two components. There are three distinct growth regimes in hetero-epitaxy [11,12,20]: arsenic rich, optimum and indium rich. Films nucleated under arsenic and indium rich conditions exhibit characteristic defects [20] and have severely degraded electrical properties [11,12,20].

There is some disagreement as to the conditions leading to optimum material quality, with some authors reporting that it is necessary to grow under an In-stable (4×2) reconstruction [11,12]. To investigate these claims we grew a series of InAs epilayers onto (100) GaAs substrates at a

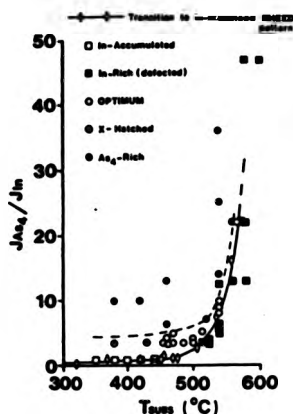


Fig. 4. The effects of varying the substrate temperature and As_4 :In flux ratio of the nucleation of InAs onto (100) GaAs.

fixed growth rate of $2.0 \pm 0.1 \mu\text{m}/\text{h}$ over a wide range of growth temperatures and As_4 :In flux ratios. Fig. 4 illustrates the correlation between morphology, reconstruction and growth conditions. The best InAs grown in these experiments was grown under a diffuse (1×1) reconstruction using a minimised As_4 flux and growth temperatures in the range 450–550°C. Unintentionally doped films with thicknesses over 5 μm were typically n-type with 77 K mobilities of $6 \times 10^4 \text{cm}^2 \text{V}^{-1} \text{s}^{-1}$ at $5 \times 10^{15} \text{cm}^{-3}$. Typical residual defect levels were 8×10^2 to $3 \times 10^3 \text{cm}^{-2}$, significantly lower than the oval defect levels on GaAs grown in parallel experiments. The use of minimised As_4 fluxes at lower growth temperatures led to the growth of mirror-shiny epilayers under a clear (2×4) reconstruction, but the 77 K mobilities of undoped layers grown under these conditions ($T_s = 300$ –450°C) were always $< 3 \times 10^4 \text{cm}^2 \text{V}^{-1} \text{s}^{-1}$ at $n > 1 \times 10^{16} \text{cm}^{-3}$.

The boundary between optimum and In-rich growth conditions was exactly delineated by a clear and unambiguous transition to a (4×2) reconstruction (fig. 4). All epilayers grown under the (4×2) reconstruction at As_4 :In flux ratios

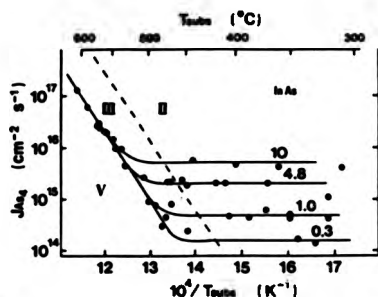


Fig. 5. The MBE surface phase diagram of (100) InAs. The surface reconstructions seen within Regions II, III and IV correspond to those seen in the same regions of the (100) GaAs phase diagrams (figs. 2 and 3).

> 0.5:1 were heavily defected with hillocks orientated along the [011] direction. These defects are described elsewhere [20]. As noted above, very similar defects were seen on GaAs grown within the temporally unstable area of Region III of the GaAs phase diagrams. Comparison of figs. 2, 3, 4 and 5 will show that the growth conditions involved are essentially equivalent. We were unable to identify an In-stable condition leading to the growth of good quality InAs under the (4×2) reconstruction.

7. The surface phase diagram of (100) InAs

In addition to the experiments described above, InAs was deposited onto (100) InAs substrates and onto thick InAs buffer layers grown on (100) GaAs substrates under optimum conditions. It was found that mirror-shiny and substantially un-defected InAs could be grown under the (2×4) and (1×1) reconstructions at $As_4:In$ flux ratios as high as 40:1, confirming an earlier report [12] that "As-rich growth" is, in fact, a nucleation condition which does not apply to homoepitaxy. Unfortunately the non-availability of semi-insulating InAs substrates has hampered investigations into the electrical properties of these films. However, the elimination of the arsenic rich nonopti-

mum growth condition does allow a full InAs surface phase diagram to be constructed.

Fig. 5 is in the MBE surface phase diagram of (100) InAs for four fixed growth rates. This diagram is, although scaled differently, very similar to the GaAs phase diagram described in section 3 and many of the same comments apply. The main difference between the two diagrams is that different energies characterise the activated phase boundaries (2.6 eV for InAs, cf. 3.9 eV for GaAs) commensurate with the relative bond strengths of the two compounds. It would be interesting to have comparative data for AlAs. Fig. 5 is in excellent qualitative agreement with the recently reported results of Sugiyama [16].

It is possible to map out a "nucleation phase diagram" for (100) InAs/GaAs which closely resembles fig. 5 with additional constraints to the range of As_4 fluxes usable at a given growth rate. However, fig. 5 contains sufficient information for most purposes as the variation of the optimum nucleation temperature with growth rate simply follows the shift in T_{nc} , i.e. for best results in heteroepitaxy the grower should nucleate under a minimised As_4 flux just within the elbow of the As-to-In stabilised transition curve appropriate to the growth rate.

8. Practical applications

The surface phase diagrams of (100) GaAs and (100) InAs clearly provide a useful framework within which to specify nucleation and/or growth conditions. RHEED mapping may well prove to be an efficient way of investigating the growth of the less well studied III-V compounds and heterojunctions, especially if combined with basic growth and assessment studies. It would be particularly useful to have the phase diagrams of both components of a heterojunction as this would assist in the choice of an optimised (or compromise) combination of substrate temperature, growth rate and group V flux(es) suited to the nucleation of both materials.

Several laboratories [6,13] use surface phase transitions for routine checks on the accuracy and reproducibility of their growth conditions. This

technique offers several advantages; a non-destructive check of T_s can be made before and after every growth; surface reconstruction is system independent; there are no problems with emissivity changes, pyrometer port fogging, etc.; and compensation for variations between wafer transfer blocks and/or mounting techniques is automatic. Calibration would normally be checked under static conditions as the $c(4 \times 4)$ to (2×4) and (2×4) to (1×1) transitions are more sharply defined in the absence of a gallium flux.

Acknowledgments

We would like to thank Dr. J.J. Harris (Philips Research Laboratories, UK) for many helpful discussions. This work was undertaken whilst the authors were at the Department of Physics of the City of London Polytechnic.

References

- [1] A.Y. Cho, *J. Appl. Phys.* 42 (1971) 2074.
- [2] A.Y. Cho, *J. Appl. Phys.* 47 (1976) 2841.
- [3] J. Manias, P. Étienne and N.T. Linh, *Rev. Tech. Thomson-CSF* 8 (1976) 5.
- [4] M.B. Panish, *J. Electrochem. Soc.* 127 (1980) 2729.
- [5] J.M. Van Hove and P.I. Cohen, *J. Vacuum Sci. Technol.* 29 (1982) 726.
- [6] J.M. Van Hove, P.I. Cohen and C.S. Lent, *J. Vacuum Sci. Technol.* A1 (1983) 546.
- [7] C.E.C. Wood, C.R. Stanley, G.W. Wicks and M.B. Esi, *J. Appl. Phys.* 54 (1983) 1868.
- [8] J.M. Van Hove, P.R. Pukite, G.J. Whaley, A.M. Wowchack and P.I. Cohen, *J. Vacuum Sci. Technol.* B3 (1985) 1116.
- [9] A.Y. Cho, *Thin Solid Films* 100 (1983) 291.
- [10] F. Briones, D. Goizamo, L. Gonzalez and J.L. De Miguel, *Japan. J. Appl. Phys.* 24 (1985) L478.
- [11] W.J. Schaffer, M.D. Lind, S.P. Kowalczyk and R.W. Grant, *J. Vacuum Sci. Technol.* B1 (1983) 688.
- [12] B.R. Hancock and H. Kroemer, *J. Appl. Phys.* 55 (1984) 4239.
- [13] C.R. Whitehouse, M.T. Emeny, L. Davies, G.M. Williams and T. Martin, presented at 4th Intern. Conf. on Molecular Beam Epitaxy, York, September 1986.
- [14] J.H. Neave and B.A. Joyce, *J. Crystal Growth* 44 (1978) 387.
- [15] C.T. Foxon, *J. Vacuum Sci. Technol.* B1 (1983) 293.
- [16] K. Sogiyama, *J. Crystal Growth* 75 (1986) 435.
- [17] J.H. Neave, B.A. Joyce and P.J. Dobson, *Appl. Phys.* A33 (1984) 184.
- [18] C.T. Foxon and B.A. Joyce, *Surface Sci.* 50 (1975) 434.
- [19] B. Goldstein, D.J. Szostack and V.S. Ban, *Surface Sci.* 57 (1976) 733.
- [20] R.A.A. Kubiak, E.H.C. Parker, S. Newstead and J.J. Harris, *Appl. Phys.* A35 (1984) 61.
- [21] H. Poth, H. Bruch, M. Heyen and P. Balk, *J. Appl. Phys.* 49 (1979) 285.

The Electrical Properties of Doped Silicon, Grown by Molecular-Beam-Epitaxy (MBE)

R. A. A. Kubiak*, S. M. Newstead, W. Y. Leong, R. Houghton, and E. H. C. Parker

Solid State MBE Research Group, Sir John Cass Faculty of Physical Sciences and
Technology, City of London Polytechnic, 31 Jewry Street, London, EC3N 2EY, UK

T. E. Whall

Department of Applied Physics and Physical Electronics, Portsmouth Polytechnic,
Park Building, King Henry I Street, Portsmouth, Hampshire, PO1 2DZ, UK

Received 9 July 1986/Accepted 26 August 1986

Abstract. Measurements of the Hall coefficients and of the resistivity of MBE-grown Si, doped with P, As, Sb, B, and Ga in the concentration range 10^{14} to 10^{20} cm⁻³, were carried out at 77 K and at 300 K. With the exception of Ga-doped Si, the measured mobilities were close to or higher than those of bulk materials at both temperatures. The Mott metal/non-metal transition has been observed in the present epitaxial materials and the measured values for the critical impurity concentration at which the transition occurs, agree with values reported by other workers for bulk silicon.

PACS: 72.20, 73.60

Previous studies [1, 2] of co-evaporation doped MBE-grown Si:Sb and Si:Ga [3] indicated that, at medium to high doping levels, the measured Hall mobilities were smaller than those of bulk Si. This arose from the propensity of the Sb and Ga dopants to segregate on the epilayer surface, which necessitated high adlayer coverages (≈ 0.1 monolayer) to achieve the maximum doping levels, and resulted in a disruption of two-dimensional planar growth [1, 4]. With the advent of more sophisticated doping methods such as "potential-enhanced doping" and the use of other dopants, notably B [7, 8], this fundamental limitation was overcome. An investigation of the Hall mobilities of materials grown within our laboratory using these more advanced co-evaporation doping techniques has been carried out in order to meet the need for a rigorous assessment of the majority carrier transport

properties of silicon grown by MBE. The results of this work are summarized in the present paper.

1. Experimental

MBE-grown Si layers were uniformly doped by co-evaporation from B [7, 8], Ga [9], P [10], As [5], and Sb [2-6] sources. The techniques are described in detail elsewhere [1-10]. Nominally undoped epilayers were characterized by Hall-effect and photoluminescence measurements [11], were found to be n-type and the residual impurity was identified as phosphorous which was present in the concentration range 5×10^{13} to 5×10^{15} cm⁻³. Rutherford back scattering, He⁺ dechanneling, secondary-ion mass-spectroscopy and electrical profile measurements were compared and indicated that, within measurement error, complete dopant substitutionality was achieved and that donor exhaustion occurred at 300 K [5] with all intentionally introduced dopant species except Ga.

* Present address: VG Semicon Ltd, The Birches Industrial Estate, Imberhorne Lane, East Grinstead, Sussex, RH11 9 1XZ, England

The Hall measurements [12] were facilitated by depositing the epilayers onto substrates of the opposite carrier type, leading to junction isolation of substrate conduction. Cross-shaped samples were formed by etching to eliminate contact-area effects [12] and ohmic contact was achieved by smearing Ga-In eutectic onto the contact areas which were then overlaid with Au foil. In the case of lightly-doped material, surface-oxidation was removed from the contact area prior to application of the eutectic to ensure good ohmic contact. Good junction isolation was initially ensured by inspecting the I-V characteristics of the junction and by verifying that the measured conductivity of the epilayer was independent of the magnitude of the applied voltage. Poor junction isolation generally lead to low measured mobilities and such non-representative data were discarded. The thicknesses of undoped epilayers (6–40 μm) were sufficient to ensure that depletion effects [13] could be ignored. The linear dependence of the Hall voltage on applied magnetic field was checked and all the usual precautions to eliminate thermomagnetic effects, including sample-current and magnetic-field reversals, were undertaken [14].

The carrier concentration n (or p) and the Hall mobility μ_H have been obtained from [14]

$$n \text{ (or } p) = r R_H \sigma, \quad (1)$$

$$\mu_H = \sigma / n \text{ (or } p) e,$$

where R_H is the Hall coefficient, σ is the conductivity, e is the electronic charge and r is the Hall factor which is set equal to unity.

2. Results

2.1. Comparison of Data on MBE-Grown and Bulk Materials

Figures 1 and 2 show the measured Hall mobilities at 77 and 300 K of n-type (Si:P, Si:As, Si:Sb) MBE-grown Si, plotted against the carrier concentrations at 77 and 300 K. The solid lines represent the Hall mobilities of bulk Si:As computed from (1) with $r=1$ and the data of Morin and Maita [15]. All the 300 K mobilities of epitaxial and bulk materials agree to within the experimental error. The 77 K mobility of P and As-doped epitaxial material are also in good agreement with mobilities measured on As-doped bulk Si over the entire doping range. In the case of Si:Sb epilayers, the measured 77 K mobilities coincide with bulk mobilities [15] at dopant concentrations below $5 \times 10^{17} \text{ cm}^{-3}$. At higher doping levels the mobilities measured in the Si:Sb epilayers are substantially higher than those measured in As-doped bulk materials. This feature is more clearly illustrated in

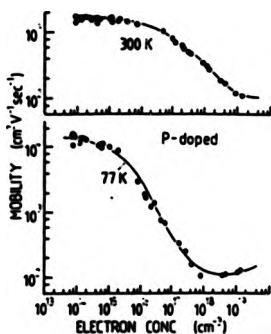


Fig. 1. Electron mobilities μ in MBE-Grown Si:P at 77 and 300 K versus electron concentration n at 77 and 300 K. Carrier concentrations in excess of $5 \times 10^{19} \text{ cm}^{-3}$ have been obtained by controlled introduction of the dopant [10], whereas lower electron densities are associated with residual impurities. In the latter case, only randomly selected representative results on MBE-grown Si are included from the very large data base available. The solid line represents bulk mobility values derived from the measurements of Morin and Maita [15] on Si:As

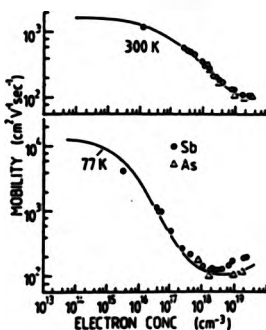


Fig. 2. Electron mobilities μ in MBE-grown Si:Sb and Si:As at 77 and 300 K, compared with measurements made by Morin and Maita [15] on bulk Si:As and Si:Sb (solid line)

Fig. 3 and its origin is not known. The present measurements are also in agreement with studies on bulk materials [15], in showing that the mobilities at 77 K increase slightly for electron concentrations above 10^{18} cm^{-3} (Fig. 3).

Mobility data for p-type MBE-Grown Si:B and Si:Ga are compared with values obtained for bulk

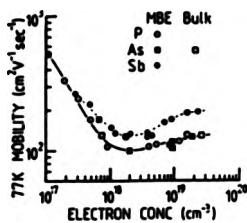


Fig. 3. A comparison of the 77 K electron mobilities of MBE-grown Si:P, Si:As, and Si:Sb. At doping levels exceeding approximately $5 \times 10^{17} \text{ cm}^{-3}$ the mobilities in Si:Sb are greater than those in Si:As and Si:P.

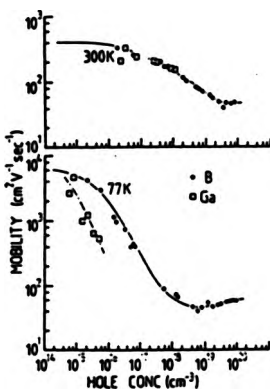


Fig. 4. Hall mobilities μ in MBE-grown Si:B and Si:Ga at 77 and 300 K compared with measurements [15] on bulk Si:B (solid line).

Si:B [15] in Fig. 4. The measurements made on B-doped epilayers are in excellent agreement with results for bulk Si at both 77 and 300 K. Hall mobilities measured on Ga-doped MBE material at 300 K are close to those obtained on bulk Si:B [15], whereas the 77 K mobilities of the Ga-doped epilayers are significantly lower than the 77 K mobilities of B-doped bulk Si. The lower mobilities in the epilayer as compared to the bulk material could be due to the fact that Ga-doped material usually becomes heavily dislocated at doping levels in excess of $5 \times 10^{17} \text{ cm}^{-3}$ [16] or that the three-dimensional adlayer structure formed during Ga-doping [9] produces an inhomogeneous doping distribution.

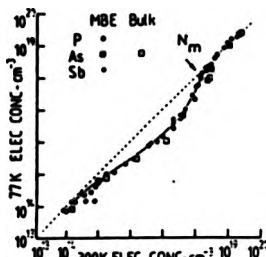


Fig. 5. The electron concentration n at 77 K of n -type bulk and MBE-grown silicon plotted versus the electron concentration at 300 K. N_m denotes the critical donor concentration for the occurrence of the Mott transition. The broken line corresponds to the situation in which the electron concentration is independent of temperature.

2.2. The Metal/Non-Metal Transition in the Silicon Impurity Band

It is anticipated on theoretical grounds [17] that, with the exception of Ga, in excess of 90% of the atoms of the various dopant species should be ionized at 300 K and, as mentioned in Sect. 3.1, this has been experimentally verified. However, as expected from the ionization energies of the dopants employed in this investigation [17], there is a rapid decrease of the carrier density for doping levels in the range 10^{16} to 10^{18} cm^{-3} as the temperature is lowered. This is shown in Figs. 5 and 6 which indicate that, in this composition range, only 10% of the dopants are electronically active at 77 K. At doping levels below 10^{16} cm^{-3} , the carrier concentrations at 77 and 300 K are approximately equal, which is attributed to the fact that donor or acceptor exhaustion is present at temperatures down to 77 K in the more lightly doped materials [17].

When the doping levels exceed about 10^{18} cm^{-3} there is a disappearance of the measured dopant ionization energy and the measured carrier concentration at 77 K becomes equal to that at 300 K for both n and p -type material. This behaviour is believed to be associated with a Mott [18] non-metal to metal transition in which, for high impurity concentrations, conduction occurs in the impurity band. The transition is also apparent in photoluminescence experiments [19] as exciton suppression. Critical dopant concentrations N_m for the occurrence of the Mott transition in the various materials have been determined from Figs. 5 and 6 and are given in Table I. As shown in the table, our values of N_m are in reasonable agreement with the result of Yamanouchi et al. for Si:P [20] which has also been obtained from Hall

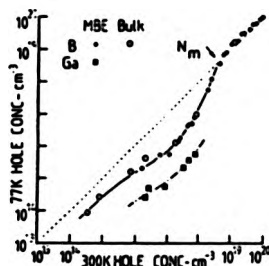


Fig. 6. The hole concentration at 77 K of p-type bulk and MBE-grown silicon, plotted versus hole concentration at 300 K. N_m is the critical acceptor concentration for the occurrence of the Mott transition. The broken line corresponds to the situation in which the hole concentration is independent of temperature.

Table 1. Critical dopant concentrations for the metal-non-metal transition

Dopant	N_m (cm^{-3})		
	This work*	Ref. [20]	Ref. [21]
P	2×10^{18}	4×10^{18}	3.5×10^{18}
As	4×10^{18}		6.4×10^{18}
Sb	2×10^{18}		3.0×10^{18}
B	5×10^{18}		
Ga	Solubility limit too low		

* The maximum error in the estimated values of N_m is approximately 30%.

data, and with values of N_m deduced from capacitance measurements [21].

Yamanouchi et al. [20] have found that, in Si:P, the mobility measured at 4.2 K increases with dopant density for concentrations in excess of N_m . This behaviour, which has been ascribed to the displacement of the Fermi level into the conduction band at high doping levels [22], is also observed in the present materials at 77 K, for all dopants except Ga, as shown in Figs. 1-4.

3. Conclusions

Comparison of the present results with data on the electrical properties of bulk silicon suggests that, except for Si:Ga, earlier difficulties in doping MBE-grown Si have been overcome.

References

- U. König, E. Kasper, H.J. Herzog: *J. Cryst. Growth* **52**, 151 (1981)
- R.A. Metzger, F.G. Allen: *J. Appl. Phys.* **55**, 931 (1984)
- Y. Ota: *Thin Solid Films* **106**, 1 (1983)
- R.A.A. Kubiak, E.H.C. Parker: "MBE of Si and Related Materials", in *The Surface Physics of Semiconductors and Heterogeneous Catalysis*, ed. D. Ring, D. Woodruff (Elsevier, Amsterdam 1987) to be published
- R.A.A. Kubiak, W.Y. Leong, E.H.C. Parker: *Appl. Phys. Lett.* **46**, 563 (1985); *J. Electrochem. Soc.* **132**, 2738 (1985)
- H. Jörke, H. Kibbel: *Electrochem. Soc. Proc.* **85-7**, 194 (1985); *Appl. Phys. Lett.* **47**, 511 (1985)
- R.A.A. Kubiak, W.Y. Leong, E.H.C. Parker: *J. Vac. Sci. Technol.* **B3**, 592 (1985)
- R. A. A. Kubiak, W.Y. Leong, E.H.C. Parker: *Electrochem. Soc. Proc.* **85-7**, 169 (1985)
- S.S. Iyer, R.A. Metzger, F.G. Allen: *J. Appl. Phys.* **52**, 5608 (1981)
- R.A.A. Kubiak, G. Patel, W.Y. Leong, R. Houghton, E.H.C. Parker: *Appl. Phys. A* **40**, 7 (1986)
- R.A.A. Kubiak, W.Y. Leong, R. Houghton, G. Patel, E.H.C. Parker: In preparation
- L.J. van der Pauw: *Philips Res. Rep.* **13**, 1 (1958)
- S.M. Sze: *Physics of Semiconductor Devices* (Wiley, New York 1969)
- E.H. Purley: *The Hall Effect and Related Phenomena* (Butterworth, London 1960)
- F.J. Morin, J.P. Marra: *Phys. Rev.* **96**, 28 (1954)
- R. Houghton, R.A.A. Kubiak, W.Y. Leong, E.H.C. Parker: In preparation
- J.P. McKelvey: *Solid State and Semiconductor Physics* (Harper & Row, London 1967)
- N.F. Mott, E.A. Davis: *Electronic Processes in Non-Crystalline Materials*, 2nd ed. (Clarendon, Oxford 1979)
- A. Sandhu, B. Hamilton, R.A.A. Kubiak, W.Y. Leong, E.H.C. Parker: *Electrochem. Soc. Proc.* **85-7**, 68 (1975)
- C. Yamanouchi, K. Mizuguchi, W. Sasaki: *J. Phys. Soc. Jpn.* **22**, 859 (1967)
- T.G. Castner, N.K. Lee, G.S. Cieloszyk, G.L. Salinger: *Phys. Rev. Lett.* **34**, 1627 (1975)
- H. Fritzsche: In: *The Metal-Non-Metal Transition in Disordered Systems*, ed. by L.R. Friedman, D.R. Tunstall (SUSSP, Edinburgh 1980) p. 193

THE BRITISH LIBRARY DOCUMENT SUPPLY CENTRE

On the growth of (100) GaAs and (100)
InAs by molecular beam epitaxy

TITLE

AUTHOR

S.M. Newstead

Attention is drawn to the fact that the copyright of this thesis rests with its author.

This copy of the thesis has been supplied on condition that anyone who consults it is understood to recognise that its copyright rests with its author and that no information derived from it may be published without the author's prior written consent.



THE BRITISH LIBRARY
DOCUMENT SUPPLY CENTRE
Boston Spa, Wakefield
West Yorkshire
United Kingdom

21

REDUCTION X

D82142